MASTER OF SCIENCE THESIS

Effect of irregularities in the under layer on the stability of Xbloc^{Plus} concrete armour unit

by

I. van den Berg

bam

TU Delft

Master of Science Thesis

Effect of irregularities in the under layer on the stability of Xbloc^{Plus} concrete armour unit

to be publicly defended at the Delft University of Technology,
on Monday May 28, 2018 at 2:30 PM

Author:
Ileen van den Berg

De Constant Rebecquestraat 98
2518 RG, Den Haag
ivdberg@hotmail.com

Graduation committee:

Prof.dr.ir. S.G.J. Aarninkhof	Delft University of Technology, Chair
Dr.ir. B. Hofland	Delft University of Technology
Ing. C. Kuiper	Delft University of Technology
Ir. B. Reedijk	BAM Infraconsult bv
Ir. R. Jacobs	BAM Infraconsult bv

Delft University of Technology
Faculty of Civil Engineering and Geosciences
Stevinweg 1, Building 23
2628 CN Delft / PO-box 5048
The Netherlands
(+31)15 2789802

BAM Infraconsult bv
H.J. Nederhorststraat 1
2801 SC Gouda / PO-box 268
The Netherlands
(+31)182 590510

List of trademarks used in this study:

- Delta Marine Consultants is a registered trade name of BAM Infraconsult bv, the Netherlands
- Accropode is a registered trademark of Artelia (Sogreah Consultants), France
- Xbloc is a registered trademark of Delta Marine Consultants, the Netherlands

The use of trademarks in any publications of Delft University of Technology does not imply any endorsement or disapproval of this product by the University

Preface

This thesis is written as the final work to complete the Master's programme Hydraulic Engineering with specialisation Hydraulic Structures of the faculty of Civil Engineering and Geosciences at Delft University of Technology. The subject for this research was formulated in cooperation with BAM Infraconsult bv. They provided the research facilities and contributed to the knowledge necessary to achieve the research goals.

Many people have contributed to the process of forming this report, both direct and indirect. I would like to thank my graduation committee for their guidance and supervision. First and foremost I would like to thank my daily supervisor Bas Hofland, for his endless enthusiasm for anything related to research in coastal protections and for always providing me with the right amount of inspiration. Whenever I would get stuck in the process you provided me with a flood of information, confusing me at first but ultimately resulting in the best ideas. Second, I would like to thank Stefan Aarninkhof for keeping an eye on the bigger picture and maintaining the added value of the study for BAM and the field of research as a whole. Although Coen Kuiper has been added to my committee at a later stage, he has been indispensable in increasing the quality and comprehensibility of my report. Thank you for reading my full report and providing me with the right remarks.

Furthermore, I would like to thank my supervisors and colleagues of BAM Infraconsult bv. I am very grateful for the opportunity given to me, to perform my own physical model tests and to contribute to the development of the Xbloc^{Plus} armour unit. I never thought that my graduation thesis would be something I could enjoy, but the interesting subject and great colleagues made the impossible possible.

Lastly I would like to thank my friends and family. Especially my parents and sister, who have supported me throughout my studies. Thank you for having faith in me and for being (exorbitantly) proud of me.

This report finalizes my years as a student and writing this makes me nostalgic. I am so very grateful for the memories I have made and the people I have met. Without them, I would not have been the person I am today and I am exited to experience what the future will bring me.

I. van den Berg
The Hague, May 2018

Summary

The Xbloc^{Plus} is a new type of single layer armour unit for breakwaters. The key difference between earlier single layer armour units is that the unit is not only placed in a regular grid, but also with a regular orientation. The main benefit of this is that it can directly be seen whether the unit is placed correctly. Additionally, the placement always takes place with the same repetitive movement, as is preferred by crane drivers. The benefits to the placement procedure would however be reduced when the requirements for the under layer become very tight. Since the time that is saved during placement of the armour units, then would be lost during the profiling of the under layer. This has led this study to focus on the influence of irregularities in the under layer on the stability of the Xbloc^{Plus} and the allowed tolerances for the placement of the under layer.

In the process of obtaining a stable armour unit, multiple researches have been conducted. The final shape has been further optimised by adding a hole in the middle of the unit and increasing the interlocking capacity. Better interlocking increased the connection between the units and thereby improved the resistance. The hole increased the porosity and thereby reduced the overpressure underneath the armour layer. Which is a result of a difference in water level inside and outside of the breakwater. The increase in stability due to the enlargement of porosity, validated earlier findings that the acting failure mechanism is extraction due to the overpressure.

The stability was expected to be mainly effected by the amount of interlocking. Subsequently, the amount of interlocking is determined by the relative angle between the armour units. For this research physical model tests have been performed to check that hypothesis. Multiple tests have been conducted with different radii of convex and concave shapes in both long shore and cross shore direction. The goal was to find the critical relative angles of each combination of shape and direction. The convex shape in cross shore direction was the only irregularity that caused failure and proved to be critical. The relation between the relative angle and the stability number resulted to be linear, instead of the expected drop of stability at a certain critical value. The relation showed significant spreading, for which tests with small deviations from the design profile seem to form the upper bound and large deviations the lower bound. Thereby indicating that the level of stability is not only determined by the relative angle but also by the deviation from the design profile.

In succession of the tests with specific shapes and directions, more realistic tests have been performed with micro irregularities and S-profiles. The convex shape in cross shore direction proved to be critical for these configurations as well. Furthermore it was found that for large S-profiles, sudden failure could occur without previous indication of loss of interlocking. Further analysis of the divergent failure behaviour of large S-profiles indicated that the arched shape of the profile enabled the lifting of the armour layer. A mechanism similar to the buckling of beams. The pressure inside the breakwater, the drag of the down-rush and the weight of the upper part of the slope, cause the initial distortion of the profile to be enlarged.

The differences between the measurements of the profile before and after the tests, showed that the similar movements occur for smaller S-profiles and the tested convex shapes in cross shore direction. The movement could even be seen in tests that have not

failed. Which implies that the arching mechanism that causes sudden failure for large S-profiles, also induces the loss of interlocking for other convex shapes.

A simplified model of the forces on the convex sections in the profile indicates that the enforcing of the arching mechanism mainly depends on the length and steepness of the downward part of the convex section and the flatness of the upward part of the convex section. These findings correspond with the test results and explain why the stability performance is the highest for the short length scale micro irregularities and lowest for the large scale S-profiles with large deviations from the design profile.

Evaluation of the effect of irregularities is performed with the tolerances of the regular Xbloc, which are also intended to be used on the Xbloc^{Plus}. To prevent differences in stability due to the size of the under layer, the tolerances are expressed in the unit size (D_n) instead of the under layer grain size (D_{n50}). The resulting tolerances are maximum 0.25 D_n for the deviation from the design profile and maximum 0.1 D_n deviation between subsequent measurements along the profile. The profile is measured every 10m of the breakwater and subsequent measurements along the profile have a distance of 0.3 D_n. The requirements are a little more liberal than the tolerances of the regular Xbloc since the tolerances of the largest under layer grain size are taken as a starting point. The test results indicate that the tolerances are sufficiently safe, with potential for more liberal requirements.

Contents

List of Symbols

Symbols and abbreviation used in the study are defined below. Specific combinations of certain symbols and abbreviations are further explained in the text to avoid misinterpretation.

List of Latin Symbols

Symbol	Description	Unit
D_n	Nominal median diameter of armour layer	m
D_{n50}	Nominal median diameter of under layer	m
H_s	Significant wave height obtained from spectral analysis	m
F_n	Normal force	N
F_p	Pressure force	N
F_z	Gravity force	N
$F_{z\perp}$, $F_{z//}$	Perpendicular and parallel components of gravity force respectively	N
K_D	Stability parameter	-
M	Stone or unit mass	kg
N_{comp}	Stability parameter used for comparison	-
N_s	Stability number	-
r, r_r	Radius and hypothetical critical radius respectively	m
W_{50}	Median weight of under layer	kg

List of Greek Symbols

Symbol	Description	Unit
α	Design slope angle	°
α_R	Relative angles between neighbouring units	°
β	Measured slope angle of downward part of convex shape relative to design slope	°
γ	Peak enhancement factor of JONSWAP-spectrum	-
Δ	Relative buoyant density	-
θ	Measured slope angle of upper part of convex shape	°
ρ_s, ρ_c	Stone and rock densities respectively	kg/m^3
σ	Standard deviation	m
ϕ	Measured slope angle of downward part of convex shape	°

List of abbreviations

Abbreviation	Description
AL	Armour layer
ARC	Active Reflection Compensation system of wave maker
DMC	Delta Marine Consultants
PSD	Power spectral density
SWL	Still water level
UL	Under layer

Chapter 1: Introduction

Concrete armour units for breakwaters exist in many different types and new types keep being developed. Generally speaking, two layer systems were most commonly applied in the past, but the single layer systems became more popular since the eighties. Examples of single layer systems that have been commonly used, are the Accropode, Core-loc and Xbloc. The units of these systems are installed in an irregular pattern to maximise the interlocking capacity and thus the stability of the units. The dependence of the stability on an irregular pattern means that the stability has a relatively large spatial variability. A second drawback is that crane drivers often prefer a regular installation method, so it can be seen directly if the unit is installed properly. This has caused the development of breakwater armour units that have a maximum stability performance and are installed in a regular pattern.

Delta Marine Consultants, the in-house engineering firm of BAM Infra, has developed the Xbloc, a concrete armour unit with a regular placement pattern. The Xbloc is an interlocking unit with a high stability performance which is installed in a regular placement grid, but with a random orientation. The regular placement facilitates the placement procedure, but experience with the Xbloc placement showed that the random orientation required much more attention during execution than was expected during the development. This led to the incentive to develop the Xbloc^{Plus}, with both regular placement and orientation. The course of the development has been determined by multiple researches resulting in the shape of the Xbloc^{Plus} as depicted in figure 1.1. More research is still being conducted to obtain knowledge about the behaviour of the new unit in various situations.

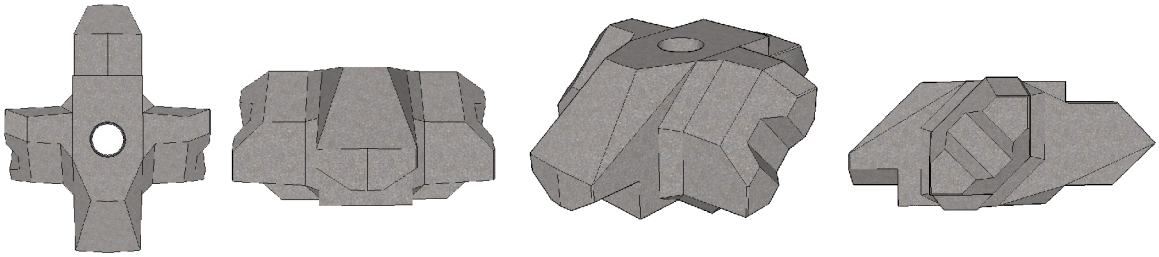

Figure 1.1: Shape of Xbloc^{Plus}, f.l.t.r. top view, front view, isometric view and side view

The incentive for the development of the Xbloc^{Plus} was to facilitate the placement procedure with respect to both ease and time. This means that fast and easy placement is a key aspect for the Xbloc^{Plus} to gain ground in the market. The advantage of easy placement however, is significantly reduced when the tolerances for the under layer become very small in order to maintain the required level of stability. Up to 20 to 30% of the construction time is spent on achieving a smooth under layer [Perrin et al., 2017]. Therefore the sensitivity of the stability for irregularities in the under layer is an important factor for the workability as well as the required construction time.

This has led this research to focus on the influence of the under layer on the stability, resulting in the **main question** of this research:

What is the effect of irregularities in the under layer on the stability number of the Xbloc^{Plus} concrete armour unit?

Which can be translated in the **goals** to:

- *Assess the level of stability of Xbloc^{Plus}*
- *Determine the execution tolerances of the under layer for which the required stability number is maintained*

1.1 Approach

The knowledge on stability is based on semi-empirical formulas and not all phenomena's are fully understood yet. Physical model tests are used to understand and demonstrate the physical processes that can not fully be modelled numerically yet. Each design that is based on analytical calculations is therefore validated by physical modelling. With the development of a new armour unit, much is still unknown and physical modelling tests are the most reliable method to assess the behaviour.

As can be extracted from the goals following from the main research question this research is focussed on two main aspects, the level of stability of the elements itself and the effect of the under layer on this stability. The answer to both of the aspects will be found by first defining and answering the sub-question within these aspects. The required sub-questions and how these will be answered is described in this section.

1.1.1 Level of stability

The behaviour of the unit with regards to its stability must be understood, before conclusions can be formed about the effect of the under layer. The level of stability of the previous versions of the Xbloc^{Plus} have been assessed by Vos [2017] and Rada Mora [2017]. They both stated that the main failure mechanism is the build up of pressure underneath the armour layer, causing units to be pushed out of the armour layer. Vos proposed to increase the porosity and the interlocking capacity to increase the stability. Both of these recommendations have been applied in different versions of the unit. By assessing how the changes have effected the stability, the conclusions of previous research can be validated and the relative importance of the porosity and interlocking can be determined. This results in the first sub-question:

How have the changes between the different versions of the Xbloc^{Plus} affected the level of stability?

1.1.2 Sensitivity to under layer configuration

The tolerances for execution will be based on the sensitivity to irregularities in the under layer configuration. These irregularities will be roughly the size of the armour units or smaller, because it is expected that the tolerances will not allow large deviations from the design profile.

The sensitivity to irregularities in the under layer is assessed with physical model tests in which intentional irregularities are created. Even without the intentional irregularities the configuration of the under layer is not completely smooth due to the natural roughness of the under layer. The effect on the stability is therefore determined by comparing the stability with a reference case without intentional irregularities.

The irregularities of the under layer that are most seen during construction are, overall irregularities due to a high spatial variability of the placed under layer and S-profiles created by the waves after placement. In order to understand the behaviour as a result of the irregularities, the influence of the different shapes and directions must be understood. This results in the second sub-question:

How do irregularities in the under layer with both convex and concave shapes and in cross shore and long shore direction affect the stability of the Xbloc^{Plus}?

For each combination of shape and direction a hypothesis is formed. In he model tests these hypothesis are either validated or refuted. By performing tests around, above, and beneath the hypothetical value, the critical value or trend is to be found.

To arrive at a conclusion on the effect of the intentional irregularities, the exact size of the irregularities must be known. The configuration of the tests must be measured accurately, so the size of the irregularities can be extracted from the measurements. Which gives the third sub-question:

How can the configuration of the under layer be measured sufficiently accurate within the limitations of time and costs?

The goal is to ultimately state tolerances for execution that can be applied in practice. From this follows the fourth sub-question:

What are the practical achievable execution tolerances for the under layer of the Xbloc^{Plus}?

Subsequent to the tests to determine the critical values, tests will be performed with different configurations of overall irregularities and S-profiles. The tests are to evaluate whether the stated critical values are also valid in the more realistic configurations. Subsequently, requirements are set which can be measured in practice and ensure that the critical values are not exceeded.

1.2 Thesis outline

This first chapter introduces the problem statement, the questions that must be answered and how these answers will be found. In chapter 2, preparatory research is done by evaluating the conclusions of previous studies, determining how the accuracy of the tests results could be approved and how the test results might be implied in practice. In the next chapter, chapter 3, the knowledge of the stability of the unit is applied to predict how the stability will be influenced by the irregularities. These hypotheses are implemented in the test program which is stated in chapter 4. Also the model set-up is described in this chapter, which has been based on the preparatory research that was conducted. Chapter 5 describes the processing of the data obtained from the 3D-models of the test

configuration profiles. The results of the processing of the test data is presented in chapter 6, along with the observations of the tests and the test results. Further analysis of the test results is conducted in chapter 7 and the intended tolerances are evaluated. The last chapter describes the concluding answers to the research questions and possibilities for further research are stated in the recommendations.

Chapter 2: Preparatory research

The answer to the main research question is found by first finding the answer to the several sub-questions. Part of these sub-questions is answered by conducting the model tests, but the other part is meant to improve the accuracy of the tests and to formulate tolerances that are applicable in practice.

In this chapter the answer to part of the sub-questions is found. First, the development of the Xbloc^{Plus} is described and the results of previous research is evaluated. This is used to understand how the stability is influenced. Thereafter, the method for data recording is elaborated to obtain the most accurate test results within the limitations of costs and time. Lastly, the current techniques and most applied methods and future possibilities for monitoring of the under layer configuration in practice are discussed.

2.1 Development of Xbloc^{Plus}

The design of breakwaters has been in development since the 18th century and is fully described by Tanimoto and Goda [1992]. The incentive to decrease construction costs and increase the applicability led to increasingly slender concrete amour units that relied on interlocking for stability. First in double layer systems and later on in single layer systems. The systems are placed irregular to increase the interlocking capacity. The result of irregular placement however is also a large spatial variability. A second drawback is that crane drivers often prefer a regular installation method, in which it can be seen directly if the unit is installed properly. On top of this, cases of breakage of the slender armour units on multiple breakwaters proved that the structural integrity was insufficient when the unit size increased.

Armour type	Shape core	Placement grid	Orientation
Dolos	Slender	Irregular	Irregular
Xbloc, Accropod ect.	Robust	Regular	Irregular
Xbloc^{Plus}	Robust	Regular	Regular

Table 2.1: Key changes between types of armour units

The problems caused a new type of armour unit to be developed, with both a robust central section and high interlocking capacity. One of these units was the Xbloc, developped by Delta Marine Consultants, the in-house engineering firm of BAM Infra. Additional to the robust central section and high interlocking capacity, the unit was also placed in a regular placement grid. Only the orientation of the units is still irregular. The regular placement grid decreases the spatial variability and facilitates the placement procedure. The orientation of the units however proved to be more a point of attention than was expected. The problem remained for crane drivers that it is difficult to see directly whether the unit is placed well. Additionally, crane drivers prefer to repeat the same movement instead of using a random orientation. This gave the incentive to develop a new armour unit with not only a regular placement grid, but also a regular orientation. An overview of the key changes between the different types of armour units are also given in table 2.1.

It is possible to place the regular Xbloc with uniform orientation, but this results in an increase in material of 30%. With the regular Xbloc in uniform orientation as starting point, all material that was not contributing to the stability was removed and the shape optimised. Resulting in the first version of the Xbloc^{Plus} in the shape as can be seen in figure 2.1.

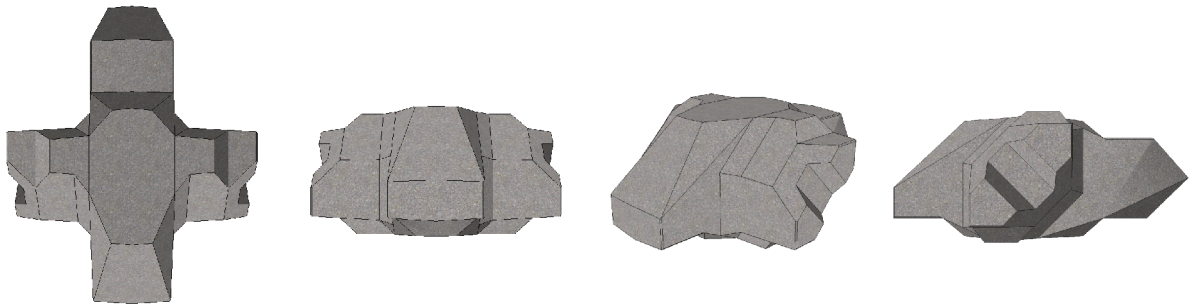

Figure 2.1: Shape of Xbloc^{Plus}, f.l.t.r. top view, front view, isometric view and side view

The stability of the first version of the Xbloc^{Plus} was tested by Vos [2017] during her Master Thesis, with both dry pull-out tests and hydraulic model tests in deep water. One of the conclusion of Vos was that failure occurred as a result of the build up of pressure underneath the armour layer and it was recommended to increase the porosity and the interlocking capacity.

The porosity was increased by adding a hole, as depicted in the left picture of figure 2.2. Resulting in the second version of the unit, which was tested by Rada Mora [2017] and Jiménez Moreno [2017] with hydraulic model tests. The tests were performed in shallow water and with a lower crest height in order to measure the overtopping rates. The tests were performed with both a 1:2 and a 3:4 slope and with differing wave steepness, resulting again in the conclusion that the failure mode is due to overpressure. Between the different slope angles there was no clear difference in moment of failure, possibly because the stability is gained both by interlocking and friction. Furthermore the unit was less stable for the waves with lower steepness.

The interlocking was increased by applying a right angle at the nose and tail of the unit instead of a chamfer. Resulting in a shape as depicted in figure 2.2.

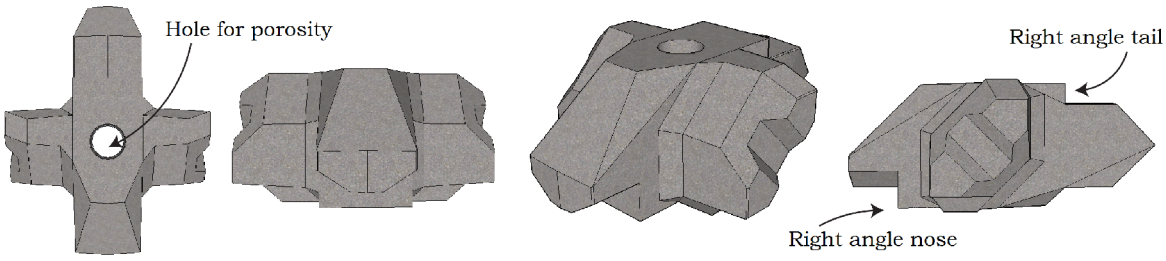

Figure 2.2: Changes of Xbloc^{Plus}, f.l.t.r. top view, front view, isometric view and side view

The difference between the third and the fourth version of the Xbloc^{Plus} is that for the fourth version the hole in the unit has been changed in a funnel shape. This means that the hole is slightly bigger at the bottom of the unit than at the top, which can be seen in figure 2.3. The reason for this change is that is makes it easier to remove the mould during production. Additionally the top hole is slightly larger (increase of 8%) and the

bottom hole is 1,3 times the size of the top hole. Thereby increasing the porosity and decreasing the amount of material.

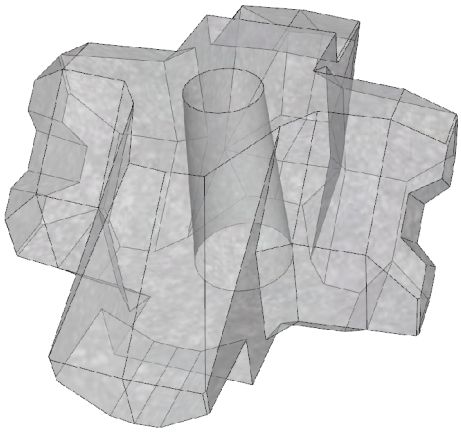

Figure 2.3: Final Xbloc^{Plus}

No further changes have been made, which is why version four is seen as the final version and is referred to when the Xbloc^{Plus} is mentioned.

2.2 Stability

The validation of the conclusions and recommendations of Vos [2017] and Rada Mora [2017] is done by comparing their results with the results of successive versions. With this information the importance of the influence of both permeability and interlocking can be derived and the stability better understood.

2.2.1 Description of stability

The most commonly used description of the armour stability for breakwaters is described by Hudson:

$$M = \frac{\rho_s H_{sc}^3}{K_D \Delta^3 cot\alpha} \tag{2.1}$$

Which can be simplified to:

$$\frac{H_{sc}}{\Delta d} = \sqrt[3]{K_D \ cot\alpha} \tag{2.2}$$

Most breakwaters have a steep slope between 1:1.5 and 3:4 and therefore the Hudsons formula is often further simplified into the stability number. Which gives the relationship between the structure and the wave conditions. To determine the stability number multiple definitions of H and d are possible, the most applied configuration is stated by Van der Meer [1987]:

$$N_s = \frac{H_s}{\Delta D_{n50}} \tag{2.3}$$

Representative wave height

As described in equation 2.3, the wave height is usually described with H_s, which is the significant wave height. This assumes a certain relation between H_s and H_{max}, from which the latter actually has a direct relation to the occurrence of failure according to Angremond et al. [2008].

The different versions of the Xbloc^{Plus} have been tested with different water depths in front of the structure due to the presence of a foreshore. The foreshore changes the ratio between H_s and H_{max} and thereby changes the H_s for which failure occurs. To overcome this difficulty for test comparison, Vos [2017] has determined that the most representative wave height is the $H_{0.1\%}$. To check this statement the test of Rada Mora [2017] have been added to the graph of Vos.

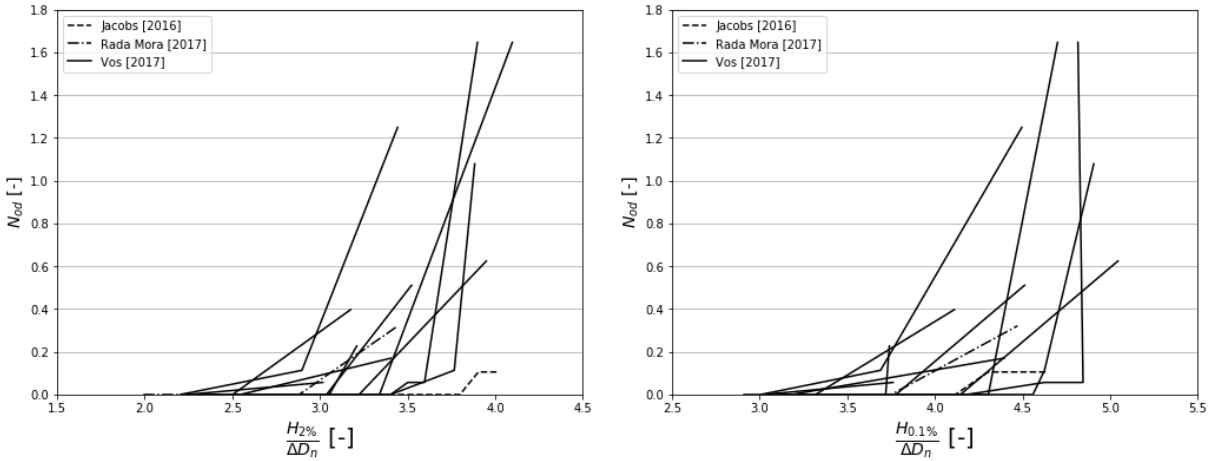

(a) Comparison based on $H_{2\%}$ **(b)** Comparison based $H_{0.1\%}$

Figure 2.4: Comparison of different tests on Xbloc^{Plus} V1

In figure 2.4 it can be seen that the result of Rada Mora is within the spreading for both $H_{2\%}$ and $H_{0.1\%}$. However because the $H_{0.1\%}$ gives the best result when all three studies are taken into account, $H_{0.1\%}$ is still considered to be the best representative wave height for comparison.

This wave height however will only be used when it is necessary due to a difference in water depth in front of the structure. When possible it is still preferred to apply H_s because it is statistically more reliable than the $H_{0.1\%}$, which is largely based on the highest few waves.

Representative diameter

D_n is the most used diameter to describe the size of concrete armour units. It is the median nominal diameter and is in case of concrete armour units represented by the rib of a cube with the same weight as the concrete unit. It is described the following way:

$$D_n = \left(\frac{M}{\rho_c}\right)^{1/3} \tag{2.4}$$

The area one unit protects is not taken into account and therefore part of the effectiveness can not be measured with this parameter. However, because all units that are compared are of the same size this will not influence the results.

Stability parameter
Resulting from the previous paragraphs, the stability parameter that is applied during the comparison of the previous tests is:

$$N_{comp} = \frac{H_{0.1\%}}{\Delta D_n} \tag{2.5}$$

During the rest of the study the standard stability number is used as:

$$N_s = \frac{H_s}{\Delta D_n} \tag{2.6}$$

The design value of the Xbloc^{Plus} is N_s=2.5. This value does not include safety and therefore model test should be stable up to a 25% overload of N_s=3.2. The stability number does not take into account the effects of the wave period, permeability, number of waves and the damage level. These parameters will thus not be considered during the study and kept constant as to not influence the test results.

2.2.2 Governing mechanisms

The previous research done by Vos [2017] and Rada Mora [2017] determined that the structure failed as a result of overpressure underneath the armour layer. The overpressure is a result of a difference in water level inside and outside of the breakwater and is maximum during down rush. Vos recommended to reduce the pressure by increasing the porosity and to reduce the effect of the overpressure by increasing the interlocking.

The conclusions of Vos are validated by comparing the results of Vos to the results of later versions. By comparing the results of version one and two the effect of the increase in porosity is assessed. The effect of interlocking is determined by comparing the stability of version two and three. The complete evaluation can be found in appendix A.

Permeability
The results of the tests with a slope of 3:4 and a wave steepness of 0.04 for version one [Vos, 2017] and version two [Rada Mora, 2017] based on the stability comparison parameter are summarised in table 2.2.

Version	Occurance of rocking	First unit fully displaced	Failure
V1	3.0 - 4.2	3.0 - 4.5	3.7 - 4.9
V2	4.3	> 4.9	> 4.9

Table 2.2: N_{comp} of V1 and V2, with wave steepness 0.04

The table shows that version two performs better than version one on all aspects. This validates the conclusion of Vos that failure occurs due to overpressure and that this can be improved by increasing the permeability.

Interlocking
Another conclusion of Vos is that the stability could be increased by increasing the interlocking. To validate this conclusion and determine the influence of interlocking, the tests of version two and version three have been compared. For version two the results of Rada Mora [2017] are used. The results of version three are obtained from Jacobs [2017], which is an internal report of DMC and has not been published.

Because failure occurred for neither versions with a test set up of a 3:4 slope and a 0.04 wave steepness. The results of a steepness 0.02 and 0.06 are used and summarised in table 2.3. The values used are the values of the stability comparison parameter for which the first unit is displaced. This is because neither rocking nor complete failure occurred for version three.

Version	Steepness 0.02	Steepness 0.06
V2	3.7	4.6
V3	> 4.2	> 4.9

Table 2.3: N_{comp} at moment of first displacements for V2 and V3

The results confirm the conclusions of Vos regarding the effect of interlocking and validates that interlocking indeed has a positive effect on the stability. Because no failure occurred for version three, no qualitative conclusion can be formed over the relative importance of the effects of porosity and interlocking.

2.3 Data recording model tests

The two most important data sets that need to be measured during the tests are the wave heights and the irregularities in the structure geometry. The goal is to choose the methods such that the data is recorded accurately within the limits of costs and time. In this section the choice for measuring methods is made for both data sets and the level of accuracy is assessed.

2.3.1 Waves

The wave heights are measured with gauges, which measure both the incoming and the reflected waves. The signals of the incoming and reflected waves are separated with the method of Mansard and Funke [1980] and by using three gauges. The level of accuracy of the method is influenced by the distance between the gauges. To obtain an accurate result the method should be valid for the range of wave lengths that contains the largest part of the energy of the spectrum. For which range the method is accurate has been studied by Wenneker and Hofland [2014].

The chosen set-up for the gauges in the DMC flume has a distance of 0.4m between the first and the second gauge (X12) and 0.3m between the second and the third gauge (X23), seen from the direction of the incoming waves. For this set-up the range of accuracy covers the largest part of the energy of the spectra, as can be seen in figure 2.5. Only the tail of the spectrum will be analysed less accurate. This part is however of lesser importance because the energy density is low and thus the influence on the total result will be small.

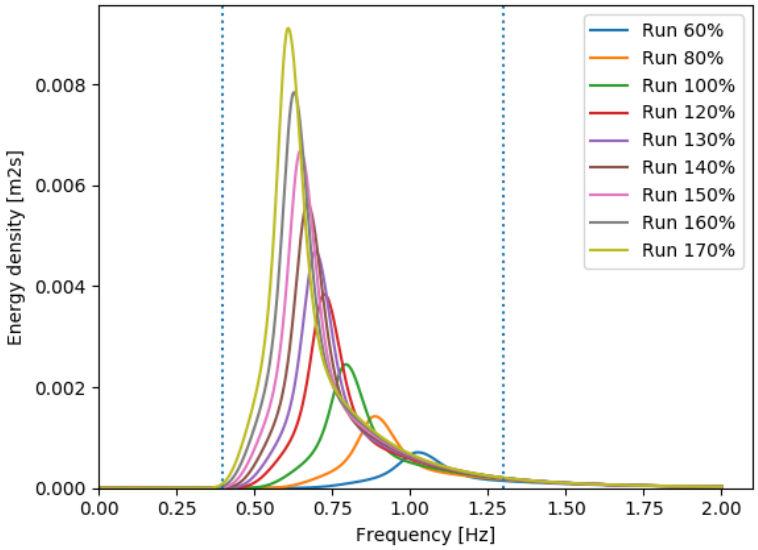

Figure 2.5: Accuracy range (X12=0.3, X23=0.4)

2.3.2 Geometry

The measurement technique for the geometry that performs best in the test set-up is determined with tests of multiple techniques. The considered methods are laser measurements, stereo photography with Python, Autodesk Recap and a semi-spherical foot staff. The techniques are evaluated in terms of costs, execution time and usefulness. The amount of usefulness is based on the completeness of the data and the level of accuracy. The effect of the under layer on the stability of the armour unit is very local and the configuration of the under layer will be different for each unit. Therefore it is important to know the local parameters in order to determine the effect adequately. The results of the evaluation are summarised in table 2.4 and the end results of all three techniques are visualised in figure 2.6.

	Costs	Time	Completeness	Accuracy
Laser	- -	- -	-	+ +
Stereo photography with Python	+ +	+	- -	- -
Autodesk Recap	+	-	+ +	+
Semi-spherical foot staff	+ +	- -	- -	- -

Table 2.4: Pro's and con's of measurement techniques

The laser measurements scores low in costs and time because accurate laser devices are very expensive and because the measurements require a lot of time if the whole slope is considered. Each measurement has a high accuracy but only over certain trajectory of the slope, therefore scoring low at completeness.

Stereo photography can be applied with regular cameras and open source software and is therefore relatively cheap. After initial calibration each measurement only takes two pictures and is thus very time efficient. However the resulting point cloud has a lot of large gaps and noise. Which is why the method scores low in both completeness and accuracy.

The use of Autodesk Recap requires a license and therefore costs money. However, the costs for the license are low and further operations on the model are done with the open source program Python. For each model up to 40 or 60 pictures have to be taken from all sides, this takes up to 15 minutes per model. A drawback is that the wave flume needs to be empty before the picture can be taken. Therefore this method takes quite some time and the technique does not score well on this aspect. The result of the technique is a 3D model of the complete slope with an accuracy of a few millimeters. Which is why the score is high on completeness and accuracy.

The semi-spherical foot staff is the most common applied measurement method in practice. It is simulated with a frame over the flume that places a semi-sphere of a certain diameter at five locations over the width. Moving the frame and the measurements are done by hand, making the method time consuming and inaccurate.

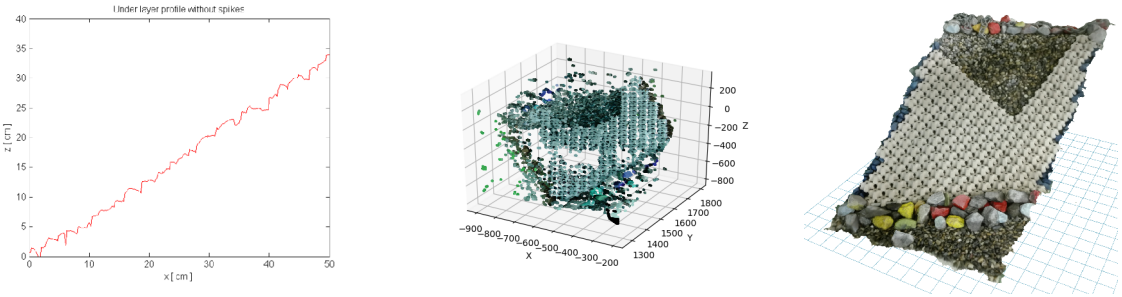

(a) Laser measurements **(b)** 3D point cloud Python **(c)** 3D model Recap

Figure 2.6: Results different measurement techniques

The method with Autodesk Recap is considered to be the most useful method for this study. It provides the highest completeness and accuracy relative to the amount of costs and time. With ReCap it is possible to measure the full slope with an accuracy of ± 3mm. Additionally it is possible to use a free student license for the Recap program, making it very cost effective. The full descriptions of the performed tests and results can be found in appendix C.

2.4 Surveying in practice

After placement the contractor is required to measure both the under and armour layer. With the measurements it is checked whether the tolerances for placement have been exceeded. In practice not the full construction area will be measured and also the survey measurements will contain errors. Therefore there has to be an additional safety margin on the tolerances that takes these factors into account. How large the errors are depends on the precision of the surveying system and the accuracy of execution of the method.

Precision is often defined as a measure for the random errors in observations. The higher the precision, the smaller the dispersion of the random errors is. In breakwater surveys the dispersion of the random errors is often expressed in terms of twice the standard deviation (2σ) or the 95% confidence level. In practical sense it means that it is assumed that 95% of the surface falls within the range of $\pm 2\sigma$ from the averaged profile [SBRCURnet, 2014], as is illustrated in figure 2.7.

The random error is expressed as the deviation of the surface from de average constructed surface. Besides the random error there is also a systematic error, which is

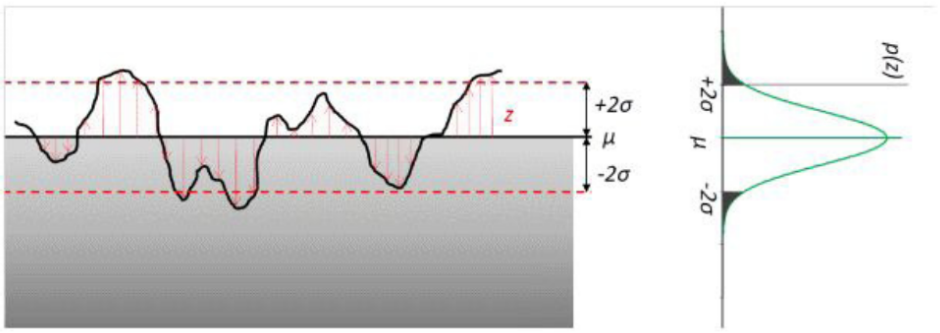

Figure 2.7: Confidence level of surface fluctuations [SBRCURnet, 2014].

defined as the difference between the average constructed surface and the designed profile. The tolerance is the allowed difference between the constructed surface and the designed profile, including measurement inaccuracies [SBRCURnet, 2014].

2.4.1 Established methods

There are multiple methods that are applied in practice. It is possible to measure the full breakwater with laser or echo-scope measurement tools, but it is not usual to measure the full construction area. Most common is to measure the cross-sectional profile at certain intervals.

The measurements of the cross-section are often done either with a semi-spherical foot staff or with the bucket of the excavator using a crane monitoring system (CMS). The precision of these methods have been stated in the CUR guideline for Construction and Survey Accuracies for the execution of rockworks [SBRCURnet, 2014].

An overview of these results is given in table 2.5, here it can be seen that the CMS has a very limited surveying precision. Since this is still the most commonly applied method, this precision will be critical for the margin on the tolerances.

Survey system	20-35mm		5-70kg		150-800kg		1-10T	
	Systematic deviation [m]	Precision [m]	Systematic deviation [m]	Precision [m]	Systematic deviation [m]	Precision [m]	Systematic deviation [m]	Precision [m]
Foot staff with plate	0.07	0.08	0.12	0.09	0.14	0.15	-	-
Excavator bucket (CMS)	0.17	0.13	0.14	0.15	0.34	0.27	0.32	0.40
Single beam echo-scope	0.08	0.08	0.08	0.11	0.09	0.18	0.06	0.26
Multi beam echo-scope	-0.03	0.06	-0.11	0.09	-0.19	0.15	-0.18	0.23

Table 2.5: Part of results from test-pit Maasvlakte 2 [SBRCURnet, 2014]

The requirements for the monitoring of the under layer of the regular Xbloc are described in the specifications for application of Xbloc by van der Zwicht [2015]. Here it

is stated that at every 10m of breakwater, the cross sectional profile should be measured with a minimal distance between the measurement points of one D_{n50} of the under layer.

The tolerances for the Xbloc are also described as a function of the size of the under layer. The maximum allowed deviation from the design profile is 0.5 D_{n50}. With an additional requirement, that maximum difference between two subsequent measurements over the cross section is maximum 0.3 D_{n50}. Both distances are measured perpendicular to the design profile.

DMC intends to apply the same monitoring requirements for the execution of Xbloc^{Plus}. The outcome of the model tests will therefore be compared with the requirements of the regular Xbloc.

2.4.2 Future possibilities

The tolerances for the Xbloc are expressed in deviations perpendicular to the design profile, with certain margins that take spatial variance and measurement errors into account. Resulting in very conservative tolerances and thereby complicating the construction process. If full area measurements become more commonly used in the future, this gives possibilities for new definitions of the tolerances which can be more precise.

A possibility for a new way of defining tolerances is by means of the Power Spectral Density (PSD) of the surface elevation. According to Jacobs et al. [2017] the PSD is a method to describe the surface topography statistically. It allows the identification of the spatial frequencies by displaying just the power (and not the phase) of autocorrelating the Fourier transform to the measured signal. Due to this process the PDS is largely unbiased by chosen scan size or pixel resolution, which makes it widely applicable. An example of a PSD is given in figure 2.8.

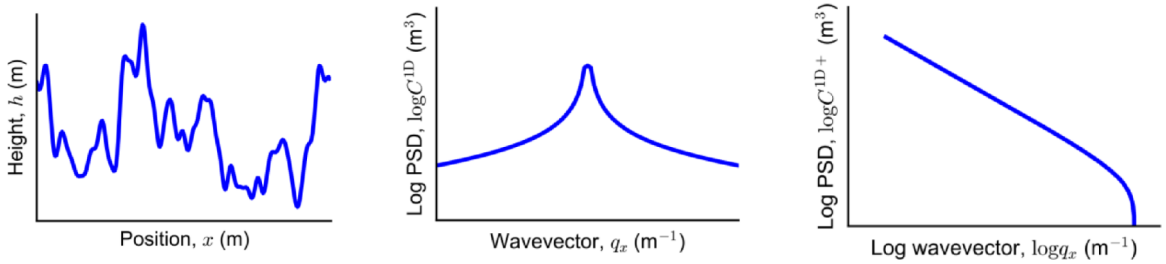

(a) Line scan **(b)** 1D PSD **(c)** One-sided 1D PSD

Figure 2.8: Example of Power Spectral Density [Jacobs et al., 2017]

In the study of Jacobs et al. [2017] from which the figure has been extracted the PSD method is applied to obtain the surface roughness of materials. The spatial frequencies of the material are extracted from the line scan (2.8a) and can be expressed in various PDS's. The 1D PSD (2.8b) is symmetrical at the vertical cross-section through the origin. Because the measured height is a real valued function and the PSD operates with complex numbers. Therefore the PDS is most commonly indicated by only showing one side (2.8c).

The benefit of this method is that not only the deviation of the surface is taken into account, but also the length scale for which de deviation occurs. However, because the PSD is a statistical description which excludes the phases, the distribution of the deviation over the area is not taken into account. For application in future use it will

have to be tested whether there is a good correlation between the PSD of the under layer and the stability of the armour layer.

Chapter 3: Hypotheses

The goal of the model tests is to obtain the critical values of the relative angles between neighbouring armour units, for which the level of stability is significantly reduced. It is expected that this will occur due to the rotation of the armour units relative to its neighbours. When the rotation becomes too large, the interlocking is no longer sufficient or the placement grid can no longer be maintained. The rotation between neighbouring units is called the relative angle and is expected to be the parameter of interest. To relate the critical relative angle to the configuration of the under layer, it is translated into a critical radius of the shape of the under layer.

The influence of the different shapes and directions is assessed, before more realistic configurations are considered. In order to choose the configurations of the test profiles of the series, an estimation of the critical relative angles is made.

In this chapter the hypotheses are stated for the critical values for both cross shore and long shore direction, for convex and concave shapes. The test plan of the research will be based on the stated hypothetical critical values.

3.1 Cross shore direction

In cross shore direction the configuration of the under layer can be either convex or concave, an example with a large length scale is visualised in figure 3.1.

(a) Convex configuration **(b)** Concave configuration

Figure 3.1: Slope configurations in cross shore direction

3.1.1 Convex

For the convex configuration it is expected that the stability is decreased when the angle of the upper unit is such that its nose is no longer interlocked behind the wings of the two lower units. This occurs when the relative angle between the upper and the two lower units is approximately 25 degrees, as is visualised in figure 3.2. With a distance between two units along the slope of 1.04 times the D_n, this occurs for an irregularity with a radius of 0.30 times the D_n.

The failure behaviour noted by Vos [2017] and Rada Mora [2017] was that extraction occurred due to a rotation of the unit with the nose upward. With this irregularity the unit is already rotated such, therefore this irregularity is expected to have a large influence on the stability.

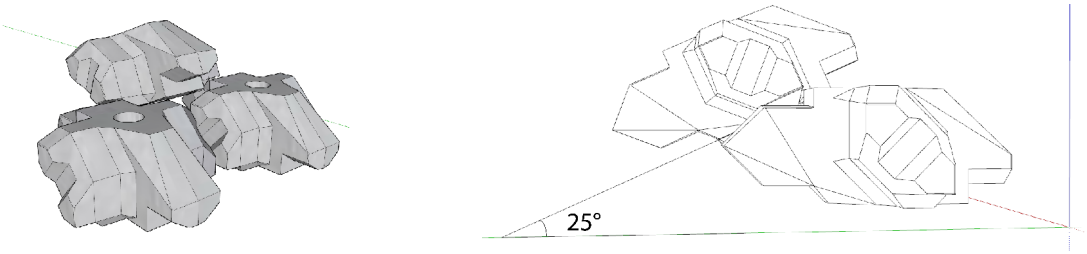

(a) Loss of interlocking **(b)** Relative angle

Figure 3.2: Theoretical critical angle for convex configuration

The expected critical radius of the irregularity is much smaller than the length of the slope. Therefore a location of the irregularity must be chosen along the length of the profile. According to Rada Mora [2017] the risk of failure is the highest just above the run-down water line, which is expected to be around 1.5 times H_s underneath the still waterline. It is chosen to place the top of the irregularity at one H_s underneath the still waterline. Causing the largest relative angles to be at the most risk prone area and this is also the expected location for the convex section of the S-profile.

3.1.2 Concave

For the concave configuration it is expected that the stability is decreased when the angle of the upper unit is such that its wings are no longer interlocked behind the two lower units. This occurs when the relative angle between the upper and the two lower units is approximately 15 degrees, as is visualised in figure 3.3. With a distance between two units along the slope of 1.04 times the D_n, this occurs for an irregularity with a radius of 0.44 times the D_n.

The armour layer fails due to extraction after rotation. With this irregularity the rotation is less likely to occur because it is already rotated in the other direction. The wings are not supported and could cause problems during placement. Due to lower quality of placement the stability could be reduced, but the effect is expected to be minor.

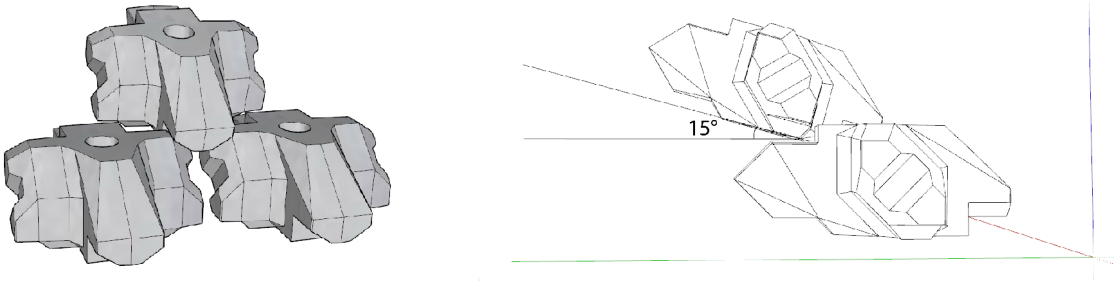

(a) Loss of interlocking **(b)** Relative angle

Figure 3.3: Theoretical maximum angle for concave configuration

The expected critical radius of the irregularity is as well much smaller than the length of the slope. As explained above the risk of failure is higher underneath the still water level, but the concave section of the S-profile is expected to be above or around water level. Therefore tests will be performed with locations both around and underneath the still water level.

3.2 Long shore direction

In long shore direction the configuration of the under layer can as well be either convex or concave, an example with a large length scale is visualised in figure 3.4.

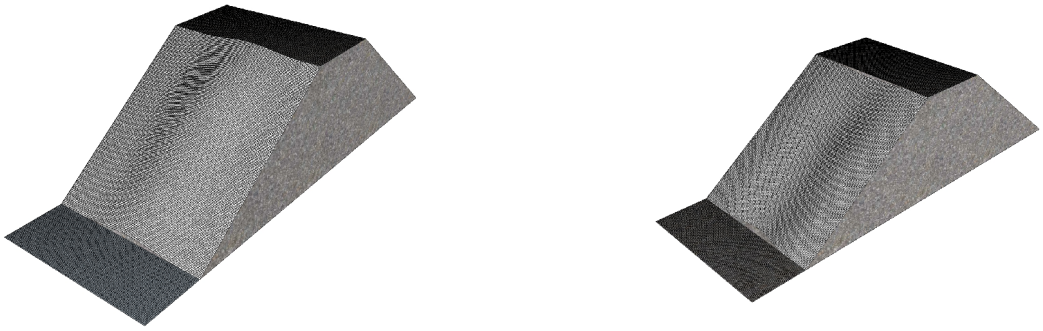

(a) Convex configuration **(b)** Concave configuration

Figure 3.4: Slope configurations in long shore direction

3.2.1 Convex

For the convex configuration it is expected that the stability is decreased when the angle between the two lower units is such that the wings of the upper unit are no longer supported by the tails of the two lower units. This occurs when the relative angle between the two lower units is approximately 40 degrees, as in visualised in figure 3.5. With a distance between two units of 1.8 times the D_n, this occurs for an irregularity with a radius of 0.30 times D_n.

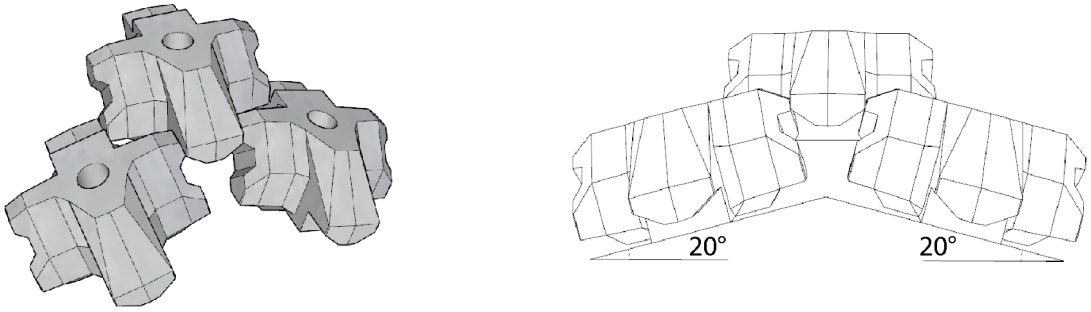

(a) Loss of interlocking **(b)** Relative angle

Figure 3.5: Theoretical maximum angle for convex configuration

It is expected that this combination of shape and direction is less critical because the unsupported unit will still be locked behind the two units that should support it. Additionally it locally increases the porosity of the armour layer which should have a positive effect on the stability. However, it will cause the placement grid to be disturbed and this can decrease the stability higher up the slope.

3.2.2 Concave

For the concave configuration it is expected that the stability is decreased when the angle between the lower two units is such, that there is not enough space to support an other unit next to the upper unit. This happens when the wings of the upper unit occupy more than half of the area of the supporting tails. The boundary for this is when the relative angle between the two lower units is approximately 20 degrees, as is visualised in figure 3.6. With a distance between two units of 1.8 times the D_n, this occurs for an irregularity with a radius of 0.60 times D_n.

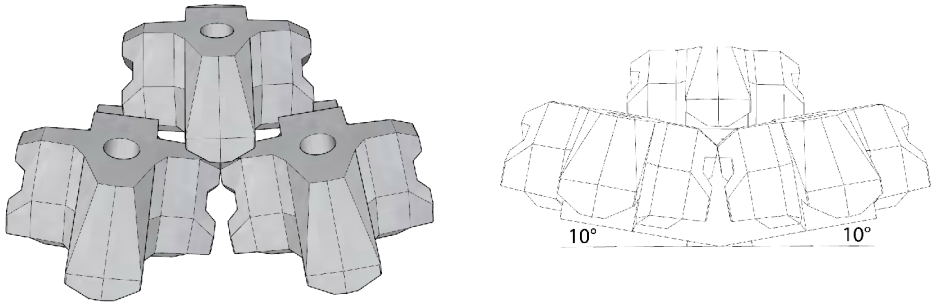

(a) Not enough space **(b)** Relative angle

Figure 3.6: Theoretical maximum angle for concave configuration

This type of irregularity is problematic for the placement, because it reduces the space at the location of the unit. A reduction in placement quality will reduce the stability. It could also effect the stability because it will decrease the porosity of the armour layer, which has a negative effect on the stability. However, because the units will still be sufficiently interlocked the effect is expected to be minor.

3.3 Common irregularities

The two types of irregularities that have been most seen by the employees of BAM are overall small scale irregularities, also referred to as micro irregularities, and S-profiles. The hypothetical influence of the above mentioned expected critical relative angels will be discussed in this section.

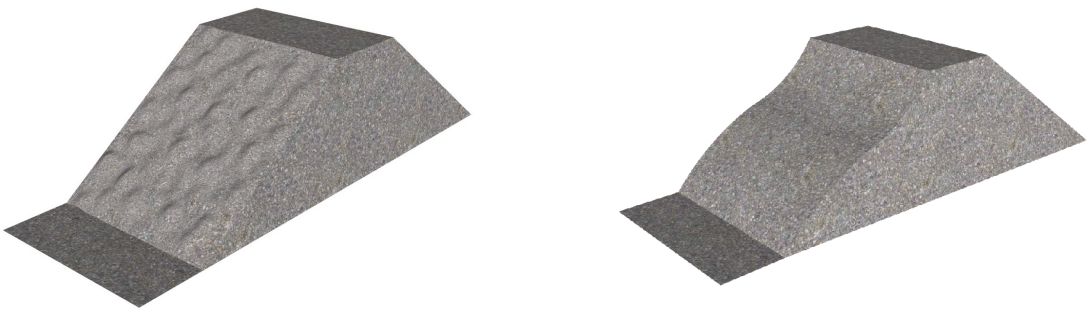

(a) Impression micro irregularities **(b)** Impression S-profile

Figure 3.7: Common irregularities

3.3.1 Micro irregularities

The micro irregularities can occur in all directions and with both convex and concave shapes, which is depicted in figure 3.7a. Due to the small length scale it only takes a small deviation from the design profile to cause a large relative angle. Therefore it is expected that this type of irregularities is critical for the determination of the tolerances.

The small length scale irregularities are always present since a rubble mound slope has a natural roughness. The hypothesis is that the critical relative angles stated in the previous section, are also valid for the irregularities with small length scale. Due to the combination of multiple directions and shapes the critical relative angle of one direction could be influenced by an irregularity in the other direction. This influence works both positively and negatively and the hypothetical critical relative angle is still expected to be the average value.

3.3.2 S-profiles

S-profiles have both a convex and a concave section in cross shore direction, as can be seen in figure 3.7b. Because the profiles are shaped by the waves, large deviations in long shore direction are not expected. The critical values stated for the convex and concave shapes in cross shore direction are expected to be valid for the S-profiles.

3.4 Conclusion

The hypothesis is that the stability is influenced by the relative angles between the neighbouring units. This depends on the underlying change of slope of the under layer. In table 3.1 all the hypothetical critical values are summarised, these values are expected to be valid for both large and small length scales.

Direction	Shape configuration	Relative angle	Critical radius
Cross shore	Convex	25°	0.30 D_n
	Concave	15°	0.44 D_n
Long shore	Convex	40°	0.30 D_n
	Concave	20°	0.60 D_n

Table 3.1: Expected critical values

It is assumed that the placement is accurate and the placement grid is maintained as well as possible. To preserve accuracy of placement the placement is expected to take more time when the irregularities are more pronounced. Error in placement is expected to decrease the stability and effect the result.

Chapter 4: Model set-up

The influence of irregularities on the stability of the Xbloc^{Plus} is determined by performing physical model tests. The tests are subdivided into seven series, each series is testing a specific type of irregularity and consists out of multiple tests. All tests are conducted with different sizes and/or locations of the irregularity. In total 28 tests have been performed, which consisted out of a total of 193 runs of increasing wave heights. An overview of all performed tests and runs within each series is given in appendix D.

4.1 Structure geometry

The aspects of the geometry are chosen such that they either resemble the situation most common in practice or are more conservative with regards to the stability of the armour units. Only the toe and the crest of the structure are more stable than would be applied in practice. The crest and toe are outside the scope of this study and build with a higher stability to prevent influence on the test results. The cross section of the structure is depicted in figure 4.1.

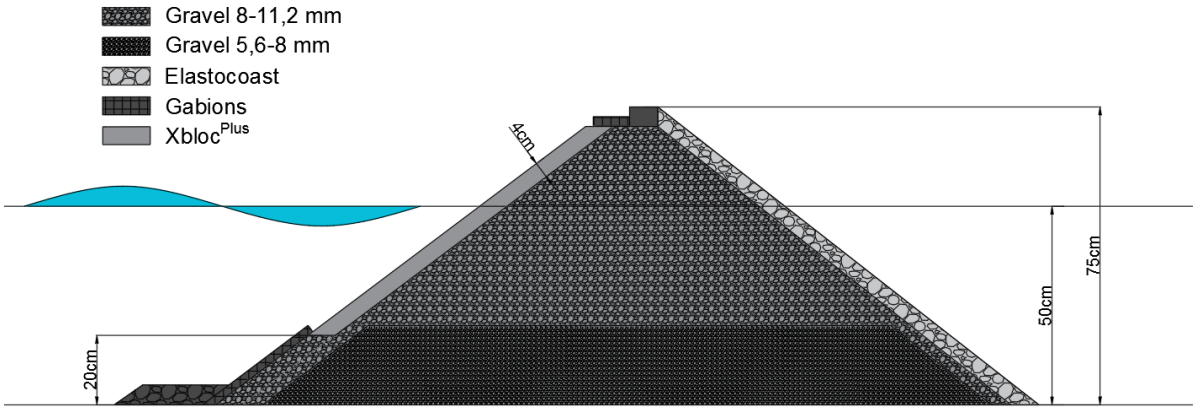

Figure 4.1: Cross section of the model structure geometry

The Xbloc^{Plus} is designed for a slope between 3:4 and 2:3. The tests are performed with a slope of 3:4 because a steep slope is expected to be more conservative with regards to the stability [Angremond et al., 2008]. The relative freeboard has both a positive and a negative relation to the stability. A large freeboard increases the mass benefiting the stability of the units in the critical region [Vos, 2017]. A small freeboard however results in more overtopping and thus in lower wave loads on the armour units. As a compromise between the two influences, the freeboard was chosen at 2.5 times the $H_{s,design}$. Which is 1.5 times the H_s of the run with the maximum tested wave height.

It is chosen to make the under layer and core of the same grading to prevent deviations in thickness of the under layer, due to the irregularities, to influence the result. This was possible because there is no real life prototype, and thus multiple gradings are possible for the core within the scaling boundaries according to Burcharth et al. [1999]. Same as in the study of Rada Mora [2017] the core is chosen to be of the standard grading

of 8-11.6mm. According to Burcharth this grading is conservative because it does not maintain turbulent flow. The W_{50} of the under layer is normally chosen as 1/10 up to 1/20 of the weight of the armour unit. In this case the chosen core grading is at the 1/20 boundary and this makes it possible to choose the same grading for the core and under layer. The under layer grading is relatively small which facilitates the placement of the armour layer but reduces the permeability of the under layer. Because both the core and the under layer have relatively low permeability, this causes a higher part of the wave energy to be reflected and therefore it is expected to give a conservative result for the stability.

To save time and prevent the necessity to drain all the water out of the flume between tests, the downward 20cm of the test slope is covered with gabions instead of Xbloc^{Plus}. The toe of the structure is not of interest and the influence of the waves may be assumed to be insignificant at more than two times the H_s below still water level. It is therefore not expected that this will influence the results. At the flume facility there was not enough material of the 8-11,6mm grading available. The downward 20cm of the breakwater is therefore made of the smaller 5,6-8mm grading. This is not expected to influence the results for the same reason as mentioned above.

4.2 Test approach

Each test starts with a low significant wave height equal to N_s=1.5, which is 60% of the design stability number. After each run the wave height is increased stepwise until failure occurs or the final run is reached. The wave steepness is calculated as the ratio between the local significant wave height and the deep water wave length, it is therefore a fictitious wave steepness. The fictitious wave steepness is used because the correlation between the wave height and period is high during storm conditions, resulting in a constant fictitious wave steepness. The wave steepness is chosen to remain constant at S_{0p}=0.04. Which is a common used wave steepness to represent wind waves in design storms [Angremond et al., 2008].

The model tests are conducted in the wave flume of Delta Marine Consultants in Utrecht. This flume is 60cm wide, 100cm high and has a length of 25m. All tests are performed with a constant water depth of 50cm and without a foreshore to prevent breaking of the waves before the structure is reached. The maximum applied wave height has a significant wave height of approximately 16cm. The waves are irregular based on a JONSWAP-spectrum with γ=3.3 and each run consists out of 1000 waves. The flume has a piston-type wave board with an Active Reflection Compensation system, which damps out the reflected waves.

4.3 Test program

The test program can be distinguished in three separate parts. The first part consists of series 1, and has the goal to determine the stability without any intentional irregularities. It is the reference case to which the other series can be compared to and the effect of the irregularities is determined with. The second part covers series 2 up to 5, which are the series with macro irregularities in different directions and shapes. The goal of this part of the test program is to either validate or counter the hypothetical critical values that have been stated in the previous chapter. The third and final part of the test program is to

simulate two kind of irregularities that are most common in practice. These irregularities are tested in series 6 and 7. The definitions and hierarchy of the test program components is explained in table 4.1.

	Component	Description
1	Test program	Total program, exists out of three separate parts
2	Part	Parts of program with each its own goal, exists out of one or multiple test series
3	Series	Series of tests with each its own type of irregularity, contains one or multiple tests
4	Test	Tests of a certain under layer configuration, contains multiple runs of increasing wave heights
5	Run	Application of 1000 waves with a certain significant wave height

Table 4.1: Hierarchy and definitions of test program components

For part II, each test within the series has a different size and/or location of the specific type of irregularity. An overview of all the different series and their specific irregularities is given in table 4.2. The target values for the size and location of the irregularities is also given in this table. The target value for the radius of the irregularity is given relative to the hypothetical critical radius. The maximum deviation from the design profile is given as Δz. The location of the irregularity along the profile is given relative to the Still Water Level, indicated by z_{SWL}. Both values are given relative to the unit size (D_n). Each test consists out of multiple runs for which the wave height is increased stepwise with either 10 or 20%.

		Irregularity type			Target size and location		
Part	Series	Direction	Shape	Test	$\frac{r}{r_{hyp}}$	$\frac{\Delta z}{D_n}$	$\frac{z_{SWL}}{D_n}$
I	1	None	Straight slope	1	n.a.	n.a.	n.a.
II	2	Cross shore	Convex	1	1.0	1.0	-3.4
			(figure 3.1a)	2	1.2	1.0	-3.4
				3	0.8	1.0	-3.4
				4	1.0	0.8	-3.4
				5	1.0	1.0	0.0
	3	Cross shore	Concave	1	1.0	1.0	0.0
			(figure 3.1b)	2	0.8	1.0	0.0
				3	1.0	1.0	-3.4
				4	1.0	1.0	-1.7
	4	Long shore	Convex	1	1.0	1.0	n.a.
			(figure 3.4a)	2	1.2	1.0	n.a.
	5	Long shore	Concave	1	1.0	1.0	n.a.
			(figure 3.4b)	2	1.0	1.0	n.a.
				3	0.8	1.0	n.a.

Table 4.2: Overview test configurations, part I and II

In part III the irregularities are present over the full length and width of the test section. In series 6 the irregularities are randomly applied, therefore the sizes are not specific but an estimated value. The values are given in table 4.3. The S-profile configurations are made by applying a certain H_s to the under layer. Multiple tests have been done with different wave height and durations of application, an overview of the differences is given in table 4.4.

		Irregularity type			Target size	
					Below SWL	Above SWL
Part	Series	Direction	Shape	Test	$\frac{\Delta z}{D_n}$	$\frac{\Delta z}{D_n}$
III	6	All	Over full slope	1	1.0	1.0
			(figure 3.7a)	2	1.1	1.1
				3	1.2	1.2
				4	1.2	1.0
				5	0.8	0.8

Table 4.3: Overview test configurations, part III series 6

		Irregularity type			Applied waves	
					$\frac{H_s}{\Delta D_n}$	Duration
Part	Series	Direction	Shape	Test		[min]
III	7	Cross shore	S-profiles	1	1.5	≈ 7
			(figure 3.7b)	2	1.5	≈ 2
				3	1.5	≈ 5
				4	1.0	≈ 10
				5	1.3	≈ 10
				6	1.4	≈ 10

Table 4.4: Overview of test configurations, part III series 7

The number of tests within each series was not known beforehand and is based on the output of the previous tests. The goal is to obtain the stability parameter for different sizes of the irregularities, so a critical value can be determined. If failure occurs during an early run, the next test is performed with an irregularity of a smaller size. Vice versa, the irregularity is increased when failure occurs at high wave heights or not at all. The irregularity is not increased beyond the boundaries of what would be realistic in practice. In that case the test program is continued with the next series. The measured configurations and wave heights of each test run are presented in chapter 6.

4.4 Methodology

Each test is performed according to the following methodology:

1. Apply required shape to under layer:
   - Cross shore direction: shape under layer with the trowel based on the lines drawn on both sides of the flume.
   - Long shore direction: shape under layer by applying a wooden template along the length of the slope.
   - S-profiles: fill flume and apply waves to the under layer, afterwards empty flume again.
   - Overall micro irregularities: rearrange under layer at random locations and with differing severities.

   In case of macro irregularities, flatten the profile with a trowel to minimise the effects of the micro irregularities. Make sure that there is enough space for the first row behind the gabion and prepare a flat surface for placement of the first row.
2. Make 40-60 pictures from all possible angles for the creation of the ReCap-model of the under layer. Make sure the targets are captured as well as possible.
3. Place the armour layer without disturbing the under layer.
4. Make 40-60 pictures from all possible angles for the creation of the ReCap-model of the armour layer. Make sure the targets are captured as well as possible.
5. Place chains on top of the bottom row of Xbloc^{Plus} and along the sides of the flume.
6. Set cameras at fixed positions above the structure and to the side of the structure, fill the flume and calibrate the wave gauges.
7. Perform runs with stepwise increase of the wave height. For each run, make a photograph from above and from the side. During the run, measure the wave heights, make a video recording from above and from the side and write down observations. After each run, stop the recordings and make photographs from above and from the side when the water surface has settled down.
8. Stop the test when one or multiple units have been extracted at the end of a run. When necessary, interrupt the run when progressive failure occurs during a run. In the case that no failure occurs the test is stopped after the final run.
9. Empty the flume until minimal 5cm below the first row.
10. Make 40-60 pictures from all possible angles for the creation of the ReCap-model of the armour layer. Make sure the targets are captured as well as possible.
11. Remove the armour layer carefully with little disturbance as possible to the under layer.
12. Make 40-60 pictures from all possible angles for the creation of the ReCap-model of the under layer. Make sure the targets are captured as well as possible.
13. Repeat the sequence for the next test.

Chapter 5: Data processing ReCap models

To verify the hypotheses and determine the tolerances, the relative angles of the test configurations are calculated. The configurations of the under and armour layer of each test are measured with a 3D-model, made with Autodesk Recap. The data is extracted from the 3D-point cloud and imported into Python for further processing. This chapter describes the sequence of the full procedure, followed by an indication of the accuracy of the required data.

5.1 Procedure

Each test configuration has been measured both at the beginning of the test and after the runs of increasing wave heights were performed. At these moments the configuration of both the under layer and the armour layer are measured, unless the damage after the test runs was too severe for the model to be meaningful. At the beginning of the test two sets of 40-60 photos were made, from which three models were created. One model of each photo set and one model of (a random selection of) the combined photo sets. The multiple ReCap models enable to estimate the accuracy and averaging over the models reduces the random errors. At the end of the tests only one set of photos was taken. This was done to save time and because this study is focussed on the configuration at construction and thus at the start of the tests. Therefore, the end configuration is considered to be of less importance. The procedure that is followed for each set of ReCap models is explained with the data of Test 1 from Series 2 as example.

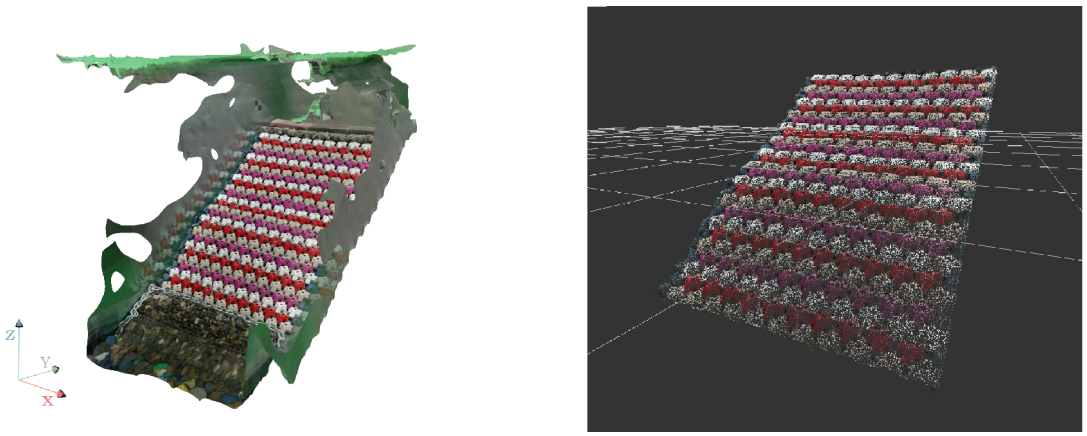

(a) ReCap Photo 3D-mesh **(b)** ReCap point cloud

Figure 5.1: Example output of Autodesk Recap programs

The ReCap program calculates a 3D-mesh and a point cloud from the set of photos, both are shown in figure 5.1. The point clouds have 41000 to 45000 points in the region of interest. The test section of the point cloud is extracted as a PTS-file, containing of each point the x,y,z-coordinates and the RGB color values. Being the z-axis upward from the

bottom of the flume, the y-axis in the length of the flume and the x-axis over the width of the flume, see figure 5.1a. The origin of the axial system is at the left side of the toe of the structure. All the models are fixed in the same axial system by four targets. Two on each side of the wave flume, one at the level of the crest and one just above the first row of armour units. Each target of each model is selected manually. To reduce errors in the target registration the zoom function of the program was used and each target has been selected on at least eight pictures.

The PTS-file is loaded into Python and restructured into a regular x,y-grid for further processing, with a grid spacing of 0.00025m. With the x,y-coordinates and the color values a top view is compiled from which the unit locations are determined with MatchTemplate by OpenCV [Docs.opencv.org, n.d.]. The unit locations are checked visually during processing, in both the compiled top view and the plot of the z-coordinates relative to the design profile, shown as example in figure 5.2.

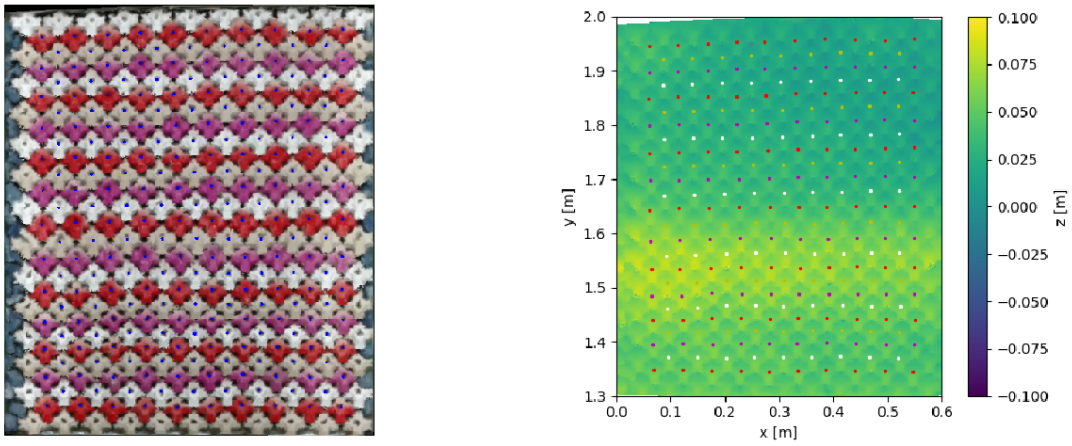

(a) Compiled top view with unit locations **(b)** Plot 3D-coordinates with unit locations

Figure 5.2: Check of unit locations

The orientation of the top of the armour unit is determined in x and y direction at the unit locations and recalculated into angles. To prevent small measurement errors from affecting the result, the slope is averaged over an area of 25mm^2, in the middle of the top of the armour unit. This area was chosen as a compromise between cancelling out model noise and preventing errors due to inaccuracy of the unit locations.

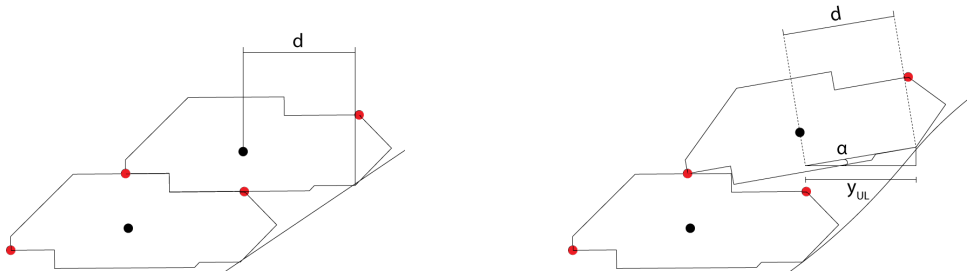

(a) Distance between found location and contact point with the under layer **(b)** Angle of unit orientation taken into account

Figure 5.3: Calculating corresponding location under layer

For the angles of the under layer the unit locations are converted to the corresponding location on the under layer. The corresponding location is taken perpendicular to the

design profile, as is depicted in figure 5.3. To prevent single grains from affecting the slope of the profile, the model is smoothed with a Gaussian filter with a standard deviation equal to the D_{n50} of the under layer. The result of smoothing is depicted in figure 5.4, in which indeed can be seen that the individual grains are smoothed out while the larger profile deviations are maintained.

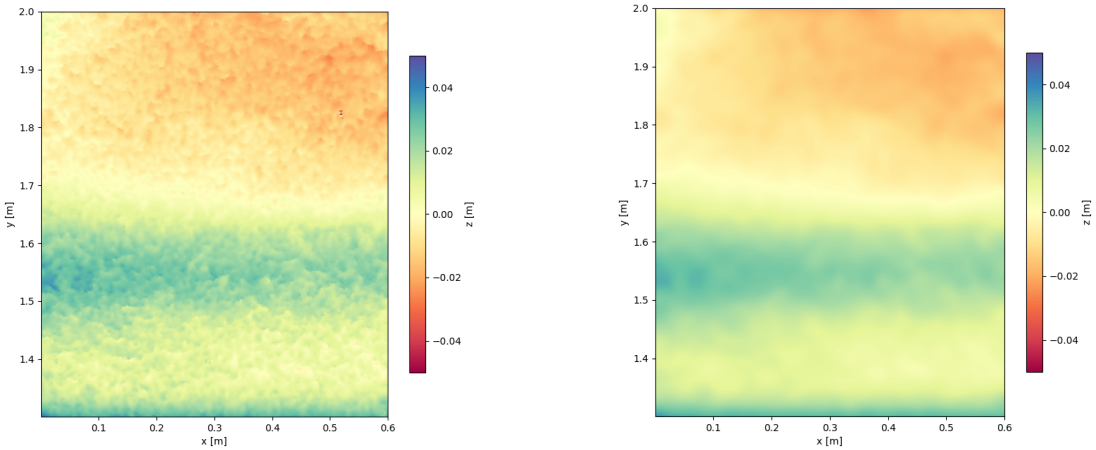

(a) Deviation from design profile

(b) Result after smoothing

Figure 5.4: Effect of smoothing under layer

Further reduction of measurement errors is accomplished by averaging the angles of each location over the three models that have been made at the same moment. After averaging, the relative angle (α_R) is calculated.

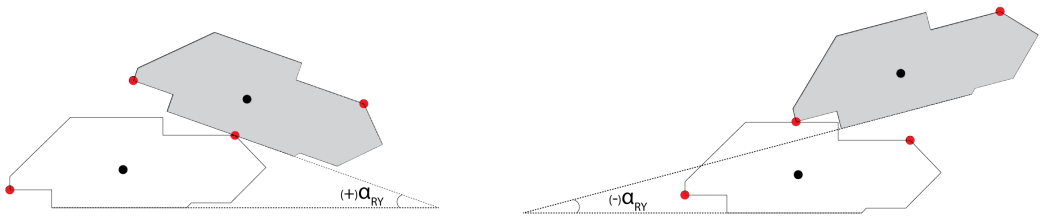

(a) Positive relative angle in y-direction (cross shore)

(b) Negative relative angle in y-direction (cross shore)

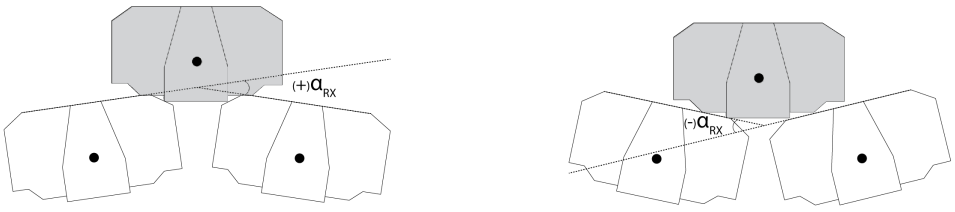

(c) Positive relative angle in x-direction (long shore)

(d) Negative relative angle in x-direction (long shore)

Figure 5.5: Definitions of relative angles, pertaining to upper units in the figures

In y-direction the relative angle (α_{RY}) is calculated as the angle of the unit minus the average angle of the two supporting units underneath. In x-direction the relative angle

(α_{RX}) is calculated as the angle of the unit minus the angle of the neighbouring unit. The exact definitions of the positive and negative relative angles for both directions is visualised in figure 5.5.

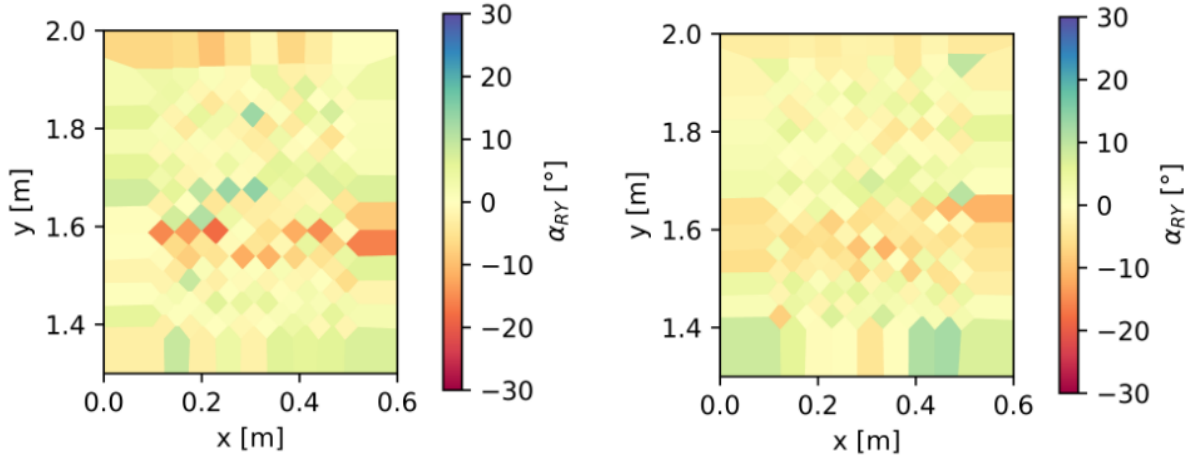

(a) Armour layer **(b)** Under layer

Figure 5.6: Calculated relative angles

The results of the relative angles are visualised at the locations of the units as in figure 5.6.The relative angle is extracted for the unit where failure occurred and plotted against the N_s for which the failure occurred. If no failure occurred the maximum measured values of α_R and N_s are plotted. The same is done with the relative angle of the corresponding under layer.

5.2 Accuracy

The three ReCap models made at the same moment are compared to indicate the accuracy of the data. For each test the three models have been compared to the average of the three models combined. The result of this is shown in figure 5.7.

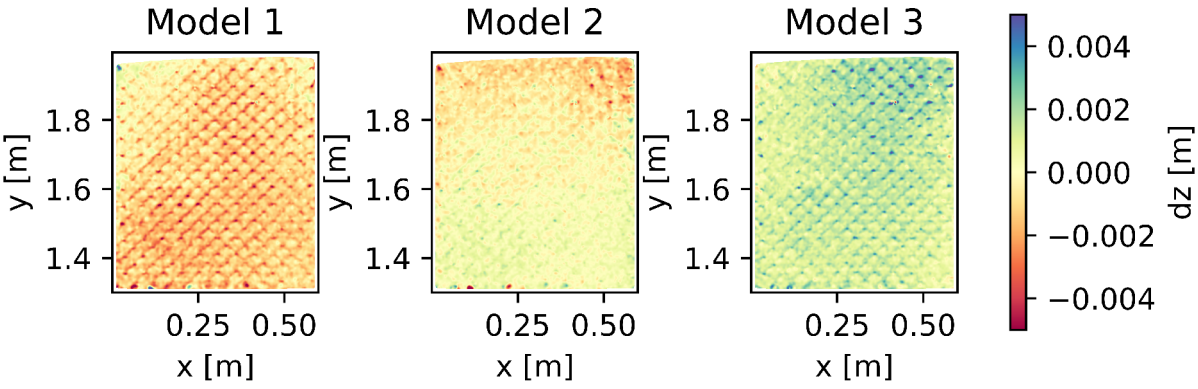

Figure 5.7: Measured difference between models of same test

The average standard deviation of each point over the three models is less than 1mm. The maximum deviation between the models is ±5mm. In figure 5.7 it can be seen that

this maximum deviation occurs at the transition between units. At the top of the unit, where the data for the units is extracted, the maximum deviation is ±3mm. For the under layer there are exceptions where the deviation is ±5mm, most models have a maximum deviation of ±3mm. The calculated angles have an average standard deviation of 2.2° for the armour layer and 0.4° for the under layer in both x- and y-direction. The errors are expected to be random and to be further reduced by averaging over the three models.

Chapter 6: Test results

This chapter describes the results of each series, the resulting values are presented and observations of the behaviour are made. The resulting values are the relative angles of the armour layer and under layer, which are extracted from the ReCap models according to the procedure explained in chapter 5. The resulting relative angles are used to validate the hypothesis of chapter 3 and are thus the key results for this study. To relate the results to the survey methods in practice [SBRCURnet, 2014], the standard deviation of the profile (σ) is also given. The standard deviation is averaged over the width of the fume and scaled by the unit size (D_n) and indicates the roughness of the test section.

6.1 Reference case

The total test sequence has been subdivided into series with different types of irregularities. The first series was conducted without any intentional irregularities and remained stable up to N_s=3.88, which is 1.55 times the design value. At this point there was no damage, but white capping occurred and the largest waves began to break, thus the wave height was not further increased.

The resulting values are $\alpha_{R_{UL}}$=8.9° and $\alpha_{R_{UL}}$=4.1° as the maximum measured relative angles of the armour layer and under layer respectively. The standard deviation of the profile (σ) averaged over the width and scaled by the unit size (D_n) is 0.08.

6.2 Cross shore convex

In the second series, the irregularity with a convex shape in cross shore direction was tested. Different sizes and locations were tested in order to determine the critical value at the most conservative location. An overview of the conducted tests and their results is given in table 6.1.

Test	Target size and location			Resulting values			Failure
	$\frac{r}{r_{hyp}}$	$\frac{\Delta z}{D_n}$	$\frac{z_{SWL}}{D_n}$	$\alpha_{R_{AL}}$	$\alpha_{R_{UL}}$	$\frac{\sigma}{D_n}$	$\frac{H_s}{\Delta D_n}$
1	1.0	1.0	-3.4	11.2	9.9	0.45	3.34
2	1.2	1.0	-3.4	9.1	6.8	0.38	> 3.90
3	0.8	1.0	-3.4	31.9	11.3	0.39	2.04
4	1.0	0.8	-3.4	18.9	7.7	0.27	3.78
5	1.0	1.0	0.0	17.3	7.4	0.29	> 4.10

Table 6.1: Overview results Series 2

It was expected that the results would show a clear critical value, in figure 6.1 however it can be seen that this is not the case. The trend seems to be linear, with a much steeper slope for the armour layer than for the under layer. The spreading is quite large and only three tests have failed, therefore it is not possible to make a conclusion yet.

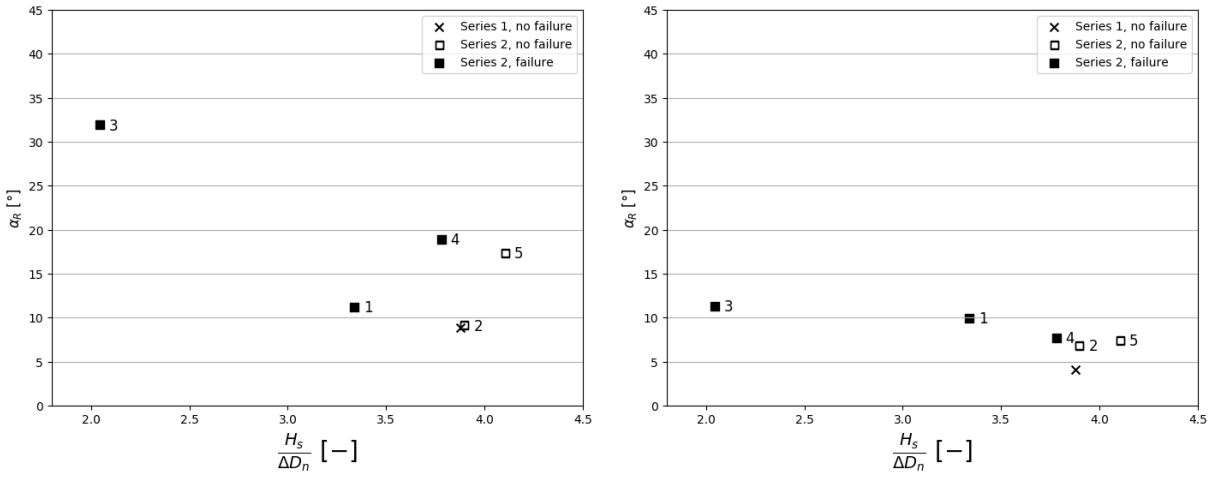

(a) Armour layer **(b)** Corresponding under layer

Figure 6.1: Relative angles of Series 2

Despite the larger relative angle at the location of failure, test 4 was more stable than test 1. This could be caused by the smaller deviation from the design profile, which implies that not only the relative angle but also the absolute deviation is of influence. This could mean that the trend line is through test 1 and 3, with an upward shift when the deviation from the design profile is reduced. Test 3 failed very early, but the configuration also had a large relative angle. Visual observations were made of insufficient interlocking for two subsequent rows.

Another observation is that test 5, where the irregularity was located around the waterline, performed better than test 1 despite the larger relative angle of test 5. Thereby confirming that the location at the run-down waterline is more critical than around the waterline. The beginning of failure was at the top of the irregularity for all failed tests, the top of the irregularity being the point with the largest deviation from the design profile. At this point the slope is same as the design profile, thereby excluding the slope as the cause of failure.

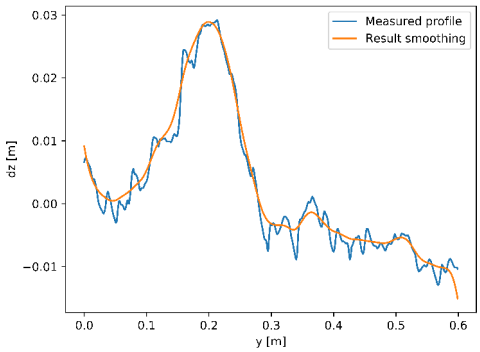

Figure 6.2: Effect of smoothing on the deviation from the design profile

Almost all corresponding relative angles of the under layer are smaller than the resulting relative angles of the armour layer. The under estimation of the relative angle of the under layer is a result of the smoothing filter. The filter reduces the extremes and thereby influences the calculated relative angle. The effect is depicted in figure 6.2.

Especially at the irregularities with a large deviation and small radius, as is the case for test 3. Because the tolerances will be based on the relative angles of the under layer the under estimation results in more conservative tolerances.

6.3 Cross shore concave

The third series of tests conducted with concave irregularities in cross shore direction. Because failure did not occur for the expected critical radius, the radius of the irregularity was reduced. Until the slope above the irregularity became too steep and also the change of slope on the downside of the irregularity could not become any larger, because failure started to occur at the convex section underneath the concave irregularity. Subsequently tests with lower locations were conducted, to check if this would be more critical. An overview of the conducted tests and their results is given in table 6.2.

Test	Target size and location			Resulting values			Failure
	$\frac{r}{r_{hyp}}$	$\frac{\Delta z}{D_n}$	$\frac{z_{SWL}}{D_n}$	$\alpha_{R_{AL}}$	$\alpha_{R_{UL}}$	$\frac{\sigma}{D_n}$	$\frac{H_s}{\Delta D_n}$
1	1.0	1.0	0.0	15.7	8.6	0.40	3.34
2	0.8	1.0	0.0	24.9	19.2	0.36	> 3.90
3	1.0	1.0	-3.4	24.3	14.2	0.38	2.04[1]
4	1.0	1.0	-1.7	18.2	11.7	0.33	3.78

Table 6.2: Overview tests and results Series 3

As can be seen in figure 6.3, none of the tests failed at the concave irregularity. Even though the expected critical value of a relative angle between the armour units of 15° was exceeded multiple times. Visual observations also confirmed that the wings of multiple units were no longer supported by the underlying units. Therefore, it can be concluded that the concave irregularity in cross shore direction is not critical for the stability of the armour layer.

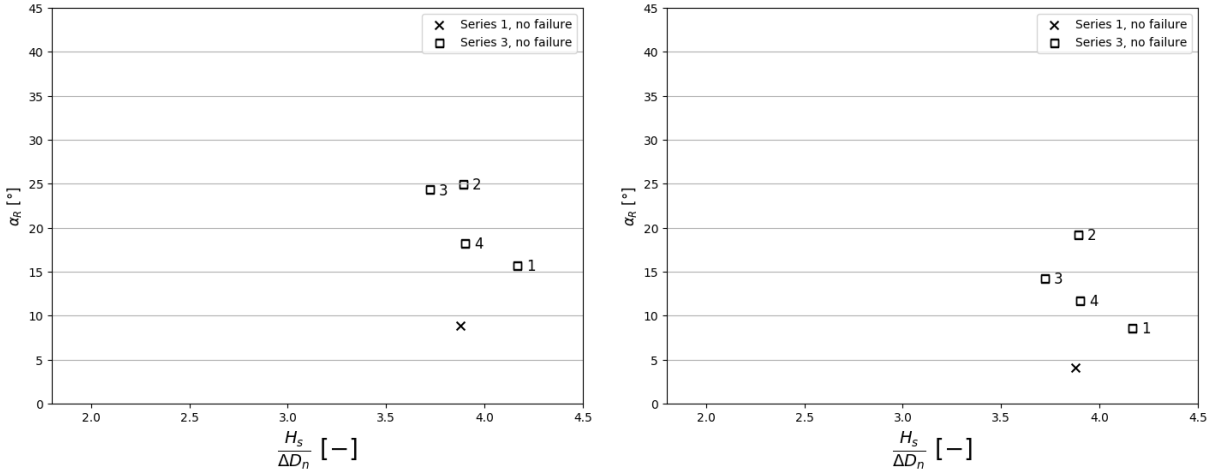

(a) Armour layer **(b)** Corresponding under layer

Figure 6.3: Relative angles of Series 3

[1] failure at convex section

6.4 Long shore convex

The convex shape in the long shore direction was tested in series 4. Because the irregularity could be applied over the full length of the slope there was no variation in location between the different tests. The first test resulted in a largely distorted placement grid, with multiple units that were insufficiently supported. Still no extraction of any units occurred and thus no failure was registered. Despite the absence of failure there did arise gaps at the top part of the slope due to settlements. Therefore, it was chosen to not further increase the irregularity. An overview of the conducted tests and their results is given in table 6.3.

Test	Target size and location			Resulting values			Failure
	$\frac{r}{r_{hyp}}$	$\frac{\Delta z}{D_n}$	$\frac{z_{SWL}}{D_n}$	$\alpha_{R_{AL}}$	$\alpha_{R_{UL}}$	$\frac{\sigma}{D_n}$	$\frac{H_s}{\Delta D_n}$
1	1.0	1.0	full height	37.3	32.7	0.10	3.34
2	1.2	1.0	full height	14.1	22.5	0.15	> 3.90

Table 6.3: Overview tests and results Series 4

The obtained relative angles that were measured during this series are depicted in figure 6.4. What is striking in this figure, is that for test 2 the angles of the under layer were larger than for the armour layer. Indicating that the armour layer has the ability to reduce the irregularities present in long shore direction. Limited for the condition that the units are still supported by their underlying units. Because for test 1, at the locations where the units were not supported, the relative angle of the armour layer was larger. At all other locations the relative angle of the under layer was smaller as can be seen in figure 6.5.

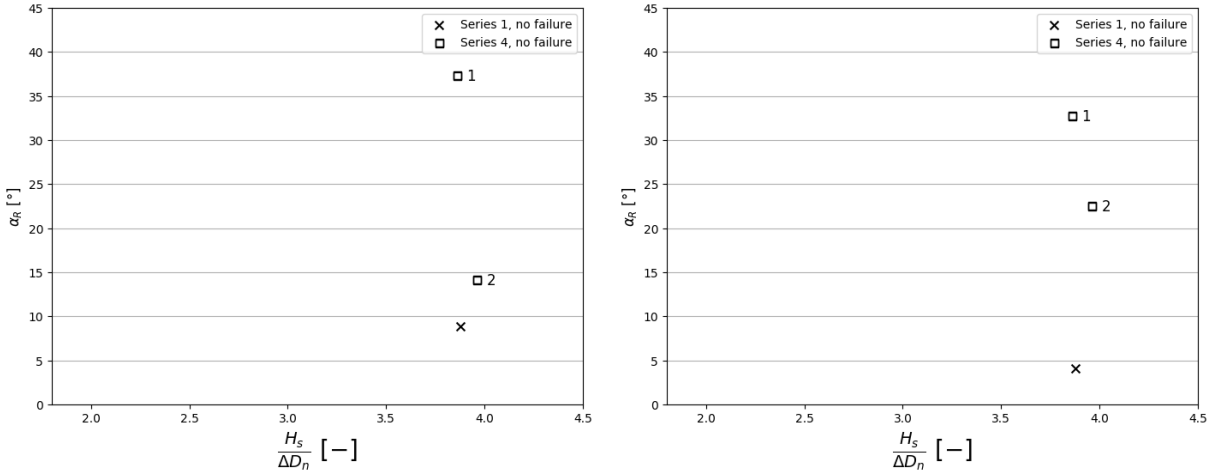

(a) Armour layer **(b)** Corresponding under layer

Figure 6.4: Relative angles of Series 4

This reduction in relative angle between the armour layer and the under layer is caused by transferring part of the deviation in z-direction to a change in grid spacing in y-direction. Being the z-axis upwards from the bottom of the flume, the y-axis in the length of the flume and the x axis over the width of the flume (see figure 5.1a).

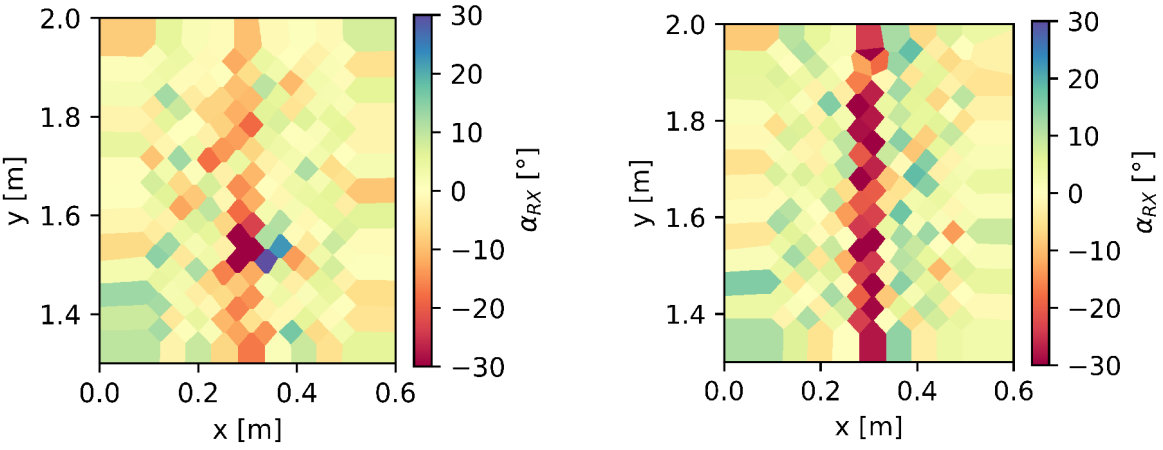

(a) Armour layer

(b) Corresponding under layer

Figure 6.5: Measured relative angles of armour units Serie 4, Test 1

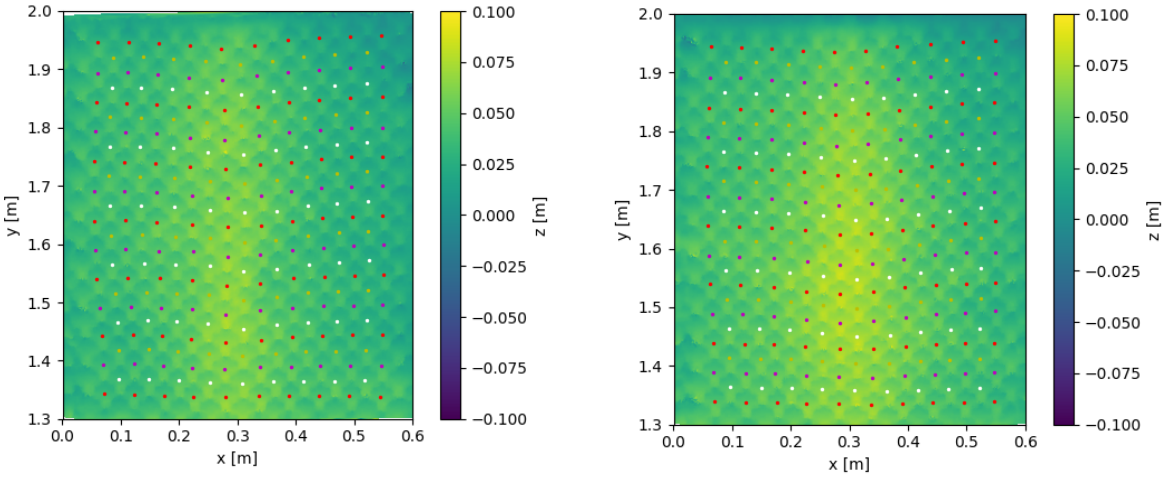

(a) Test 1, z relative to design profile

(b) Test 2, z relative to design profile

Figure 6.6: Change of placement grid due to convex irregularity in long shore direction

The change of grid was apparent in both tests as is visualised in figure 6.6. Here the deviation from the design slope is plotted, in which the shape of each unit is visible and the location of each unit is indicated with a dot. At the bottom row the dots are all in line in x-direction, but at the top of the slope a definite curve can be seen for both tests.

Overall it can be concluded that the irregularity in long shore direction with a convex shape does effect the grid spacing and can influence the amount of settlements, but is not critical in the determination of the tolerances.

6.5 Long shore concave

The fifth series of testing was conducted with a concave shape in long shore direction. Also in this series failure did not occur and it resulted to be difficult to create the irregularity such that the units were too closely packed. Same as with the convex shape, the effect of the irregularity was reduced due to a change in the grid spacing.

The effect of the irregularity was due to change in grid spacing largest at the toe,

Test	Target size and location $\frac{r}{r_{hyp}}$	$\frac{\Delta z}{D_n}$	$\frac{z_{SWL}}{D_n}$	Resulting values $\alpha_{R_{AL}}$	$\alpha_{R_{UL}}$	$\frac{\sigma}{D_n}$	Failure $\frac{H_s}{\Delta D_n}$
1	1.0	1.0	full height	15.7	10.4	0.09	3.34
2	1.0	1.0	top 3/4	11.6	15.2	0.16	> 3.90
3	0.8	1.0	top 3/4	13.9	24.9	0.23	2.04

Table 6.4: Overview tests and results Series 5

outside the influence of waves. Therefore, in the second and third tests the irregularity was introduced only at the highest 3/4 of the slope. However, it still proved that a large irregularity has little effect and it was chosen to continue with the next series after three tests. An overview of the conducted tests and their results is given in table 6.4.

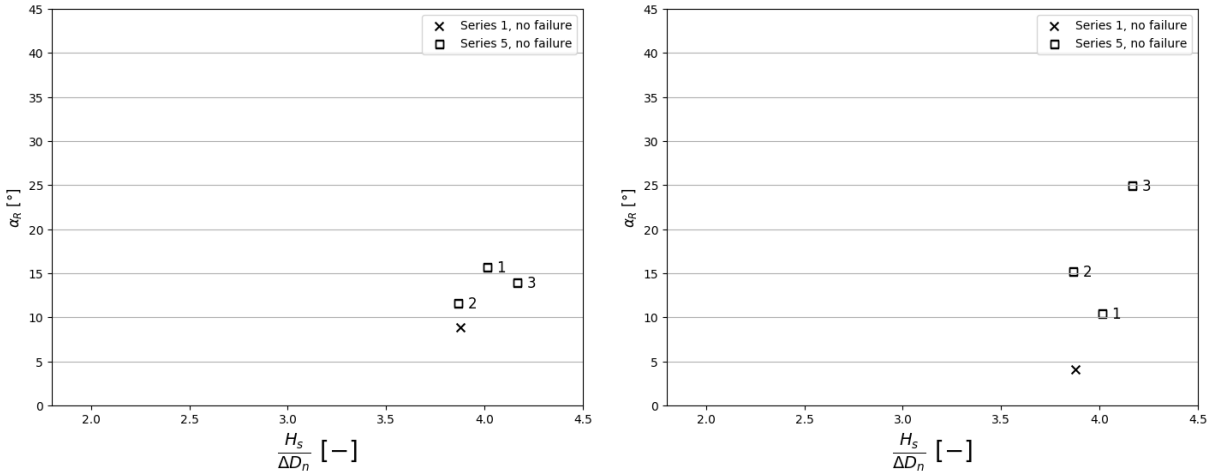

(a) Armour layer **(b)** Corresponding under layer

Figure 6.7: Relative angles of Series 5

In figure 6.7 it can be seen that no failure occurred even though the hypothetical critical value has been exceeded. Visual observations confirmed that at some locations the wings of neighbouring units were touching each other, but the stability was unaffected. Therefore it is concluded that the irregularity in long shore direction with concave shape is not critical.

6.6 Micro irregularities

After each combination of direction and shape has been tested separately, it was tested whether the behaviour remained the same when the irregularities were not applied over the full height but at random locations. In series 6, a total of five tests were conducted, each with a new configuration which has been randomly made. It has been attempted to make differing severities of micro irregularities. The results of the tests are depicted in 6.8.

During the profile creation it was noted that is was quite difficult to create large relative angles in the under layer. Either the slopes became to steep or the irregularity was so local that is did not have an immediate effect on the armour layer. It can be seen

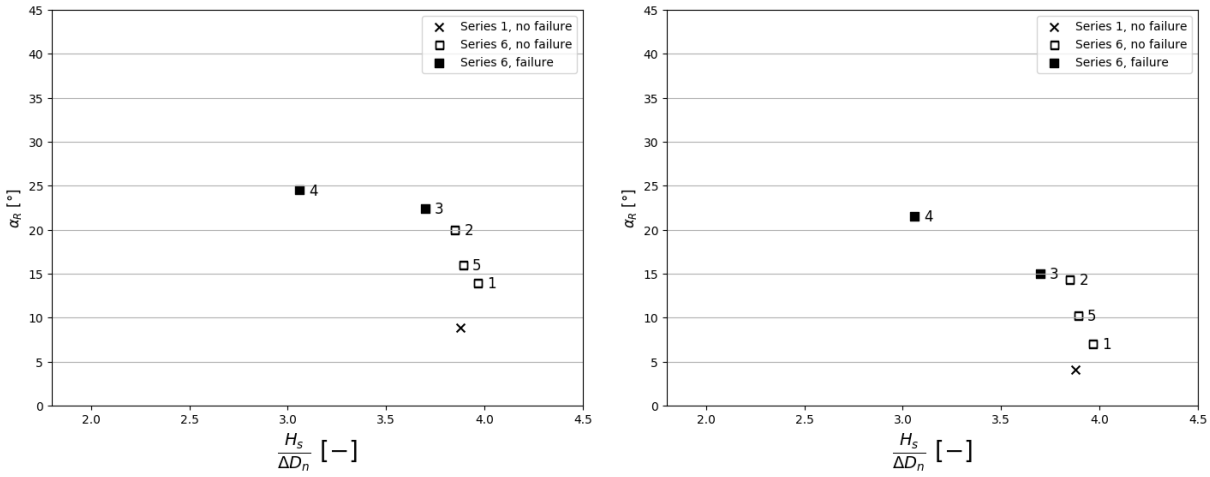

(a) Armour layer **(b)** Corresponding under layer

Figure 6.8: Relative angles of Series 6

in the figure that only the highest relative angles indeed resulted in failure. In both cases this was due to a convex shape in cross shore direction, which is in line with the previous observations.

Test	Target size Below SWL $\frac{\Delta z}{D_n}$	Target size Above SWL $\frac{\Delta z}{D_n}$	Resulting values $\alpha_{R_{AL}}$	Resulting values $\alpha_{R_{UL}}$	Resulting values $\frac{\sigma}{D_n}$	Failure $\frac{H_s}{\Delta D_n}$
1	1.0	1.0	13.9	7.0	0.12	> 3.96
2	1.1	1.1	20.0	14.3	0.23	> 3.85
3	1.2	1.2	22.4	15.0	0.31	3.70
4	1.2	1.0	24.5	21.5	0.18	3.06
5	0.8	0.8	16.0	10.2	0.14	> 3.89

Table 6.5: Overview results Series 6

An important difference in comparison with the results of the convex shape over the full width of the flume, is that the relative angles are larger and that the trend between the stability number and the relative angle is quite similar for the armour layer and the under layer. Therefore, it can be concluded that with micro irregularities the stability of the armour layer is less sensitive and that the influence of the under layer on the armour layer is more direct.

6.7 S-profiles

In series 7 the convex and concave shape in cross shore direction were combined into an S-profile. These S-profiles were created by applying different wave heights for different durations on to the slope without armour layer. An overview of the conducted tests and their results is given in table 6.6. The wave heights applied to the under layer and at moment of failure of the armour layer are expressed in N_s of the armour layer to make the values dimensionless.

Test	Applied waves $\frac{H_s}{\Delta D_n}$	Applied waves Duration [min]	Resulting values $\alpha_{R_{AL}}$	Resulting values $\alpha_{R_{UL}}$	Resulting values $\frac{\sigma}{D_n}$	Failure $\frac{H_s}{\Delta D_n}$
1	1.5	≈ 7	9.1	1.5	1.14	2.58
2	1.5	≈ 2	13.8	0.5	0.73	> 3.92
3	1.5	≈ 5	18.9	3.4	1.21	2.53
4	1.0	≈ 10	9.0	9.9	0.54	3.51
5	1.3	≈ 10	15.7	7.1	0.94	3.72
6	1.4	≈ 10	16.1	7.0	1.10	3.04

Table 6.6: Overview tests and results Series 7

Remarkable in this series is that test 1 and 3 fail relatively early. Especially since it was visually observed that all units were sufficiently interlocked. Figure 6.9 confirms this observation since it can be seen that the relative angles are not very high for the armour layer and strikingly low for the under layer. Additionally, the behaviour during failure was unlike the behaviour of earlier failure. Normally the failure would occur due to one or two units that were extracted and the damage progress would be slow. In this case the whole armour layer was lifted around the top of the convex shape. The top being the point of the convex shape with the largest deviation from the design profile. If the lift was high enough the armour layer would break and within 10 minutes the whole armour layer would have come down the slope.

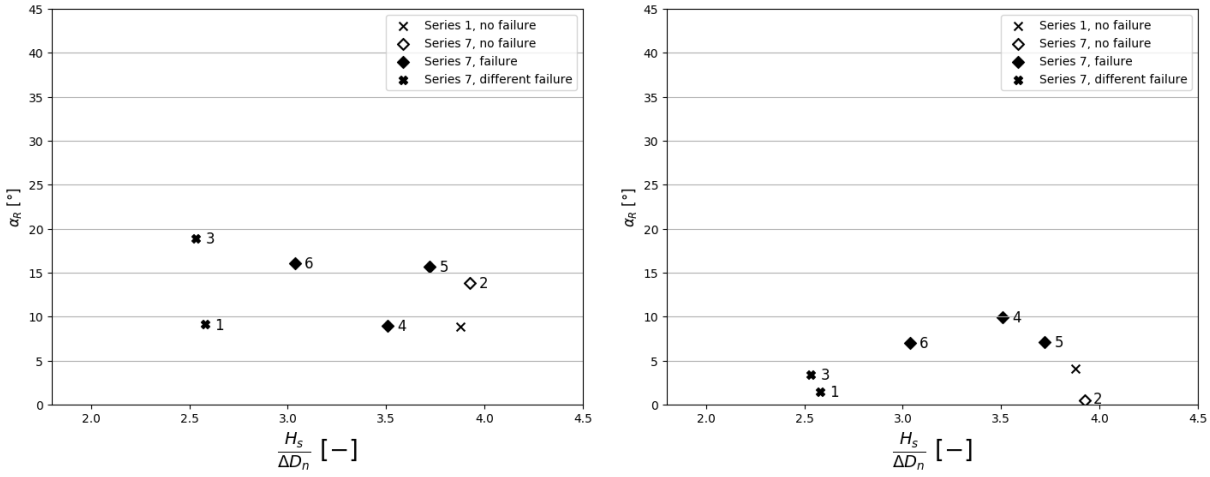

(a) Armour layer **(b)** Corresponding under layer

Figure 6.9: Relative angles of Series 7

In the other cases of damage, which occurred at higher wave heights, the behaviour would be more similar to the behaviour of the convex shape in cross shore direction. With the exception that when failure occurred, two or three rows above the point of extraction had a sudden settlement. Indicating that there was a hollow gap at this location between the armour layer and the under layer. Visual observations were made that there was a large amount of plunging waves, which plunged directly at this location and thereby could have caused this gap. The hollow space between the armour layer and under layer indicates that there is a certain pressure between the armour units that maintains the arch in the armour layer without support of the under layer.

6.8 Correspondence armour layer and under layer

The angles of the armour units are influenced by the configuration of the under layer. The above plots of the resulting relative angles show that the values of the armour layer and under layer are not the same, although a similar trend can often be seen. To find the amount of correlation between armour layer and under layer the angles and relative angles of the under layer are plotted against the respective value of the armour layer. For series 4 and 5 the angles in x-direction are plotted, for all other series the y-direction. The result of this is depicted in figure 6.10 and 6.11. Every detected unit of each test is depicted per series with the linear regression line of the points. The measure of precision (p-value), the measure of correlation (r-value) and the standard deviation of the slope is given. The 95% confidence bound of the linear regression line is between the dotted lines.

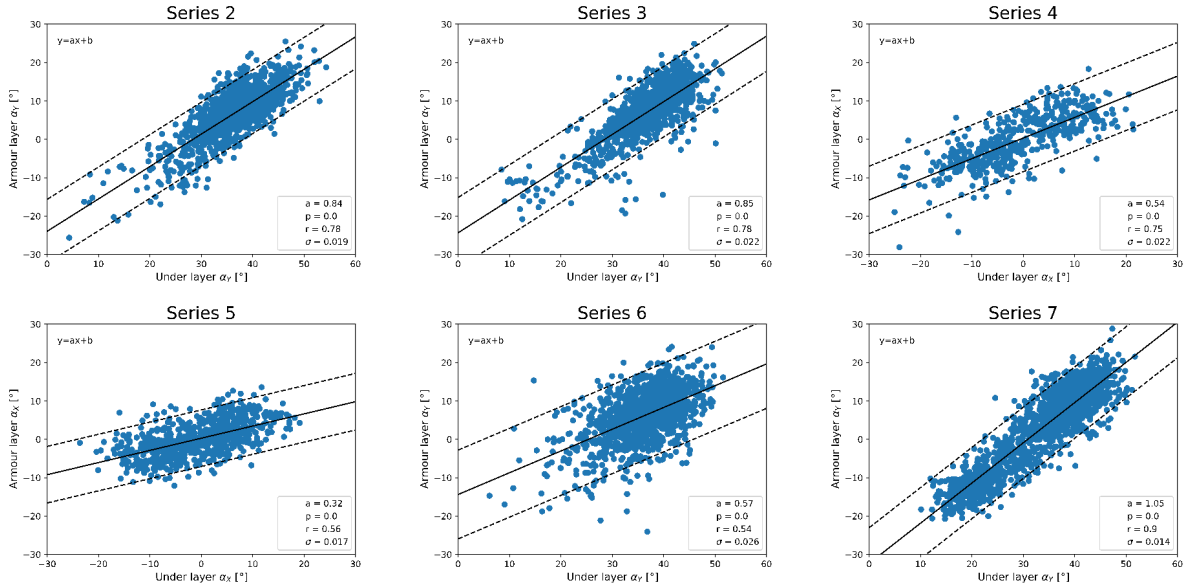

Figure 6.10: Correlation angles armour layer and under layer

The correlation of the angles is strong for series 2, 3, 4 and 7. The spreading of series 6 is larger and the correlation is reduced due to the influence of irregularities in the x-direction. The slope of series 4 and 5 is relatively small, confirming the observation that the armour layer is less sensitive for irregularities of the under layer in x-direction. The high correlation of series 7 is caused by the large range of angles that is present in the test section. Similar trends are observed for the relative angle, but the correlation between the armour layer and the under layer is in all series significantly reduced. This is caused by a smaller range in the measured angles and a larger spreading due to the additional calculation step.

The regression line of series 7 is the most reliable because of the high correlation between the armour and under layer and due to the wide range and equal spreading of the measured angles. The slope of this regression line is larger than 1.0, indicating that the armour layer slightly overreacts in relation to the under layer. Which was also seen at the other results in this chapter, with exception of series 4 and 5. The difference could be caused by the under layer smoothing that cancels out the influence of individual grains and thereby slightly reduces the irregularities in the under layer. The influence of the smoothing in the x-direction is much smaller because the contact area between the unit

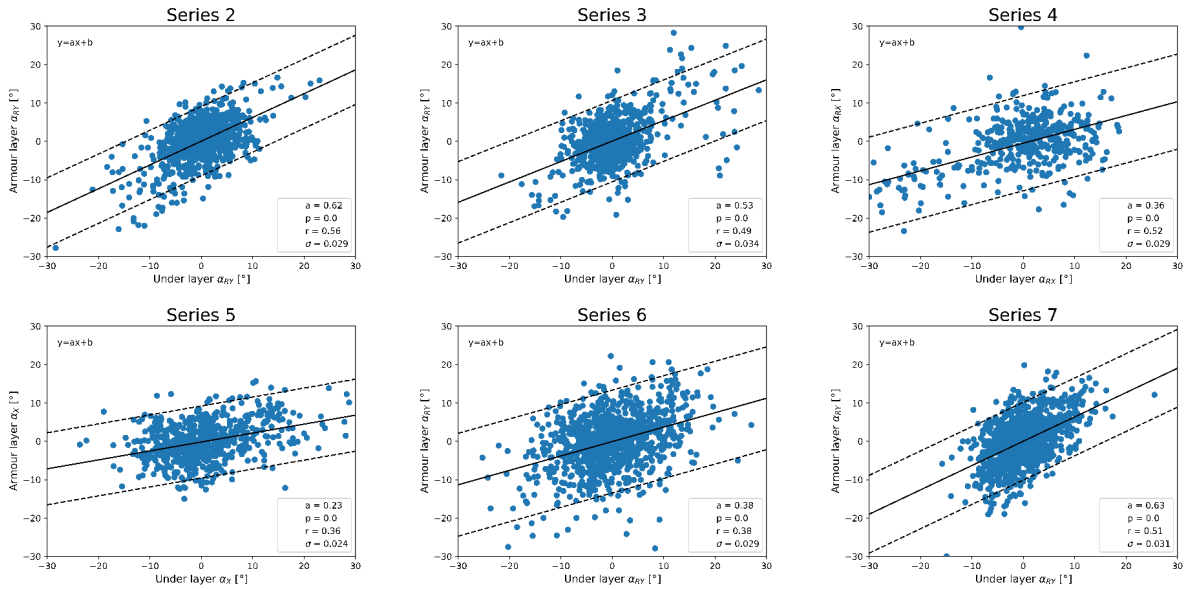

Figure 6.11: Correlation relative angles armour layer and under layer

and the under layer is larger.

6.9 Placement time

The placement time of the model armour layer was expected to increase due to the irregularities. Figure 6.12 shows however that the placement time remains seemingly constant throughout all the series. Also during placement it was observed that the configuration does not increase the difficulty of placement. Even when the units are not sufficiently interlocked there is only one way to place the unit.

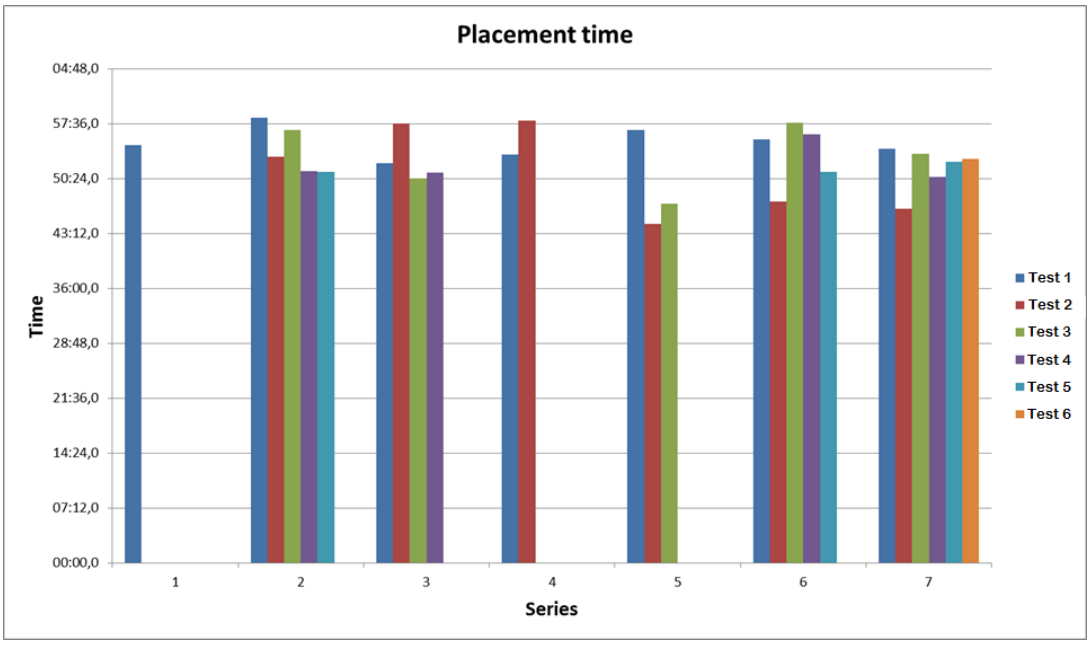

Figure 6.12: Measured placement time of series

In reality placement will be more difficult because the crane operator has a less favourable view point and the positioning of the unit is less direct by crane than it is by hand. It is proposed however to design a hydraulic system which fits into the hole of the armour unit. With this system the unit can be rotated and translated in every direction and thus can be placed with high precision. Additionally, the placement is assisted by the programmed GPS locations. Same as in the model tests, there is only one way to place the unit due to the regular pattern and orientation. Therefore the effect of the irregularities on the placement time is not expected to differ much in reality.

6.10 Power Spectral Density

The use of the Power Spectral Density (PSD) was seen as a future possibility to define the tolerances. The test results indicate that both the relative angle (change of slope) and the deviation from the design profile are expected to influence the stability. The PSD's from the slope and the change in slope are found by taking the first and second derivatives of the PSD of the deviation respectively. The resulting PSD's of the tests with the micro irregularities (series 6) are depicted in figure 6.13. It shows that no correlation is found with the level of stability, for neither the PSD's of the deviation from the design profile, the slope or the change in slope. Since no difference can be seen between the failed tests 3 and 4 and the other tests of series 6.

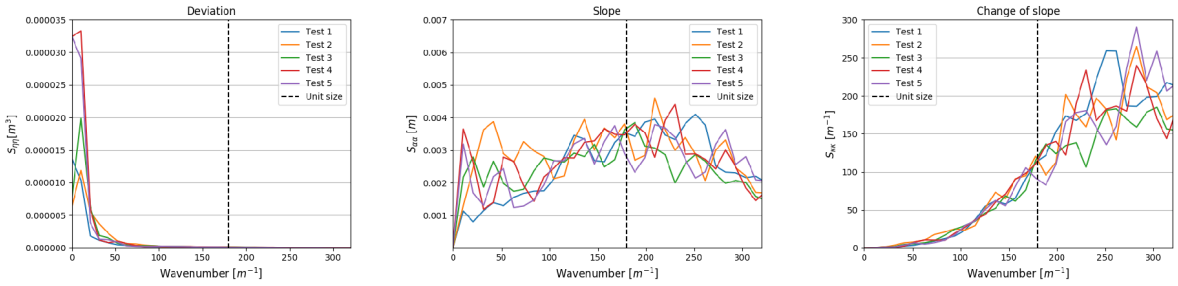

Figure 6.13: Power Spectral Densities of series 6 (micro irregularities)

Chapter 7: Analysis

In this chapter the relationship between under layer configuration and stability of the Xbloc^{Plus} is analysed. First, the divergent behaviour of some of the S-profiles compared to the other convex shapes is assessed. This information is then used for further analysis on the aspects of the irregularities that influence the stability behaviour. Subsequently, the implications for practice are determined and the tolerances for execution are deducted.

7.1 Failure mechanism

Two types of failure have been observed during the model tests. The first is the extraction of one or multiple adjacent units due to overpressure inside the breakwater which overcomes the interlocking capacity. This is the type of failure which has also been observed in the previous studies of Vos [2017] and Rada Mora [2017]. Another failure mechanism however occurred for the two largest S-profiles. The analysis of the forcing of this mechanism is discussed in this section, followed by the implication of the presence of this mechanism for the development of the loss of interlocking.

7.1.1 Divergent failure behaviour

In section 6.7 it was observed that the S-profiles in tests 1 and 3 of series 7 failed very abruptly and with a fast failure progression. This behaviour is divergent from the other failure cases where the loss of interlocking was seen beforehand.

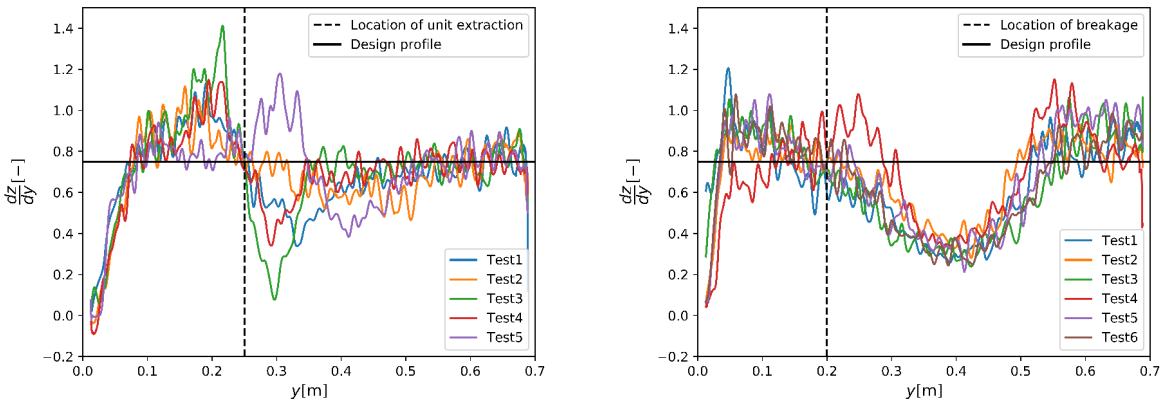

(a) Convex shape in cross shore direction (Series 2)

(b) S-profiles (Series 7)

Figure 7.1: Slopes of profiles

The different behaviour of tests 1 and 3 in comparison with series 2 and the other tests of series 7, could be caused by multiple factors. One of which is the slope at the downside of the profile, which is very steep. Causing the under layer to be unstable and to consequentially push the armour layer out. In figure 7.1 the slopes of series 7 are

compared with series 2. It can be seen that the slopes are not steeper than in the tests of series 2 or the other tests of series 7. Also the location where the slope is maximum is not where the armour layer breaks for test 1 and 3. Making it unlikely that the steep slope is the main cause of the failure.

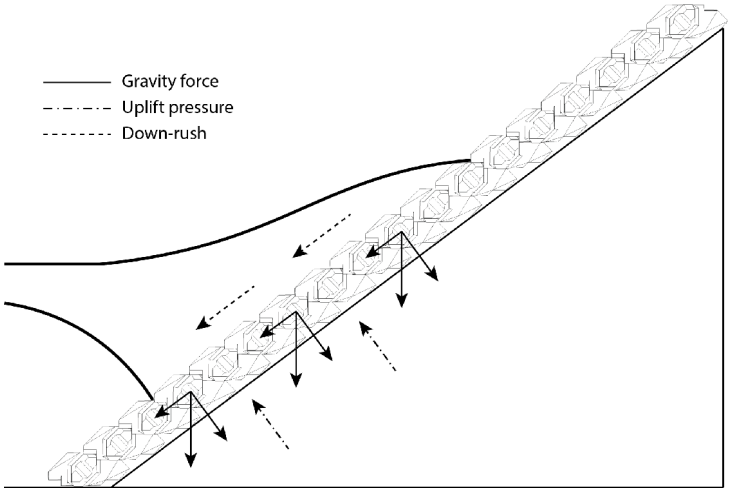

Figure 7.2: Directions of main acting forces on a straight profile

In figure 7.2 the main forces that act on the slope are depicted. The main cause of failure for the Xbloc^{Plus} is extraction due to overpressure during run-down. The resistive force is gravity, enlarged by the interlocking capacity. The gravity force is subdivided into components parallel and perpendicular to the slope. The perpendicular component counteracts the force due to overpressure. The parallel component is partially counteracted by friction with the slope and the remaining force rests on the lower units, thereby enlarging their weight and keeping them in place. The force due to the drag of the down-rush is considered to be in the same direction as the slope and counteracted by both friction and the resistance of the toe.

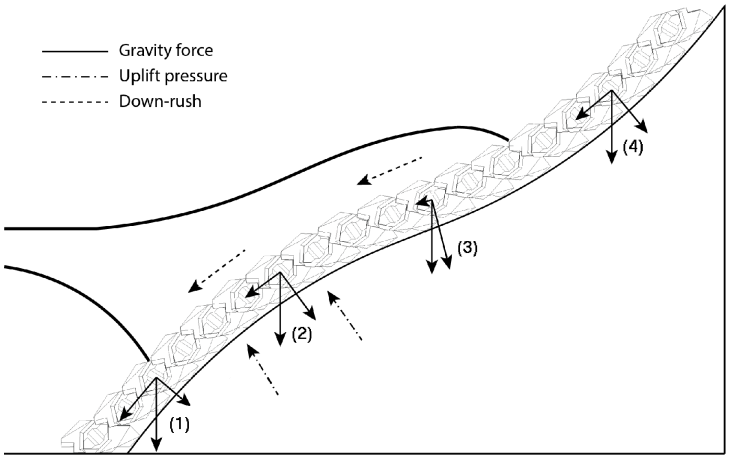

Figure 7.3: Directions of main acting forces on a S-profile

In case of a S-profile the same test-runs have been performed and thus the same forces are expected to have been applied. The fact that failure occurred for the S-profile and not for the straight slope is due to a different distribution of the forces. The change in slope over the profile causes the parallel and perpendicular components of the gravity force to

differ over the profile. The resistance is reduced due a reduction of the perpendicular gravity force resting on the steep lower part of the slope (1) and a reduction of the parallel gravity force (3) weighing on the lower convex section. The force due to the overpressure and the drag of the down-rush are still present and are not expected to be decreased. The weight of the upper part of the slope (4) induces a buckling effect, similar to the buckling of beams. For a straight beam, a force along the axis increases the resistance against forces acting perpendicular to the axis. In case of a beam which is already distorted sideways however, a force along the axis of the beam will increase the distortion. Resulting in the units on top of the convex section (2), to be pushed away from the slope and fail. The mechanism is caused by the arched shape and is therefore further referred to as the 'arching mechanism'.

7.1.2 Simplified model

The divergent failure behaviour is influenced by factors along the whole profile and the distribution of forces is different everywhere. To increase the understanding of the arching mechanism and deduct the most influential factors a simplified model is used. The full explanation of the deduction of the model can be found in appendix E.

As a result of the profile shape not only the distribution of the forces changes, but also the point of contact between the neighbouring units is different. As is visualised in figure 7.4. The visualisation shows that at the concave section the rotation points are at the nose of the units. The line of pressure between the units is thereby further away from the supporting under layer. The forces between the units (Fn) are increased and the perpendicular component of the gravity force (Fz) is reduced. This makes it more probable for the pressure force (Fp) to push the units away from the slope. At the convex section the center of mass is behind the point of rotation resulting in a tendency of the unit to rotate toward the slope.

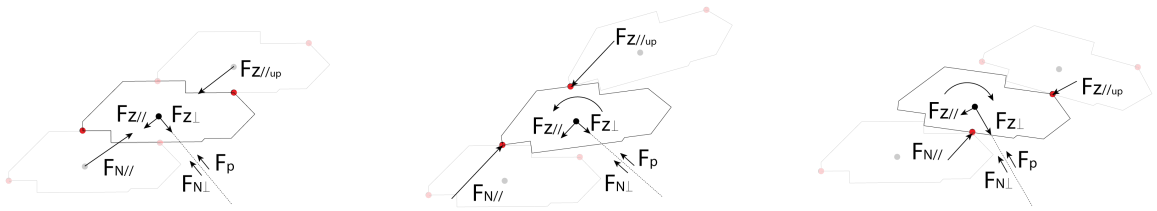

(a) Straight slope **(b)** Concave section **(c)** Convex section

Figure 7.4: Difference in contact points between units

The knowledge of the analysis on a single unit in the different sections is used to model the full slope. The bottom part of the S-profile is a straight slope, but it is a steeper slope than the units are designed for. Therefore the forces on the units are similar to the concave shape. At concave sections the normal forces between the units are very large and thus is the interlocking strong. To simplify the model the steep downward section of the slope is modelled as a rigid body. At the convex section the normal forces between the units are reduced, but since the units are still interlocked they are also modelled as a rigid body.

The transition between the steep downward slope and the convex section is the point of breakage, modelled with a hinge. The point of breakage is at the transition between

the units that want to rotate forward (figure 7.4b) and want to rotate backward (figure 7.4c). This is the location with the largest positive deviation from the design profile, where failure was also observed during the model tests. With these simplifications the S-profile can be schematised in a model as depicted in figure 7.5. The top part of the profile is modelled by a force on the rigid bodies, depicted as $Fz_{//up}$.

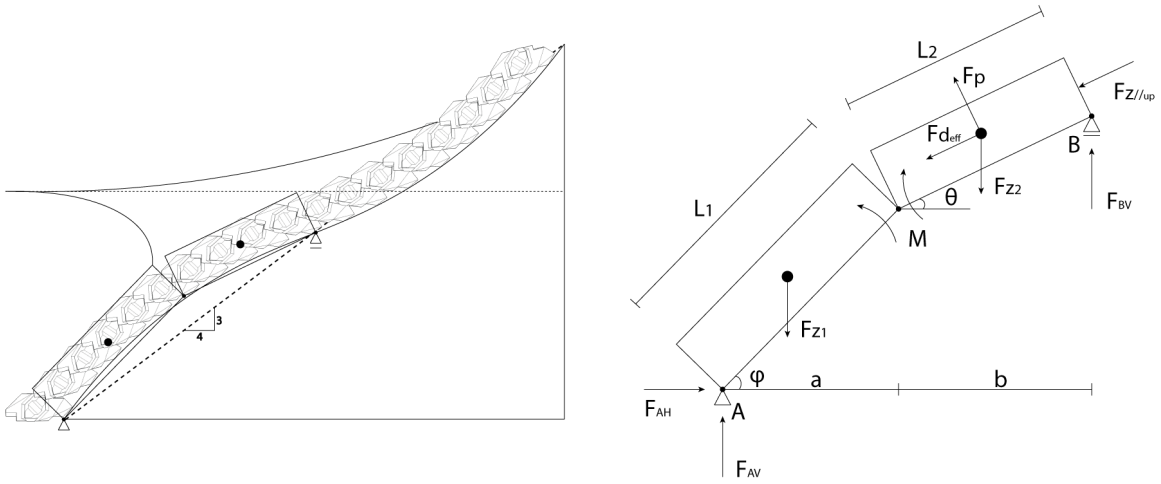

(a) Schematised S-profile **(b)** Simplified model

Figure 7.5: Schematisation of S-profile into simplified model

A further simplification is made by assuming that the pressure force (Fp) and the effective drag force (Fd_{eff}) mainly act on the upper rigid body. This simplification is valid because both forces are mainly present in the area between run-down and still water level. The effective drag force is the drag force of the down rush minus the friction of the under layer.

From the model it can be deducted that if the effect due to the effective drag, the weight of the units up-slope of the model and the pressure force, is larger than the resistance caused by the weight of the units, a rotation is caused. The rotation pushes the two rigid bodies away from the slope and causing the hinge between the bodies to be extended, simulating the loss of interlocking. The model indicates that L1, ϕ and $Fz_{//up}$ have a positive influence on the rotation, meaning that an increase amplifies the rotation around A. While θ has a negative influence on the rotation. The contributions of ϕ and θ are considered to be most important. The reasoning behind the relations can be found in appendix E.

7.1.3 Correlation with test results

To verify if the arching mechanism is the acting failure mechanism, the found relations of the simplified model are compared with the test results. In figure 7.6 the profiles of series 7 are depicted. It can be seen that the profiles of test 1 and 3 have the largest deviation from the design profile. Causing a large ϕ, a small θ and a large $Fz_{//up}$ due to the steep upper slope. Indicating that the relations deduced from the model correspond with the test results.

For further validation, the 3D-models made before and after the tests are compared to check the movements of the armour layer. The fast damage progression of series 7 tests 1 and 3 however, made it impossible to link the measured difference between before

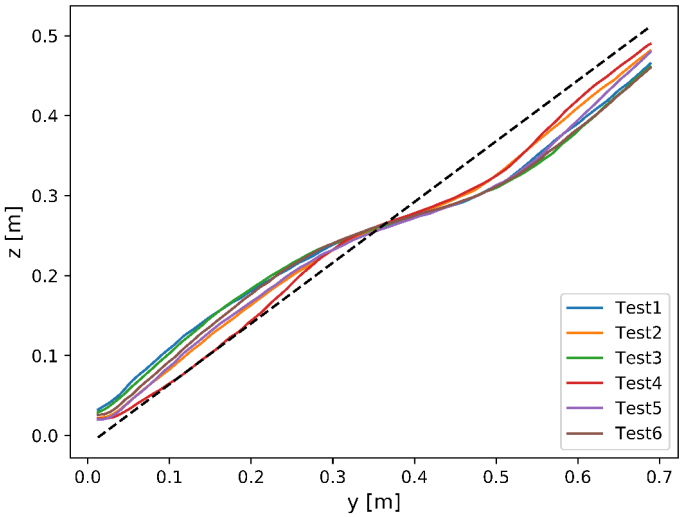

Figure 7.6: Cross sectional profiles of series 7

and after the tests to the cause of failure. The results of multiple other tests did show that the downward part of the convex section moved away from the slope while the top part of the convex section settled. Some of the results are depicted in figure 7.7, the rest is presented in appendix D.

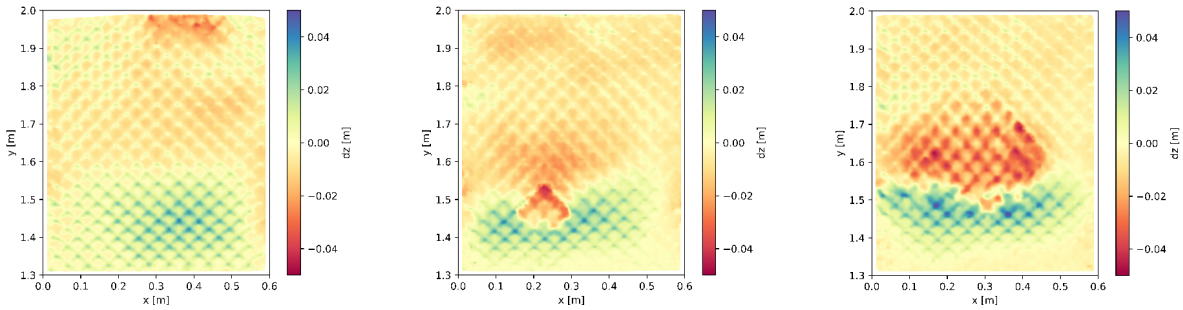

(a) Series 2, test 2 (convex shape)

(b) Series 7, test 5 (S-profile)

(c) Series 7, test 6 (S-profile)

Figure 7.7: Measured difference between start and end of tests

The results of both series 7 (S-profiles) and series 2 (Convex shape) show that the bottom part of the convex section moves away from the slope. This indicates that the arching mechanism plays a role in the failure of smaller S-profiles and other convex shapes as well as of large S-profiles. The effect is smaller because the failure is not direct, but slow progressing. In case of slow progression the mechanism induces the loss of interlocking, thereby enabling units to be extracted from the amour layer. This process is visualised in figure 7.8. The slow progression confirms that a smaller L1 reduces the effect of the mechanism, again confirming the simplified model findings.

Slow progression of the mechanism occurs when the modelled rigid bodies are pushed away from the slope but the hinge is not enough extended to cause loss of interlocking. The created space between the lower rigid body and the slope will be filled due to instability of the under layer, preventing the rigid bodies to move back to their original location. Eventually the loss of interlocking occurs and units are extracted, resulting in failure of the armour layer.

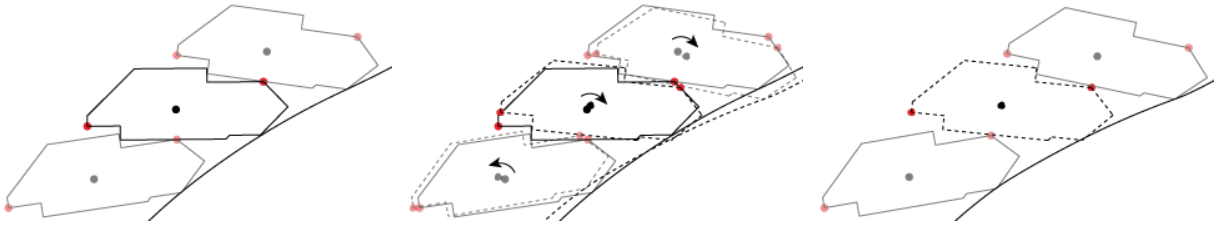

(a) Original position **(b)** Movement of armour units **(c)** Extraction of unit

Figure 7.8: Rotation of amour units causing loss of interlocking

The measured movements do not fully correspond with the simplified model, for which the top part of the convex section should be lifted. The simplified model however does not take the behaviour of the under layer into account. When the downward part of the convex section moves away from the slope, the under layer will move with it. Since the under layer is not stable without the weight of the armour layer. The movement will cause the upward part of the convex section to settle.

The influence of the arching mechanism in the development of loss of interlocking, also explains the influence of the deviation from the design profile on the stability of the armour units. A larger deviation has a larger ϕ, thereby amplifying the arching mechanism and causing an earlier loss of interlocking.

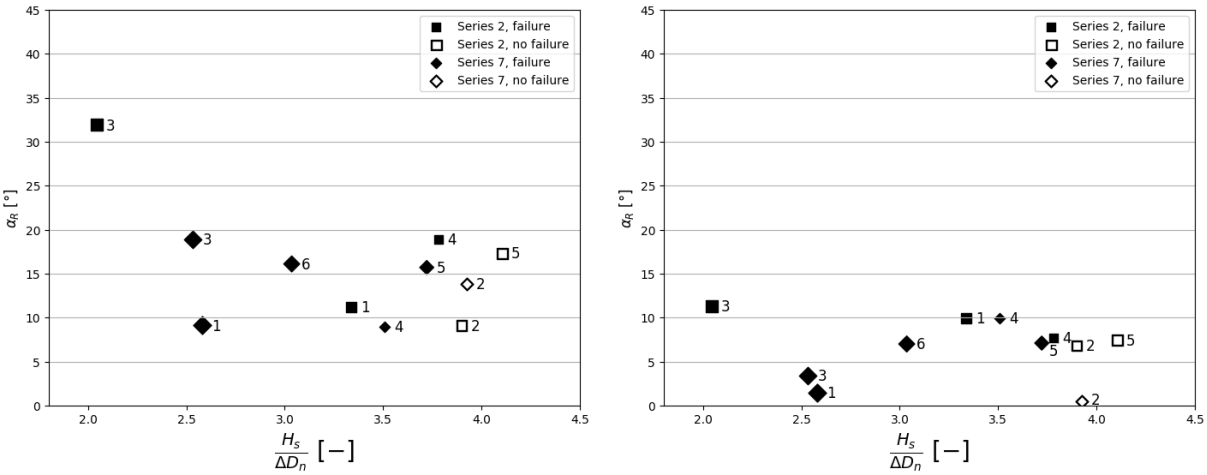

(a) Armour layer **(b)** Corresponding under layer

Figure 7.9: Influence of the deviation from the design profile

To confirm this the results of series 2 and 7 are further analysed. In figure 7.9 the relation between the relative angle and the stability number has been plotted with the marker size scaled by the deviation from the design profile. It can be seen that the scatter of the relation indeed correlates with the amount of deviation. An exception is test 4 of series 7, performing worse than test 5 of the same series, despite a smaller deviation. The length scale (L1) of test 4 however is smaller than test 5, thereby causing a steeper slope. The location of the irregularity higher up the slope causes test 5 to be less critical. Thereby explaining why test 5 of series 2 performs better than test 4, despite the larger deviation. The exact maximum deviations perpendicular to the design profile are given in table 7.1.

The influence of the arching mechanism on micro irregularities is expected to be

	Test	Maximum deviations		Difference
Series 2	1	+ 0.024m	- 0.015m	0.039m
(Convex)	2	+ 0.017m	- 0.015m	0.032m
	3	+ 0.030m	- 0.010m	0.040m
	4	+ 0.017m	- 0.010m	0.027m
	5	+ 0.018m	- 0.010m	0.028m
Series 7	1	+ 0.038m	- 0.047m	0.085m
(S-profile)	2	+ 0.019m	- 0.034m	0.053m
	3	+ 0.036m	- 0.054m	0.090m
	4	+ 0.013m	- 0.035m	0.048m
	5	+ 0.023m	- 0.045m	0.068m
	6	+ 0.030m	- 0.051m	0.081m

Table 7.1: Maximum deviations perpendicular to design profile

insignificant due to the local character of the irregularities. This corresponds with the observations that failure only occurred when the unit had insufficient interlocking from the beginning. The absence of the influence of the deviation from the design profile also explains the higher stability in relation to the relative angle in comparison to the other types irregularities.

The local character and the high stability of the micro irregularities make it reasonable to assume that the effect of the arching mechanism is insignificant and the reduction of stability is fully determined by α_R. For the other irregularities however it is found that the stability is strongly influenced by steepness of the bottom part of the convex shape. As was indicated by the results depicted in figure 7.9. The steepness of this section is expressed by β, the value of β is estimated from the test measurement as is exemplified in figure 7.10.

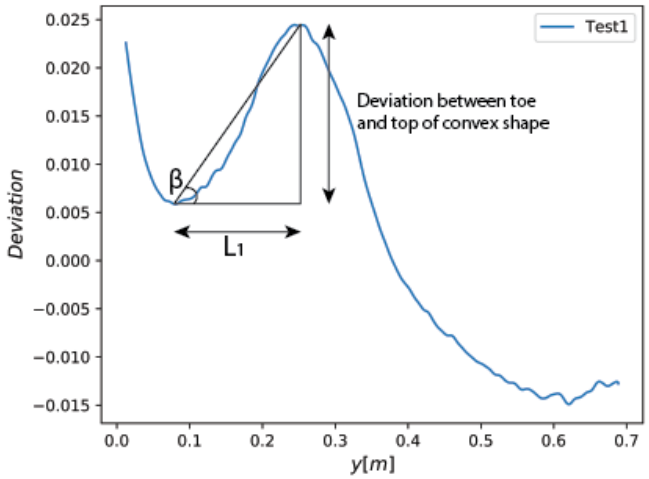

Figure 7.10: Example estimation of β

The influence of β on the relation between the stability and α_R is in correspondence with the simplified model, because the orientation of the rigid bodies can be fully described by the combination of β and α_R. It is assumed that the sizes of the forces do not change. The orientation of the rigid bodies however effects the line of loading of the

forces and thus the lever arm relative to rotation point A. When it is assumed that the pressure force on the upper rigid body is fully counteracted by the gravity force. Than the lever arm of the resistance is determined by β, which describes the orientation of the lower rigid body. The orientation of the upper rigid body determines the lever arm of the loads causing the rotation and is influenced by the combination of α_R and β. The definition of α_R is the relative angle at the location of failure and β is the angle of the downward slope relative to the design profile. As is visualised in figure 7.11.

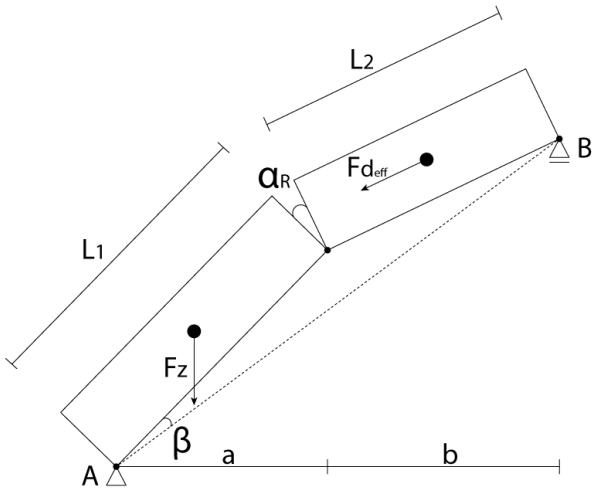

Figure 7.11: Visualisation α_R and β

In figure 7.12 the sum of α_R and β is plotted against the stability number. For both under layer and armour layer the correlation between the sum of α_R and β and the stability number is high and located around the values of the micro irregularities (series 6). This empirical result indicates that the value of β is a good indicator of the influence of the arching mechanism. That no additional factor is necessary to obtain the good correlation, indicates that the amount of influence of the arching mechanism and the relative angle are approximately the same.

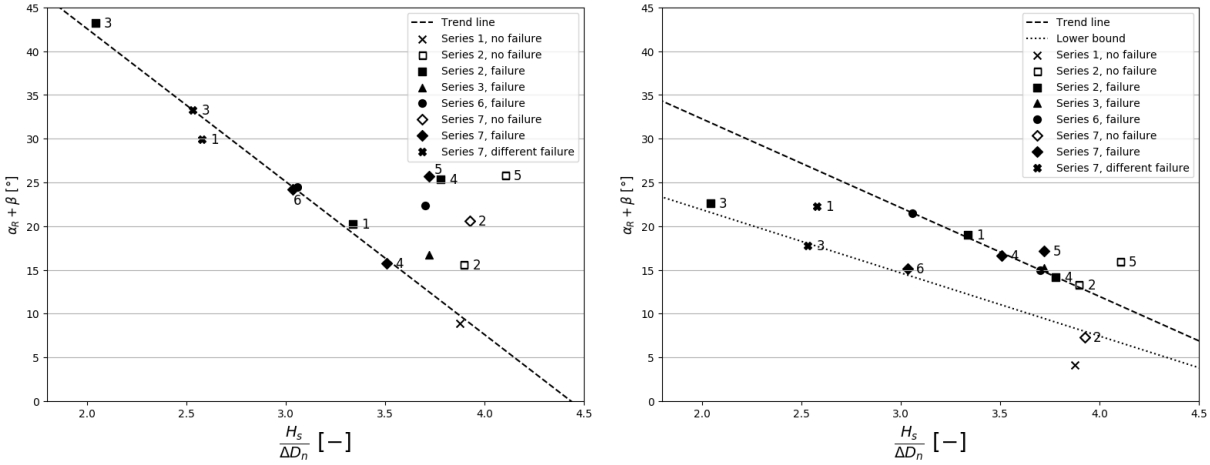

(a) Armour layer **(b)** Corresponding under layer

Figure 7.12: Sum of α_R and β in relation to the stability number

The agreement between the simplified model relations and the test results make it reasonable to assume that the arching mechanism is indeed causing the direct failure of

large S-profiles and influences development of loss of interlocking for other convex shapes. The effect of the mechanism is related to the size of β and is thus mostly dependent on the steepness of the bottom part of the convex shape.

7.2 Tolerances

From the analysis of the test results in the previous section, insight is gained into the factors that influence the failure behaviour of the armour layer. These are the relative angle of the units caused by the change in slope of the under layer and the deviation from the design profile, causing the arching mechanism to push the armour layer away from the under layer. This information is used to set the tolerances that contractors have to meet during placement of the under layer and armour layer.

The strictness of the tolerances is influenced by the reduction of stability level that is allowed while maintaining a safe design. The present design guidelines of the Xbloc^{Plus}, which have not been published officially yet, describes a design value of N_s=2.5. DMC requires the construction to be stable up to an overload of 25%. Resulting in a limit for the tolerances of N_s=3.2 as the required level of stability.

7.2.1 Under layer

As explained in section 2.4, the tolerances for the under layer of the Xbloc are maximum 0.5 D_{n50} for the deviation from the design profile and a maximum deviation between subsequent measurements of 0.3 D_{n50}. The distance between the subsequent measurements is 1.0 D_{n50}. DMC intents to use the same tolerances for Xbloc^{Plus}. In this section it is checked whether these tolerances are sufficient and if changes should or could be made.

Deviation from design profile
The deviation from the design profile must be limited because of the effect of the arching mechanism and to limit the amount of spatial variability. Liberal requirements will result in large variances, which increases the risk of exceeding the limits at unmeasured locations. The amount of spatial variability can be expressed with the standard deviation. Two times the standard deviation is the 95% confidence bound and can therefore be considered as the maximum deviation from the design profile.

Spatial variabilities of the profile configurations are expressed by the standard deviation. The results of the standard deviations of the measured profiles are given in figure 7.13. The standard deviation is calculated over the y-axis and averaged over the x-axis to avoid deviations in x-direction (long shore direction) to influence the results. To reduce the influence of the model precision on the results, the average value per test is considered to be the true value.

The maximum deviation from the design profile of the regular Xbloc is 0.5 times the D_{n50} of the under layer. Which is equal to a maximum standard deviation of 0.25 times the D_{n50}. Scaled to the model test, this results in a maximum standard deviation of 0.003m. The same as the standard deviation of the reference case, for which extra care was taken to obtain a smooth slope. In this regard, the standard deviations of the model tests are relatively large. This is not surprising since intentional irregularities have been made, causing all the test configurations to exceed the limit of the maximum deviation from the design profile. Indicating, that the tolerance is limited by the allowed spatial variability and not due to influence of the arching mechanism.

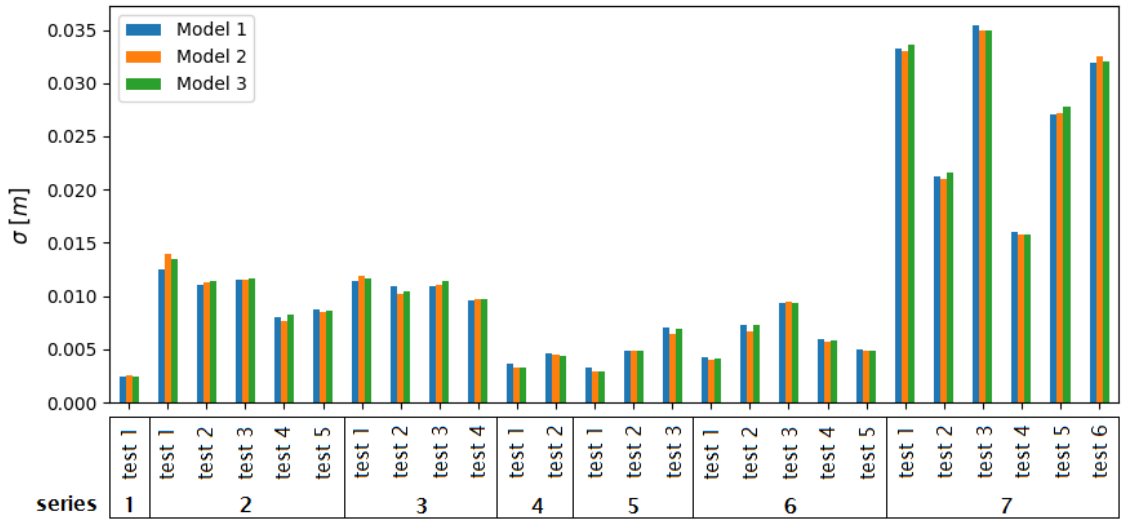

Figure 7.13: Standard deviation of under layer per test

A limit of 0.5 times D_{n50} results in a maximum deviation from the design profile of 0.23 times D_n. The minimum value of the standard deviation for which failure occurred was at test 4 of series 6, at a standard deviation of 0.006m, which would result in a maximum deviation of 0.012m and 0.4 times D_n. This means that a maximum deviation of 0.23 times D_n would be safe to use and there are possibilities for more liberal requirements. For now a value of 0.25 times D_n is chosen as maximum deviation from the design profile. Figure 7.14 shows that this limit was indeed exceeded by all test configurations.

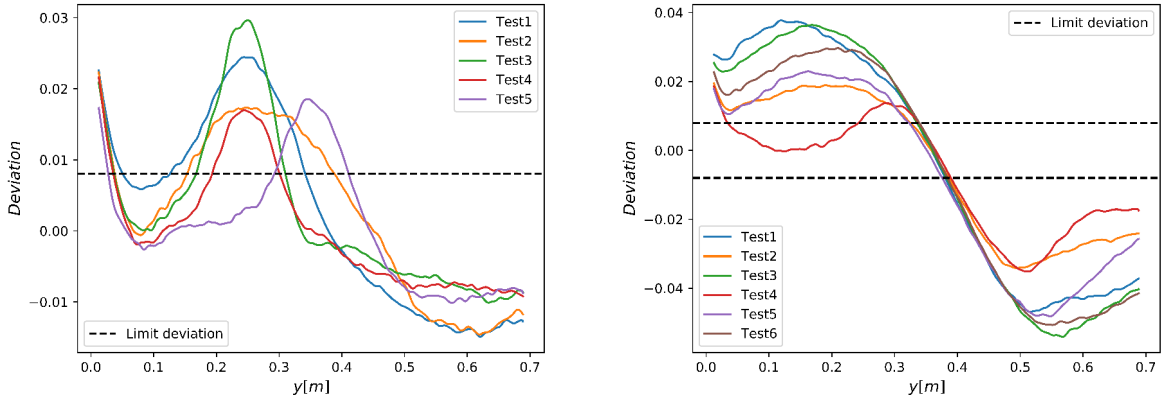

(a) Series 2 **(b)** Series 7

Figure 7.14: Deviations from design profile

Deviation between succeeding measurements

The maximum deviation between succeeding measurements is determined by the maximum allowed relative angle of the armour layer and the relative angle of the corresponding under layer. The level of stability is however not only determined by the relative angle of the amour units but also by the deviation from the design profile.

The limit on the deviation from the design profile has a positive effect on the stability. A small deviation will limit the effect of the arching mechanism and due to the limit in

spatial variability only micro irregularities are expected to occur. For micro irregularities the effect of the arching mechanism is expected to be insignificant and change in stability is considered to be fully dependent on the relative angle.

In figure 7.12 the results of the critical convex shapes are presented, corrected for the effect of the arching mechanism by adding β. The irregularities expected in practice are the micro irregularities and because of the absence of the arching mechanism β is considered to be zero.

The tolerances for profiling of the under layer are deducted from the measured relative angles of the under layer. When the trend line of the test results is taken, the maximum allowed relative angle is 21°(figure 7.12b). With the distance between two units along the slope of 1.0 times the D_n, this results in a maximum deviation between two unit locations of 0.4 times D_n. Because the limit of the maximum deviation from the design profile is 0.25 times D_n, this maximum deviation between two units can only be exceeded when over a distance between two units both maximum limits from the design profile are nearly reached. Which is very unlikely to occur over such a short distance.

An additional requirement between subsequent measurements is not expected to be necessary, but to be safe the requirement is used to remain below the lower bound of the results (figure 7.12b). This results in limit value for the relative angle of 14° and a limit deviation over a distance between two units along the slope of 0.25 times D_n.

For the regular Xbloc, measurements are taken with a distance of D_{n50} [van der Zwicht, 2015]. This results in approximately 2 to 3 measurements over the distance between two units, depending on the size of the under layer. For the Xbloc^{Plus} the maximum deviation between succeeding measurements would be 0.13 times D_n for two measurements and 0.10 times D_n for three measurements. The limit deviation between the measurements is only exceeded if the maximum value is almost reached for every measurement. This chance is very slim and it is considered to be safe to limit the deviation between succeeding measurements at 0.1 times D_n, with measurements every 0.3 D_n. Which is approximately the same as the requirements for the regular Xbloc.

Defined tolerances

In figure 7.15 the chosen tolerances of the under layer are visualised. The maximum deviation from the design profile is 0.25 times D_n, depicted by the black outer lines. The maximum deviation between succeeding measurements is 0.10 times D_n. In the figure indicated by the orange arrow.

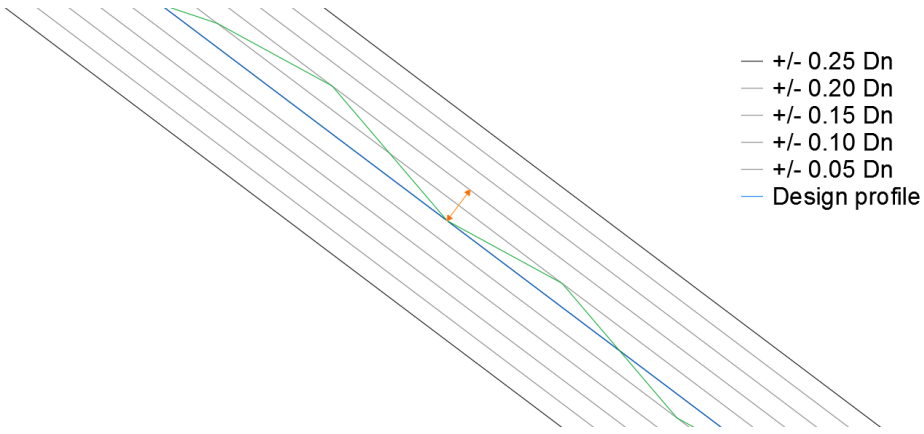

Figure 7.15: Visualisation under layer tolerances

7.2.2 Armour layer

The tolerance of the under layer are meant to facilitate the placement of the armour layer. The tolerances are stated such that the armour units can be placed at the correct place with sufficient interlocking and prevent having to redo the placement of the armour units. The placement of the armour layer can therefore be seen as an additional safety check with its own requirements.

Before placement of the armour layer it should be visually checked that there is no S-profile present. Only large S-profiles, which are easily visually observed, cause an early and abrupt failure behaviour. If a S-profile is observed, the under layer should be re-profiled.

During placement of the units, the key aspect for good interlocking capacity is that the straight angle at the nose of the unit is locked behind the two wings of the two downward units. Depicted in figure 7.16 with a red circle. The interlocking of the wings behind the right angle at the tail of the two downward units is preferred, but not a necessity. This is depicted in the figure with a smaller orange circle.

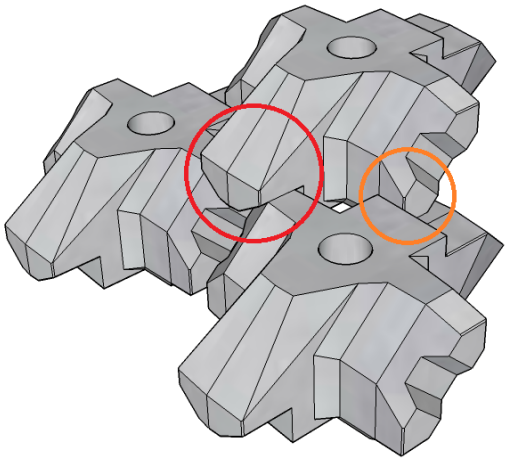

Figure 7.16: Interlocking points armour units

7.2.3 Margins

Several choices have been made to ensure safe requirements as tolerances. Firstly, the relative angles of the under layer on which the requirements are based are underestimations of the real relative angles due to the effect of smoothing. Secondly, the requirements are limited by the lower bound of the test results and multiple subsequent measurements must be close to the maximum allowed deviation to exceed this limit. Thirdly, the tolerances are based on the expected most critical location, indicating that at most locations in the cross section the stability will be higher. Lastly, the interlocking of the armour units is checked during placement. Which ensures that the stability is maintained, when the under layer is placed within the tolerances and no S-profile is created after the survey.

The multiple conservative choices indicate that the tolerances are rather strict and indicate possibilities for more liberal requirements. Therefore it is not considered to be necessary to state additional margins to take measurement inaccuracies into account.

Chapter 8: Discussion

The choices made during this research concerning the set-up of the model tests and the processing of the data, have effected the outcome of the results. The limitations of the choices made and the expected effects are discussed in this chapter.

8.1 Model set-up

In the choices for the model tests the main limitation was availability of time. To limit the amount of tests and focus mainly on the effect of the irregularities in the under layer, other parameters had to remain constant. With the result that the exact effect of the parameter remains largely unknown. The choice of the constant parameter however still influenced the result. The reasoning behind the made choices and their expected effect on the results are discussed in this section.

8.1.1 Location cross shore irregularities

The radii of the expected critical irregularities are much smaller that the length of the profile. In cross shore direction this induced an additional parameter for the location on the slope. Multiple locations have been tested but not all possible locations could be considered.

The choice for the location was based on the expected location of damage and the expected location of the irregularities shape in the S-profile. For the convex shape these locations were both estimated to be between 1.0 and 1.5 H_s below the still waterline. In figure 8.1 it can be seen that the location of the convex shape indeed corresponds well with the S-profile.

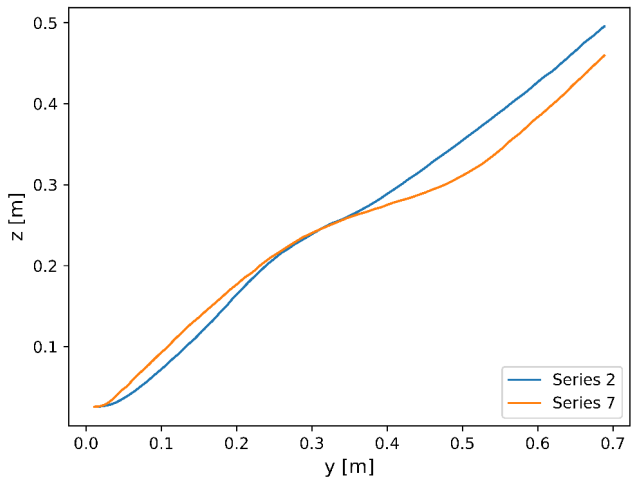

Figure 8.1: Comparison location convex shape (series 2) and S-profile (series 7)

The test higher on the profile confirmed that the convex shape was indeed more critical below the waterline. During the test with micro irregularities, failure also occurred around

the same location as the convex irregularity was placed. Thereby confirming that this is indeed the critical location.

Damage did not occur for the concave shape and thus an estimation of the effect of the location can not be given. Because the shape is not critical for the tolerances this is not considered to be of importance.

8.1.2 Under layer grain size

The D_{n50} of both the core and under layer have been chosen relatively small and of the same gradation. This choice has been made to prevent thickness of the under layer to influence the results and because a small gradation gives a conservative result with respect to the stability.

A small gradation however results in a smoother slope at a length scale of one D_n. This is counteracted by the fact that in practice a wider grading is applied and thus the gaps between the individual stones will be smaller than for a tight grading. Moreover, the requirements of the tolerances are expressed in terms of the unit size. The requirements are therefore relatively more strict for under layers with a larger grain size and are therefore required to be placed more accurately. All things considered, it is expected that the influence of the D_{n50} is small. As long as it is within the 1/10 - 1/20 W_{50} range.

8.1.3 Quality of placement

Due to experience with placement of 3000 model armour units before start of the test program, it is not expected that there is a difference in speed or quality of placement between the beginning and the end of the test program.

The quality of placement is judged on the preservation of the design grid spacing beyond expected distortions by irregularities. The quality is thus considered to be maintained when no additional errors are observed.

In section 6.9, it was observed that there is no significant difference in the required placement time between different tests and series. It was however expected that the presence of irregularities would increase the placement time. In the analysis of the test results it is assumed that placement quality is the same for all tests. The lack of increase in required placement time however, could be compensated by a decrease of placement quality.

In figure 8.2 the average, maximum and minimum grid spacing in x-direction are depicted for every series. The figure shows that with only a few exceptions, the grid spacings of all the tests are close together. The only exceptions are in series 4 and 5, which have a irregularity in x-direction. All average values are just above design value of the grid spacing and no correlation can be seen between grid spacing and placement time. The grid spacing in x-direction is a good measure for the placement quality for the irregularities in y-direction, which is the critical direction for the determination of the tolerances. The results therefore indicate that there are no large differences in placement quality besides the direct influence of the irregularities.

For the y-direction there is also no correlation visible between grid spacing and placement time, as is depicted in figure 8.3. The spreading between the minimum and the maximum values is larger than in x-direction. This indicates that the unit is more sensitive for deviations in y-direction, which is in line with the test results. It can therefore be expected that the spreading is caused by the irregularities and no additional placement

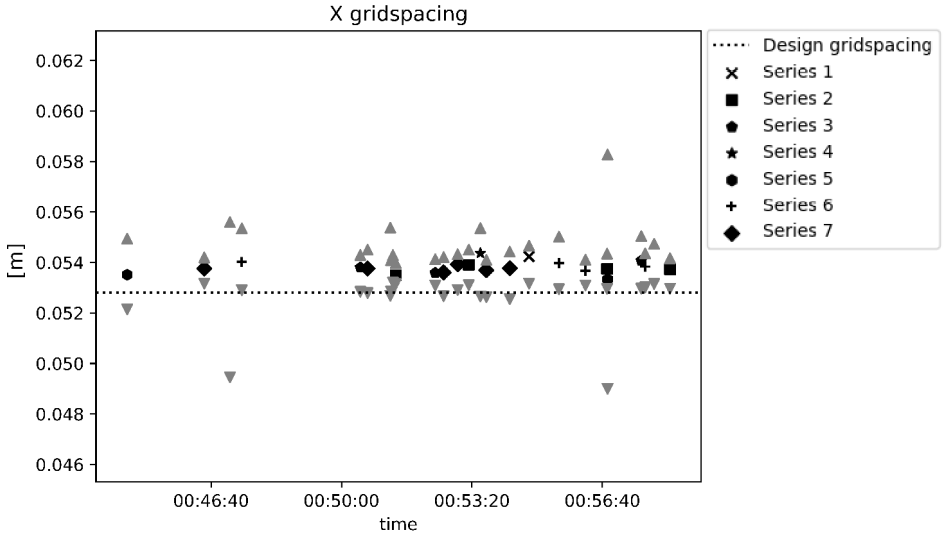

Figure 8.2: Grid spacing in x-direction relative to placement time

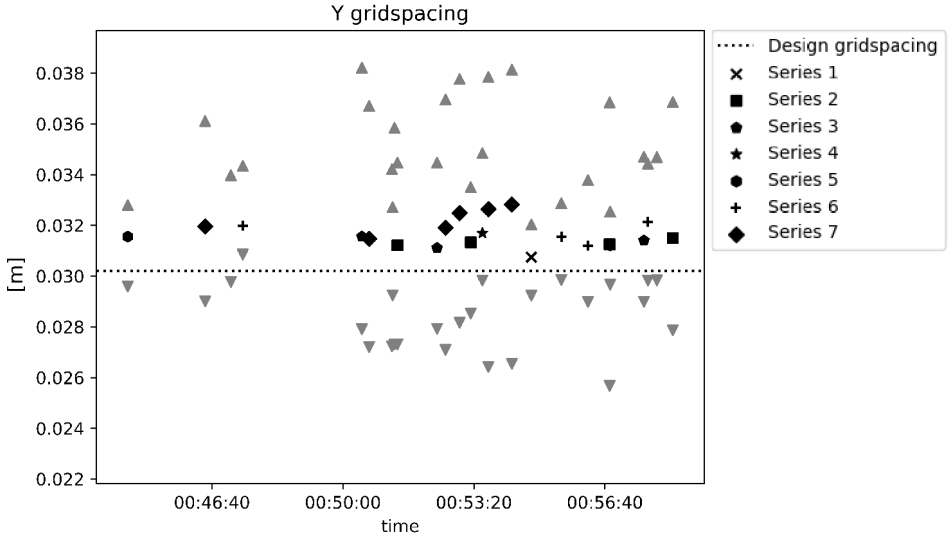

Figure 8.3: Grid spacing in y-direction relative to placement time

errors have influenced the results. That the average values are above the design values indicates that the design values might have to be adapted.

The spreading of grid spacing in y-direction could induce deviations at the crest of the structure. Since the tolerances are stricter in practice than for the test configurations, the differences at the crest are expected to be smaller. For strict requirements at the crest however it might be necessary to take additional measures and use stricter tolerances.

For irregularities in long shore direction some wash out of the under layer was observed due to the larger space between armour units. This however mainly occurred for wave overload situations and is not expected to occur within limits of the set tolerances.

8.2 Data processing

The data of the under layer configuration is extracted from the 3D-models made with Autodesk Recap. Certain steps in the creation and further processing of this data can induce errors in the outcome. Possible errors and expected effects of these errors are discussed in this section.

8.2.1 Measurement technique

During this study a consideration for multiple measurement techniques was made. However with a larger investment of time more techniques could be considered or the method with ReCap might be optimised. Or a fully open source method might be created. A more precise determination of the accuracy and the effect on the results could be made, also compared to other measurement techniques.

Measurements of the full (model) breakwater is in development and new possibilities of OpenSource software and image processing makes detailed measurements more widely available. Giving opportunities for quantitative evaluation of damage as was applied by Garcia et al. [2013] and de Leau [2017]. Another opportunity is the quantification of random placement, which has been studied by Pardo et al. [2012]. Evidently, these type of measurements provide a whole range of research possibilities with a relatively small investment.

8.2.2 Model creation

The quality of the models is influenced by the quality of the photos and the precision of target registration. In this study all models were created with at least 40 pictures, for which the out of focus pictures have been eliminated from the collection. Therefore no large differences between the quality of the models is expected.

The models are placed and scaled with four targets at fixed positions. The registration of the targets is manual and thus every target is registered on at least eight pictures. The zoom function in ReCap made it possible to reach pixel scale precision, as can be seen in figure 8.4. The targets were selected when clearly visible and from different angles to increase the measurements precision. Due to these measures the models are expected to be accurately placed into the same axial system.

The precision of the target registration could however be improved by applying sub-pixel accuracy. It has been visually attempted to register the target such within the pixel that this accuracy is reached, the method is however not reliable. Further use of OpenCV in Python could be applied to find the corner points of the targets exactly. For this research however, it was not possible to combine the functionalities of Python and ReCap to detect the targets automatically and with sub-pixel precision.

The photos used for extraction of data, were made before the application of any waves. This means that initial settlements have not been taken into account. In practice however, surveying of the under layer is also expected to be conducted directly after placement. In addition, the initial settlements are expected to be small since they have not been observed visually.

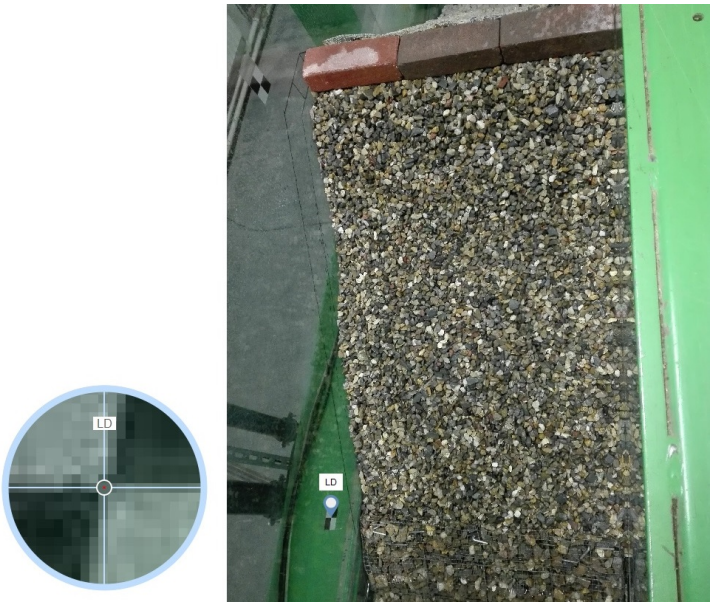

Figure 8.4: Target registration

8.2.3 Finding unit locations

The unit locations are found with MatchTemplate from OpenCV [Docs.opencv.org, n.d.]. Because the orientations of the units differ due to the influence of irregularities, the template does not always match the unit exactly. The MatchTemplate package searches for the best match and therefore most units are found correctly. This has been visually checked during the processing, as explained in section 5.1. The unit orientations of the top surface are calculated at the center of the units, to prevent points outside the top surface from being taken into account. Only for irregularities in long shore direction significant errors were observed. However, because these irregularities are not critical for the tolerances this has not influenced the results.

A higher precision for finding the unit locations could increase the accuracy of the orientations. In this research, a relative small area has been taken to determine the unit orientations. This choice was made to prevent edges and neighbouring units from effecting the results. A higher precision for the location and taking into account the horizontal rotation of the unit, will result in a larger useful surface and subsequently into a more accurate result.

8.2.4 Corresponding location unit on under layer

The location of the armour unit has been correlated with the under layer by using the horizontal distance between the center of the unit and the contact point with the under layer, in combination with the orientation of the unit. Both the found location of the units and the determined angle may contain errors. The effect of an error in the exact location of contact between the armour unit and under layer is however reduced due to the smoothing of the under layer. Additionally, the use of relative angles makes the angle at the exact location less important. This because the change in angle over a certain distance is the aspect of interest. The plots in figure 6.10 show that the correlation between the angles of the armour layer and of the under layer is strong. Which indicates that the influence of the under layer on the armour layer is determined correctly.

8.2.5 Smoothing of under layer

The smoothing of the under layer filters out the individual grains and thus reduces the small scale peaks and holes in the profile. In practice the measurements will also have some deviations from the exact profile. With the semi-spherical foot staff, the holes are reduced and the peaks are increased due to the height and width of the semi-sphere. This effect is visualised in figure 8.5, in which the resulting profile of a simulated semi-spherical foot staff measurement is depicted.

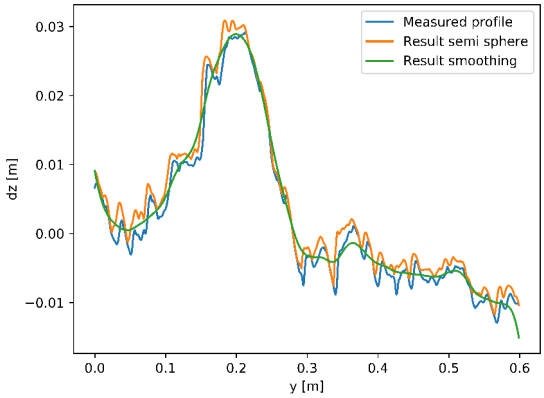

Figure 8.5: Deviation from the design profile of test 3 from series 2

In practice the distance between the semi-spherical foot staff measurements will be larger, which may cause certain peaks not to be measured. The total result is however not expected to be below the smoothed profile.

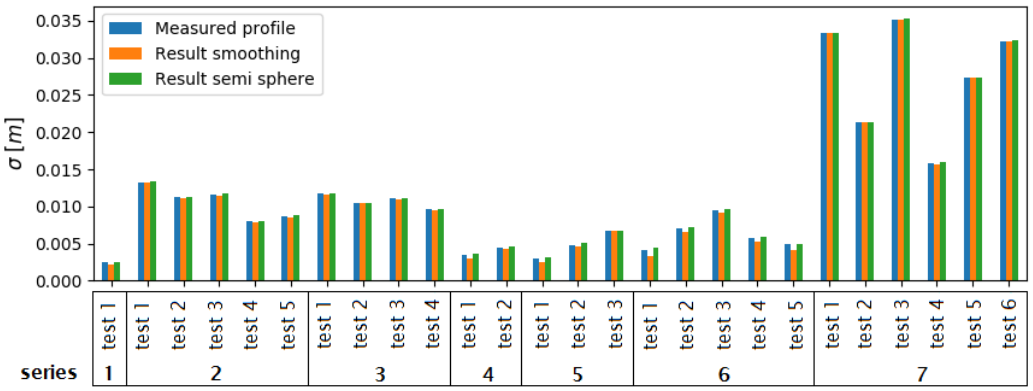

Figure 8.6: Standard deviation of different filters compared to the measured profile

In figure 8.6 it can be seen that the deviation as a result of the semi-spherical foot staff is equal to or larger than the originally measured profile. The requirement for the maximum deviation from the design profile is based on the measured profile without filter. Which indicates that in comparison with practice, the set requirements are representable and even slightly conservative.

Chapter 9: Conclusions and recommendations

The objective of this research was to gain insight into the effect of irregularities in the under layer on the stability of the Xbloc^{Plus}. The research questions stated in section 1.1 are repeated and answered in the first section of this chapter. The recommendations for further research can be found in the second section.

9.1 Conclusions

The main question of this research is:

What is the effect of irregularities in the under layer on the stability number of the Xbloc^{Plus} concrete armour unit?

The answer to this question has been found by performing 28 tests with a total of 193 runs with increasing wave heights. Each test had a different configuration of the under layer and each type of irregularity was part of a separate series. The concluding findings of the results of the tests are presented in this section.

9.1.1 Level of stability

How have the changes between the different versions of the Xbloc^{Plus} affected the level of stability?

The level of stability without any intentional irregularities is larger than N_s=3.88, which is 1.55 times the design value of the Xbloc^{Plus} of N_s=2.5. Further tests with higher stability numbers have not been performed, due to limitations of the model set-up. Therefore, the exact level of stability without intentional irregularities remains unknown.

Comparison with test results of earlier research proved that the increase of porosity and the increase of interlocking both have a positive effect on the level of stability. The beneficial effect of the increase in porosity confirms the conclusions of earlier research, that the failure of the Xbloc^{Plus} is induced by overpressure underneath the armour layer.

9.1.2 Critical configuration

How do irregularities in the under layer with both convex and concave shapes and in cross shore and long shore direction affect the stability of the Xbloc^{Plus}?

The convex shape in cross shore direction is the only shape for which failure occurred during the test program and this is thus the most critical configuration. For the convex irregularity in long shore direction settlements were observed when insufficient support was observed during placement. No extraction of any units occurred, but the structure is expected to have been weakened. For the concave irregularities in both cross shore and long shore direction, neither settlement or extraction have been observed.

The critical convex shape is affected by both the relative angle between the armour units and the deviation from the design profile. A large relative angle causes a loss of interlocking and enables armour units to be extracted by overpressure. A large deviation from the design profile enforces a failure mechanism similar to the buckling of beams, in this study referred to as the 'arching mechanism'. The pressure inside the breakwater, the drag of the down-rush and the weight of the upper part of the slope, cause the initial distortion of the profile to be enlarged. The effect of the mechanism is amplified by the deviation from the design profile, the length of the steep slope underneath the convex shape, the flatness of the area above the convex shape and the steepness of the upper slope. This causes the shape of an S-profile to be very sensitive for this failure mechanism. S-profiles with a deviation from the design profile larger than 1.0 D_n, can even fail in a brittle fashion without any previous loss of interlocking. In less severe cases the arching mechanism slowly develops a loss of interlocking and enables armour units to be extracted by overpressure.

The small length scale of micro irregularities cause the influence of the arching mechanism to be insignificant. The stability fully depends on the relative angles between the armour units and failure only occurred when the interlock was already observed to be insufficient at placement.

9.1.3 Configuration measurements

How can the configuration of the under layer be measured sufficiently accurate within the limitations of time and costs?

For this study the configuration of the profile had to be known precisely, for the full test section and without a large investment of time or money. The program Recap Photo of Autodesk proved to be the best choice to obtain these goals. The program enables to measure the full test configuration with a precision of maximum ±3mm and a standard deviation of less than 1mm. The calculated angles have an average standard deviation of 2.2° for the armour layer and 0.4° for the under layer in both x- and y-direction. The errors are expected to be random and to be further reduced by averaging over the three models made at the same moment.

Besides the ReCap program only a regular camera is necessary to create the ReCap models. The output is a digital model of a 3D mesh and point cloud, which can be further processed with Python or any other analytical software.

9.1.4 Execution tolerances

What are the practical achievable execution tolerances for the under layer of the Xbloc^{Plus}?

In practice the profile of the breakwater is measured every 10m along the length of the breakwater [van der Zwicht, 2015]. For the measurement the maximum allowed deviation from the design profile is 0.25 D_n. Additionally, succeeding measurements along the profile are allowed a maximum deviation 0.1 D_n. With a distance between the measurements of 0.3 D_n.

These requirements are a little more liberal than the tolerances of the regular Xbloc, since they are comparable to the current tolerances of the regular Xbloc for the largest under layer size (1/10 W_{50}). The requirements of the Xbloc^{Plus} are linked to the unit size

to avoid deviations in the allowed tolerances for different under layer sizes. The consequence is that in terms of under layer diameters, relatively more deviations are allowed for smaller under layer sizes. The contractors prefer to have the tolerances expressed in terms of the D_{n50}. Therefore it is recommended to translate the tolerance into the size of the under layer after the grading has been set.

As an additional check the interlocking of the units is checked during placement. The unit is sufficiently interlocked when the right angle at the nose is fixed behind the wings of the two lower units. Before placement of the units it must be confirmed visually that there is no S-profile present. Due to the strictness of the tolerances and the additional measures during placement of the units no additional margins are considered to be necessary.

9.2 Recommendations

Recommendations for further research are made, based on the observations and analysis of the test results, combined with experiences from practice.

Unit strength
The unit strength should be further researched in terms of both stability and concrete strength. Since no failure has occurred without intentional irregularities, the full capacity of the stability level remains unknown. The known capacity is already far above the design value. A reduction in the design value however results in a smaller unit size and thus more units to be placed. An optimum could be found between the amount of material and the amount of units to be placed.

The cross-sectional shape of the profile and the amount of rows, determines the weight that rests on a certain unit. At a certain point the concrete strength of the unit could become limiting. It should be checked in which situations this occurs.

Acceptable waves
Multiple configurations with S-profiles have been tested and it was found that the Xbloc^{Plus} can fail in a brittle fashion when large S-profiles are present. The tested profiles exceed the stated tolerances but often the S-profiles are created after the survey has been conducted. Therefore it would be useful to know which wave conditions are allowed in the period between placement of the under and the armour layer. With the knowledge of the creation of S-profiles and the results of the tests, an analysis should be done of the allowed wave conditions for multiple under layer sizes.

Arching mechanism
The simplified model of the arching mechanism complies with the test results of the current study. The total mechanism however is very complex and the model should be further validated and possibly adapted. Further understanding of the mechanism could be reached by measurements of the pressure build up, with numerical modelling or with more continuous measurements of the profile development.

Long term effects
In the failed tests the movements of the armour layer could be clearly seen in the measured differences between the models before and after the tests. For tests where failure did not occur, it could still be seen that below the still water level the profile extended while above the still water level the profile settled. Due to time constrictions the models have

only been made before application of any waves and after the tests. Which means that either failure had occurred or the profiles had been exposed to a significant overload. As a consequence it is unknown whether the changes in the profile are due to initial settlements, due to overloading or are a constant process.

To prevent failure of structures due to slow progressing failure it is recommended to test for the existence of any long term effects. Especially with regard to the arching mechanism, it is important to know whether long term effects could cause small deviations to fail. The movements of the cross-sectional profile might stabilise or could only occur at a certain critical wave height. Measurements between the runs can indicate how the movements develop. Another option is to increase the duration of the runs and check whether this affects the results.

Monitoring systems

The tolerances are based on measurements of the profile at every 10m of breakwater. With digital simulations of survey systems it could be checked how reliable this requirement is and whether it is still sufficient. The current survey system should also be compared with other systems to investigate whether new possibilities for survey systems might be more efficient and reliable. Different measurement systems will give different data and new methods may induce new possibilities.

With the acquired data of the test configurations different monitoring systems could be simulated and the influence of the systems could be assessed. Based on the results it could be decided to make the tolerances more liberal or to measure a different parameter than the deviation from the design profile. Especially if the full area of the breakwater is measured, the possibilities for methods to define tolerances increase and a more optimal system with regard to both ease and safety may be found.

Placement

Grid spacing measurements indicated that the average distances were larger than the design values. It should be checked what caused this deviation and whether the design values should be adapted. The value of the grid spacing is expected to depend on the slope. It should be checked if this influence is significant enough to make the design value dependent of the design slope.

The placement time and quality have been assessed based on the model measurements. It should be checked how the difference in placement in model and in real scale effect these aspects.

Since a convex shape in cross-shore direction has proven to be more vulnerable for failure it might be beneficial to place the under layer in a concave shape. This will however change the distribution of forces over the profile. It will increase the forces between the units at the steeper parts and the under layer will be difficult to place at the steep parts. Additionally, a concave shape will increase the horizontal forces at the toe. Making a more robust toe necessary. For now it is advised to attempt to place a straight slope, further optimisations might however be possible.

Bibliography

Angremond, K., Van Roode, F. C. and Verhagen, H. [2008], *Breakwaters and closure dams*, 2nd edn, VSSD, Delft.
URL: *uuid:9fdac7ea-bd42-49a7-8078-cbc9af9e35e6*

Arena, F., Soares, C. and Petrova, P. [2010], Theoretical analysis of average wave steepness related to peak period or to mean period, *in* 'International Conference on Offshore Mechanics and Arctic Engineering - OMAE', Vol. 2, American Society of Mechanical Engineers, Shanghai, pp. 595–603.

Brouwer, M. [2013], The influence of the under layer on the stability of single layer armour units Master of Science Thesis, Master thesis, Delft University of Technology, Delft.
URL: *uuid:6b142495-00d3-4ed4-a73e-65c74e30c577*

Burcharth, H., Christensen, M., Jensen, T. and Frigaard, P. [1998], Influence of core permeability on Accropode armour layer stability, *in* 'Coastlines, structures and breakwaters', pp. 34–45.

Burcharth, H., Liu, Z. and Troch, P. [1999], Scaling of core material in rubble mound breakwater model tests, *in* 'International Conference on Port Engineering in Developing Countries', Cape Town.

de Leau, J. [2017], Laboratory experiments on the stability of concrete cubes: a comparison of testing methodologies, Master thesis, Delft University of Technology.
URL: *uuid:39da4d6b-e60e-4e0e-8a37-4fda0456dd3a*

Docs.opencv.org [n.d.], 'OpenCV MatchTemplate documentation'.
URL: *https://docs.opencv.org/2.4/modules/imgproc/doc/object_detection.html?highlight=matchtemp*

Garcia, N., Eau, A., Richardson, S., Wallingford, H. R. and Kingdom, U. [2013], Physical Model Testing of the Hydraulic Stability of Single-layer Armour Units, *in* 'Coasts, Marine Structures and Breakwaters Conference', Institution of Civil Engineers, Edinburgh.

Heller, V. [2011], 'Scale effects in physical hydraulic engineering models', *Journal of Hydraulic Research* **49**(3), 293–306.
URL: *http://dx.doi.org/10.1080/00221686.2011.578914*

Jacobs, R. [2017], 2D Hydraulic Model Tests, Technical report, Delta Marine Consultants, Gouda.

Jacobs, T., Junge, T. and Pastewka, L. [2017], 'Quantitative characterization of surface topography using spectral analysis', *Surface Topography: Metrology and Properties* **5**(1).
URL: *http://stacks.iop.org/2051-672X/5/i=1/a=013001*

Jiménez Moreno, A. [2017], Experimental study on the wave overtopping performance of Xbloc+ armour unit, Master thesis, Delft University of Technology.
URL: *uuid:b4bbc14f-12db-4858-b9d8-2c1b12dd76c7*

Kirkegaard, J., Wolters, G., Sutherland, J., Soulsby, R., Frostick, L., McLelland, S., Mercer, T. and Gerritsen, H. [2011], *Users Guide to Physical Modelling and Experimentation*, CRC Press, Hull.

Mansard, E. and Funke, E. [1980], The measurement of incident and reflected spectra using a least squares method, *in* 'International Conference on Coastal Engineering', ICCE, Sidney, pp. 154–172.

Martin, F. L., Lomonaco, P. and Vidal, C. [2002], A new procedure for the scaling of core material in rubble mound breakwater model tests, *in* 'Coastal Engineering', ICCE, Auckland, pp. 2203–2215.

Ozbahceci, B. O., Takayama, T., Mase, H. and Ergin, A. [2004], 'Wave Grouping and Spectral Shape Effects on the Stability of Rubble Mound Breakwaters', *Coastal Structures* **40733**(November 2014), 113–125.
URL: *http://ascelibrary.org/doi/abs/10.1061/40733%28147%2910*

Pardo, V., Herrera, M. P., Molines, J. and Medina, J. R. [2012], Placement grids, porosity and randomness of armor layers, *in* 'Coastal Engineering', American Society of Civil Engineers, New York, pp. 1–11.

Perrin, S., Giraudel, C., Collinsworth, S. and Melby, J. [2017], Hydraulic response & placement methods for a new single-layer concrete armour unit called C- ROC ™, *in* 'Coasts, Marine Structures and Breakwaters Conference', Institution of Civil Engineers, Liverpool.

Rada Mora, B. [2017], Hydraulic performance of Xbloc+ armor unit, Master thesis, Delft University of Technology.
URL: *uuid:fbe797ef-5944-4bc1-9d25-e7448dce3d1b*

SBRCURnet [2014], Construction and Survey Accuracies for the execution of rockworks, Technical report, SBRCURnet, Rotterdam.

Tanimoto, K. and Goda, Y. [1992], Historical development of breakwater structures in the world, *in* 'Coastal structures and breakwaters', Institution of Civil Engineers, Yokohama, chapter 12, pp. 193–206.
URL: *https://doi.org/10.1680/csab.16729.0013*

Van der Meer, J. [1987], Stability of breakwater armour layers - design formulae, *in* 'Coastal Engineering', Coastal Engineering Research Counsil, pp. 219–239.

van der Zwicht, B. [2015], Specifications of Application Xbloc, Technical report, Delta Marine Consultants, Gouda.

Vos, A. B. [2017], Exploration into the mechanisms that govern the stability of an Xbloc+ v1 armour unit, Master thesis, Delft University of Technology.
URL: *uuid:dd61dbae-67ea-4a67-b5f2-b9691240f729*

Wenneker, I. and Hofland, B. [2014], Optimal wave gauge spacings for separation of incoming and reflected waves, *in* 'International Conference on the Application of Physical Modelling in Coastal and Port Engineering and Science', Coastlab, Varna.

List of Figures

List of Tables

Appendix A: Previous research

The succeeding versions of the Xbloc^{Plus} have been developed based on the conclusions of multiple studies. By comparing the results of the tests performed with different versions, the previously drawn conclusions are validated. The validation of the previous conclusions, results in statements of the influence on the stability which are used to form the hypothesis of the current study.

A.1 Influence of porosity

The influence of the porosity on the stability is determined by comparing the test results of V1 and V2. Because the tests in the current study are done with a 3:4 slope and a wave steepness of 0.04, these are also the values used for the comparison. However, for this configuration there was no failure reached during the tests of V2.

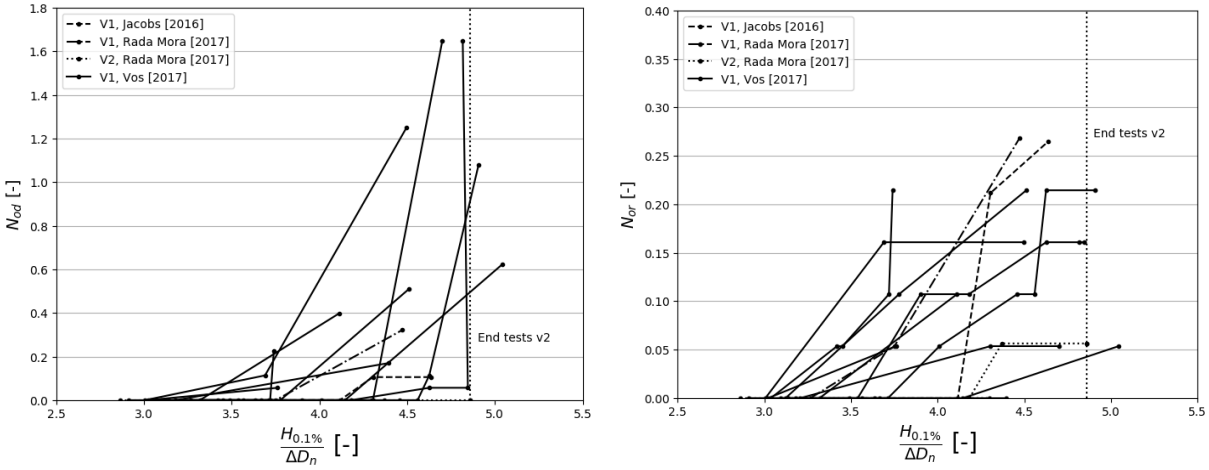

(a) Number of displaced units

(b) Number of rocking units

Figure A.1: Comparison of Xbloc^{Plus} V1 and V2, slope 3:4 and wave steepness 0.04

In figure A.1a can be seen that the tests of V2 are stopped at a point that most tests of V1 have already failed or have a larger amount of damage. According to judgement based on the start of damage V2 performs better than V2. In case of rocking, V2 also performs better than V1 for both the start and the development of rocking. This can also be seen in figure A.1b.

The differences are small and because the further development of damage is not known for V2 with a slope of 3:4 and a wave steepness of 0.04, the differences between V1 and V2 are checked with wave steepness 0.02 and 0.06. This is depicted in figure A.2.

In this figure it can be seen that for a wave steepness of 0.02, V2 performs indeed better than V1, again both for rocking and displacements. For a wave steepness of 0.06 the results of V1 and V2 are very similar, therefore it can be stated that the effect of the increase in porosity depends also on the wave steepness.

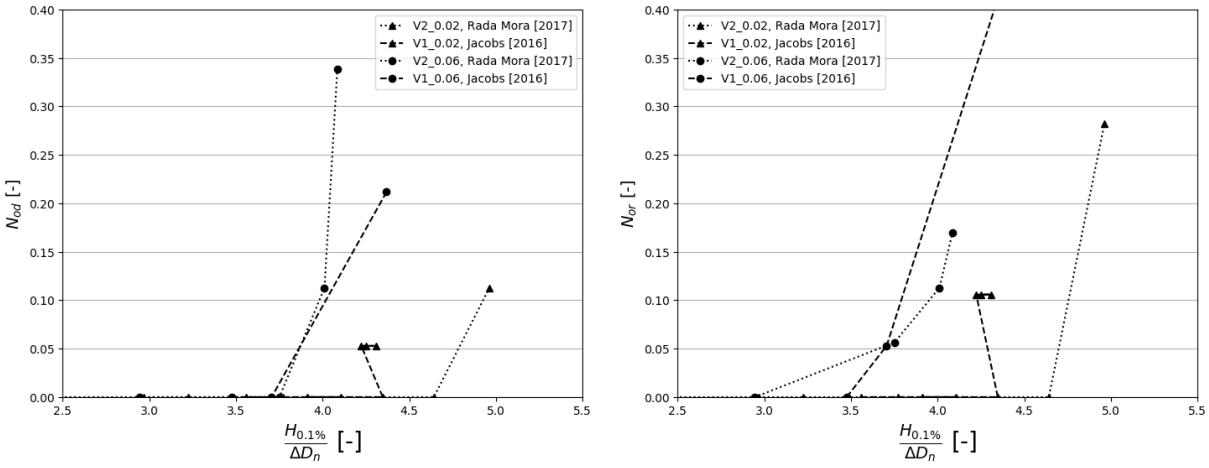

(a) Number of displaced units **(b)** Number of rocking units

Figure A.2: Comparison of Xbloc$^{\text{Plus}}$ V1 and V2, slope 3:4 and wave steepness 0.02 and 0.06

The influence of the wave steepness is caused by the shorter duration of up and down rush. Because of the limited duration of high water level outside of the structure the internal water level will increase less. This results in less overpressure during down rush and thus less effect of the increase in porosity. The effect of both the porosity and the wave steepness is depicted in figure A.3.

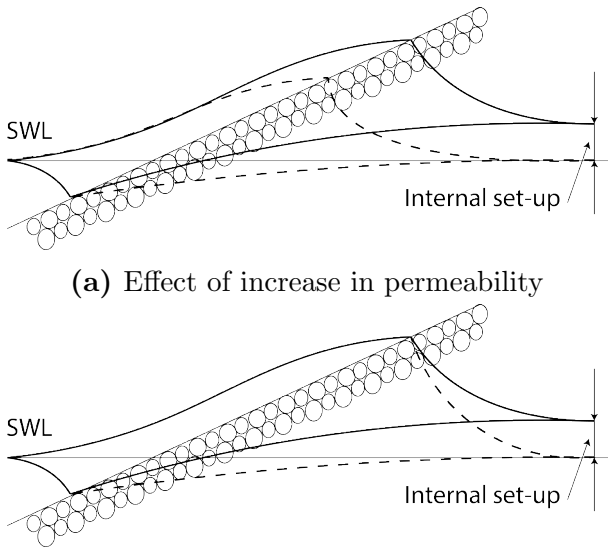

(a) Effect of increase in permeability

(b) Effect of increase in wave steepness

Figure A.3: Internal water table during up and down rush

The Xbloc$^{\text{Plus}}$ is less stable for a wave steepness of 0.06 than for a wave steepness of 0.02. That the change in porosity does not influence the stability for a wave steepness of 0.06 indicates that either the failure mechanism is different of the change in porosity is to small to have an influence. However, for a wave steepness of 0.04 the increase in porosity has increased the stability. Therefore it is concluded that for a slope of 3:4 and a wave steepness of 0.04 the conclusions of both Vos [2017] and Rada Mora [2017] are valid.

A.2 Influence of interlocking

The influence of the increase of interlocking can be determined by comparing the test results of V2 and V3. The tests of V3 are performed by Jacobs in august 2017 and is referred to as Jacobs[2017]. During the tests of V3 it was not possible to induce failure in the test-section due to the shallow water, the only failure that occurred was at the crest and at the side of the flume. To be able to further increase the wave height one test was performed with increased water depth. The result of this test is compared to the results of a similar test on V2, this is depicted in figure A.4.

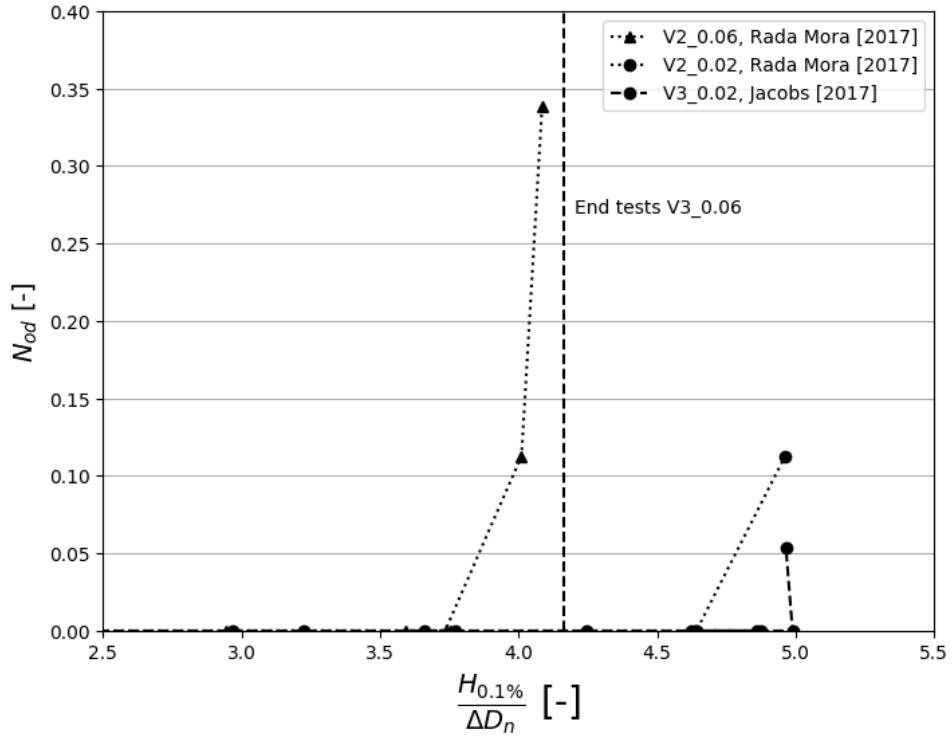

Figure A.4: Comparison of Xbloc^{Plus} V2 and V3 based on $H_{0.1\%}$ and N_{od}, slope 3:4 and wave steepness 0.02 & 0.06

In figure A.4 it can be seen that for a wave steepness of 0.02, V3 is slightly more stable than V2. However the failure of V3 occurred at the crest of the structure and only because there were not enough model units to build the crest at sufficient height. This means the intended test-section was still completely stable at this point. For wave steepness 0.04 failure did not occur for either V2 or V3 and for wave steepness 0.06 failure occurred for V2 while for V3 at higher wave height there was no observation of damage or rocking. From this it can be concluded that the increase of interlocking has a positive effect on the stability of the Xbloc^{Plus}, this validates the conclusions of both Vos [2017] and Rada Mora [2017].

Appendix B: Scaling procedure

The physical model tests are done for research purposes, this is why there is no prototype structure to be scaled. The scaling procedure is done such that it is representable as an actual breakwater structure and that the physical processes related to the stability are well represented. In this appendix the scaling procedure of the physical scale model is described. First a scale law is chosen, then the scaling effects of this law are assessed, concluding with the necessary deviations from the scale law to reduce the scale effects.

B.1 Scale law

The most common scale laws are Froude, Weber and Reynolds scaling. The choice for a scaling law is made based on which physical phenomena are most important. Waves are predominantly defined by the influences of gravity and inertia, which is why Froude scaling is most applicable. The application of Froude scaling leads to the following scale factors:

Wave height (m)	$n_H = n_L$
Time (s)	$n_T = \sqrt{n_L}$
Velocity (m/s)	$n_u = \sqrt{n_L}$
Acceleration (m/s^2)	$n_a = 1$
Mass (kg)	$n_M = n_\rho * n_L^3$
Pressure (kN/m^2)	$n_P = n_\rho * n_L$
Force (kN)	$n_F = n_\rho * n_L^3$

Because of the choice for Froude scaling the Reynolds and Weber numbers, which describe friction and surface tension forces, are scaled incorrectly. These forces are however negligible when the wave height is not smaller than 2cm, the flow is turbulent for both model and prototype and the water depth is sufficiently large.

B.2 Scaling effects

The scaling law is chosen such to induce the least scaling effects for the model. However, there are always certain phenomena that are influenced by this choice. In this case the most effects are induced by roughness and porous flow, which are not well represented by Froude scaling [Kirkegaard et al., 2011]. To reduce the influence of scaling, the effects need to be assessed and when possible reduced. In order to reduce certain effects it will be necessary to deviate from the Froude scaling.

B.2.1 Waves

It is not yet possible to scale short duration impact loads, such as wave impacts, correctly. Froude scaling will underestimate the loads that will occur in reality, because compressibility is not taken into account [Heller, 2011]. However, because of the slope of

the breakwater not the impact of the wave is the most important, but the run-up and run-down.

The influence of surface tension, described by the Weber number, can create wave motion damping of the waves that would not occur in prototype. This affect only occurs for waves smaller than 2cm and therefore does not pose a problem. The Weber number also influences the air intake when the breaking of waves occurs, but because the total energy budget remains the same this is not of high importance [Kirkegaard et al., 2011]. Because wave breaking is not expected, the scaling effect with relation to the waves is negligible.

B.2.2 Under layer

The effects of turbulence which is described by the Reynolds number, is not scaled correctly when Froude scaling is applied. The flow through the model structure and drag forces on the structure are influenced by scale effects. With Reynolds numbers above 30000 the flow is fully turbulent both in the model and the prototype and the effects will be limited.

The under layer and core can not be scaled geometrically because the small stone size will lead to viscous scale effects and reduce the permeability, causing energy to be reflected instead of being transmitted. Which results in less flow in the inner layers, increasing pressure on the armour layer, and higher run-up. By enlarging the grain sizes this effect can be reduced such that the effect becomes minimal, the procedure for this has been described by Burcharth et al. [1999].

B.2.3 Friction

The Reynolds number describes the behaviour due to friction and viscosity. The viscous effects are limited if the diameters in the model are larger than 3-5mm. The friction is of importance for the bottom friction and the friction between concrete units [Kirkegaard et al., 2011]. Bottom friction can be neglected when the water depth is large enough for the waves not to feel the bottom. Friction between the units can be scaled correctly by scaling the surface roughness, which is why the concrete armour units are modelled by plastic units. When all these aspects are taken in to account the scaling effect on the friction force is negligible.

B.2.4 Top layer

According to Heller [2011] the application of Froude scaling affects the drag-force, if the Reynolds-number is not above the critical value. This effect is less pronounced for cross-sections with sharp edges due to the fixation of flow separation. But will still be present in the upper part of the structure, where the flow will no longer be turbulent. This increases the flow resistance and the drag forces on the armour units during run-up and run-down. This effect results in a more conservative design for the armour units since lift force will increase due to the additional energy dissipation. Because the effects will be minor, and only increases the safety of the design, the effects can be neglected.

The stability of the top layer is described by the stability number (N_S). To scale this correctly, the stability number should be the same for both model and prototype. Because of the geometric scaling of the armour the density of the materials is scaled

correctly. However, in most models fresh water is used instead of salt water, reducing the buoyancy forces and affecting the stability number. This can be corrected by adjusting the weight of the model armour units or the design wave height such that the stability number is the same in both model and prototype [Kirkegaard et al., 2011].

B.3 Deviations from Froude scaling

As described above, most scale effects will be negligible. There are two cases however for which is deviated from the Froude scaling law of reduce the scale effects. In this section alternative scaling is chosen for both the under layer and the stability number.

B.3.1 Under layer

When Foude scaling is applied for the under layer and core of the structure, the Reynolds number becomes to low in the model with relation to a real scale situation. Effecting the viscous forces and permeability, causing scale effects in relation to wave-core interaction. Inducing errors in the armour stability, wave run-up, overtopping and forces on crown walls [**?**].

Alternative methods

It is difficult to scale correctly, because the wave-induced Reynolds number depends on the flux of water and this varies in time and space. The method proposed by Burcharth et al. [1999] to approximate the correct scaling, uses the time and space averaged pore velocity for the calculation of the Reynolds number in the core. The space averaging is done by choosing six characteristic points close to the armour layer and the SWL. In these points the characteristic flux velocity is calculated from the wave induced pressure gradient with the extended Forchheimer equation. The time averaged pore velocity is then used as characteristic velocity [Martin et al., 2002].

Martin et al. [2002] proposed to use four points and the RMS velocity instead of the time average velocity. However, for this method more details must be known of the prototype. Because there is no defined prototype in this case the method of Martin is not expected to provide improved scaling. Therefore the method of Burcharth is chosen as appropriate method.

Burcharth scaling

According to Burcharth et al. [1998], to avoid scale effects in the hydraulic response of the amour layer the flow fields in the core must be similar in both model and prototype. The similarity of the hydraulic gradient is acquired by the similarity of the hydraulic gradient I at geometrically similar points. The hydraulic gradient is estimated by the Forchheimer equation, which is the following:

$$I = \alpha \left(\frac{1-n}{n}\right)^2 \frac{\nu}{gd^2}\left(\frac{U}{n}\right) + \beta \frac{1-n}{n}\frac{1}{gd}\left(\frac{U}{n}\right)^2 \tag{B.1}$$

In which:

n = porosity
ν = kinematic viscosity of water
d = characteristic diameter of grains
U = discharge velocity
$\frac{U}{n}$ = pore velocity
g = gravitational constant
α, β = coefficients dependent on Reynolds number, grading and shape of grain material

For a given length scale ratio (λ) between the prototype and the model, the velocity scale is $\sqrt{\lambda}$ according to Froude scaling. In the method of Burcharth et al. [1999] the diameter is chosen such that the Froude scale law holds for a characteristic pore velocity. The characteristic pore velocity is chosen as the average velocity of a most critical area with respect to porous flow. The velocity is averaged in time over one wave period and in space over six points. Vos [2017] applied this method, which resulted in an D_{50} of 8,8mm.

B.3.2 Design wave height

The design wave height is scaled such that the stability number is the same for both model and future real life design. The stability number is determined by the wave height, the nominal diameter and the relative density. The relation between the wave height and the nominal diameter is determined by the design formula of DMC, which is as follows:

$$H_{s,design} = 2.5 * \Delta * D_n \tag{B.2}$$

In which:

$$\Delta = \frac{\rho_c - \rho_w}{\rho_w} \tag{B.3}$$

$$D_n = \sqrt[3]{V} \tag{B.4}$$

Relative density is determined by the density of the water and of the armour unit. Fresh water will be used during the tests, so the density is 1000kg/m^3. The density of the model amour units is measured by measuring the weight of 30 units in both dry and submerged situation. The average density is chosen as calculation value. The results of the measurements are shown in figure B.1. The resulting average density is 2360kg/m^3 with a standard deviation of 9,28kg/m^3.

The average dry weight of the model units is 58,4g with a standard deviation of 0,16g. With the dry weight and the calculated density, the volume and subsequently the nominal diameter are calculated. This results is a design wave height of 0,099m. As long as the future real life situation is calculated with the same design formula and the correct densities the design wave height is scaled correctly in relation to the stability number.

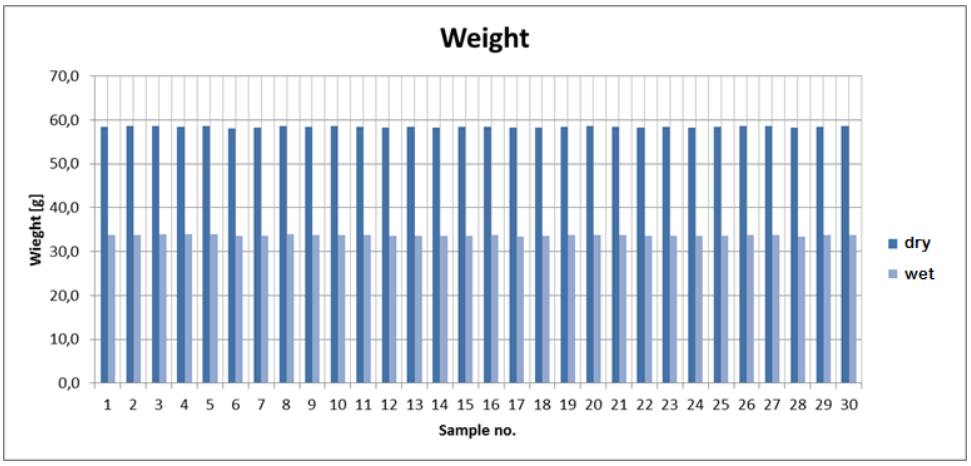

(a) Measured dry and wet weights

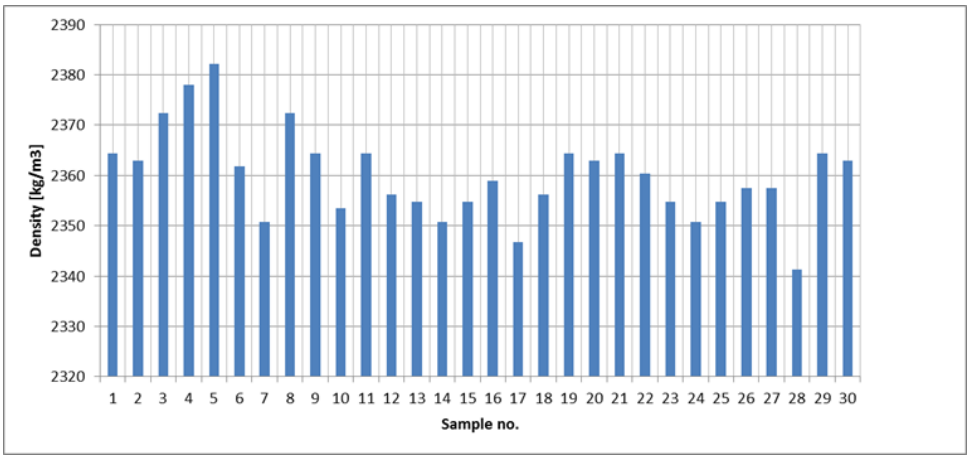

(b) Calculated densities

Figure B.1: Density measurements of model units

Appendix C: Measurement techniques

To ensure that the recorded data is as accurate as possible within the limits of costs and time the measurement techniques of the two most important data sets are discussed. To improve the accuracy certain choices are made for the set up and the applied techniques. The reasoning behind these choices is explained in this appendix.

C.1 Wave measurements

The wave heights are measures with wave gauges and the incoming and reflected waves are split with the theory of Mansard and Funke [1980]. The accuracy of this theory depends on the distance between the wave gauges as is described in de study of Wenneker and Hofland [2014]. During the experiments the water level will be measured with three wave gauges. The optimal distances between the gauges depends on the spectral shape and is derived from the results of Wenneker and Hofland. The distance is chosen such that the theory of Funke and Mansard is valid for the frequency range with the highest energy density. To determine which frequency range is of importance the spectral shape needs to be determined first. From the results of the spectrum the optimal gauge spacing is determined.

C.1.1 Wave spectra

For general breakwater design it is chosen that a young sea-state described by a JONSWAP spectrum with $\gamma = 3.3$ is most suitable and most common. The influence of the spectral shape on the stability of rubble mound breakwaters has been studied by Ozbahceci et al. [2004]. It was concluded that the spectral shape only indirectly affects the stability because it influences the occurrence probability of the extreme waves. The occurrence of extreme waves becomes higher when the spectral shape becomes more narrow which decreases the stability.

The JONSWAP spectrum is defined by H_s and T_p. The wave steepness (S_{0p}) is chosen as 4% because this is the most common wave steepness in storm conditions according to Angremond et al. [2008]. The design H_s is chosen based on the design formula of the Xbloc^{Plus}, formulated by DMC the following way:

$$H_{s,design} = 2.5 * \Delta * D_n \tag{C.1}$$

In which:

$$\Delta = \frac{\rho_c - \rho_w}{\rho_w} \tag{C.2}$$

$$D_n = \sqrt[3]{V} \tag{C.3}$$

According to Arena et al. [2010] the average steepness can be described as:

$$S_{0p} = \frac{H_s}{L_p} \tag{C.4}$$

In which L_p is the wavelength associated with the peak period. Because the wave length in deep water is described as:

$$L = \frac{g}{2\pi} T^2 \tag{C.5}$$

The peak period to obtain the required average wave steepness can be calculated with the following formula:

$$T_p = \sqrt{\frac{H_s}{S_{0p}} \frac{2\pi}{g}} \tag{C.6}$$

During the experiment the H_s will be build up from 60% of the design value until failure, with a maximum of 160%. The corresponding spectral shapes are displayed in figure C.1.

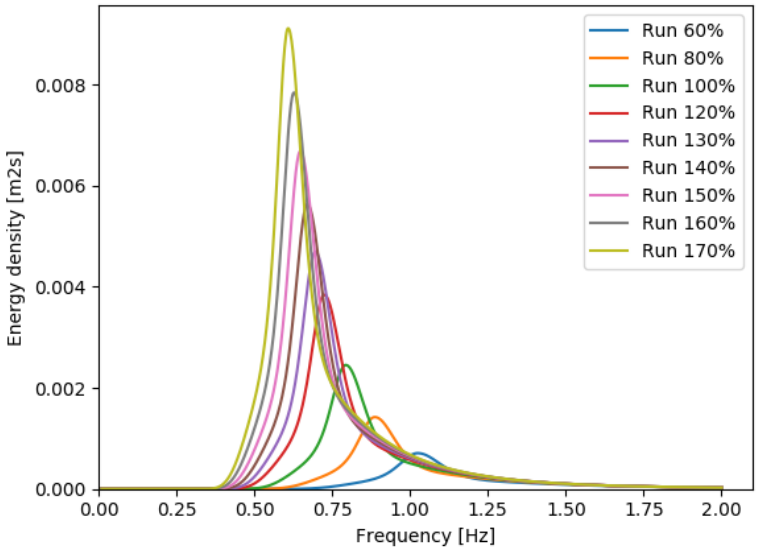

Figure C.1: Spectral shapes of separate runs

C.1.2 Optimal gauge spacing

The gauge spacing must be such that the theory of Mansard and Funke is valid for the range of wave lengths with a large energy density. The larger the part of the spectrum that falls within the range, the more accurate the wave analysis results will be. Wenneker and Hofland [2014] have calculated the error for a wide range of gauge spacing and visualised the result in a graph depicted in figure C.2.

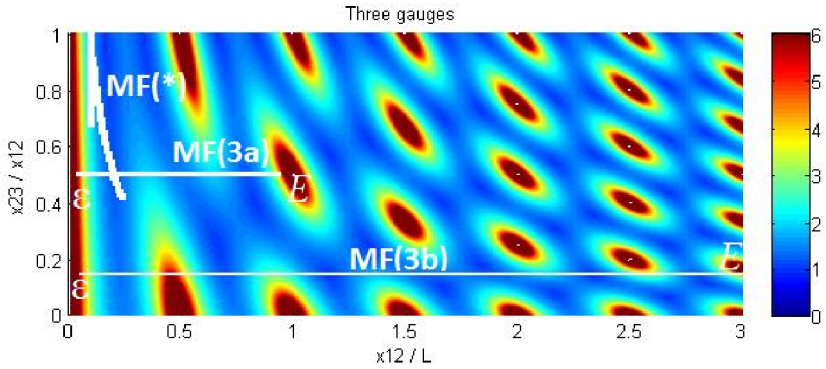

Figure C.2: Condition number as indication of error [Wenneker and Hofland, 2014]

The setup for the gages in the DMC flume has a distance of 0.4m between the first and the second gauge (X12) and 0.3m between the second and the third gauge (X23). The accuracy range of this setup is determined by first calculating the ratio between X12 and X23. Along this line the method is considered accurate for X12/L outside the dark red patches. The resulting range of accuracy is between the dotted lines in figure C.3.

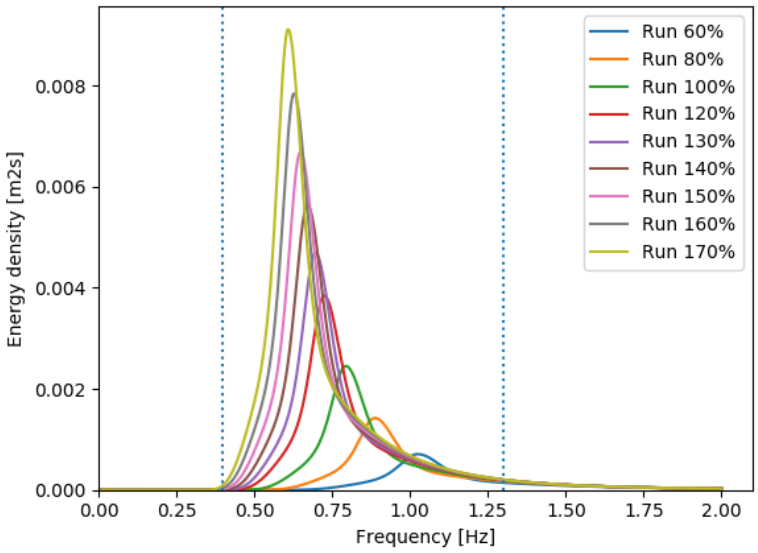

Figure C.3: Accuracy range (X12=0.3, X23=0.4)

The range covers the largest part of the spectra, only the tail of the spectrum will be analysed less accurate. This part is however of lesser importance because the energy density is low and thus the influence on the total result will be small.

C.2 Geometry measurements

To determine the sensitivity to irregularities in the under layer, it is necessary to measure these irregularities. Within the constrains of limited costs and time there are three measurement techniques that are considered for this study. The less applied techniques have been tested previous to the real tests in order to determine their accuracy.

C.2.1 Laser measuring

The more standard manner of measuring slope profiles is by laser measuring. This method was also applied in the wave flume of DMC in the study of Brouwer [2013]. Brouwer measured the slope profile at three locations and used the average of the measurements as data for his experiment.

The laser device itself is very accurate and has a maximum error of 0.75mm. However the laser is fixed to a wooden frame which is party fixed but can be moved to measure different parts of the slope, as can be seen in figure C.4a. Because the placement of the laser is done manually errors will occur which effect the accuracy of the measurements. Additionally the laser device generates some spikes in the measurements (figure C.4b) which are unrealistic and had to be corrected. Still the laser measurement technique is considered to be very accurate when attention is paid to the exact location and correction of the measurements.

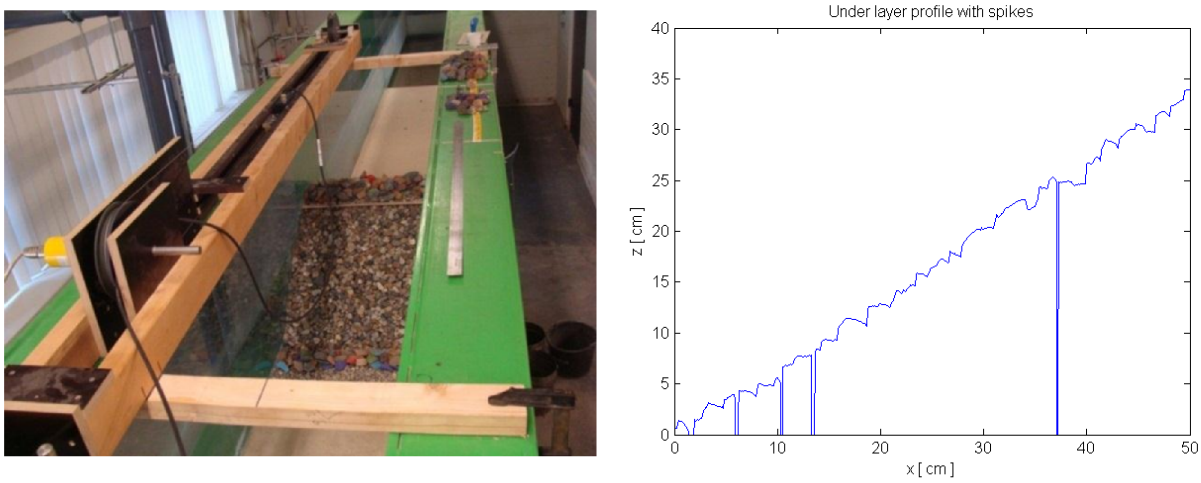

(a) Wooden frame to facilitate laser device

(b) Spikes in laser measurements

Figure C.4: Laser measurement technique [Brouwer, 2013]

The drawback of this technique is that the laser only measures a certain trajectory. For every new trajectory the laser has to be replaced in an accurate manner, which is very time consuming when a lot of trajectories have to be measured. Even with a large amount of trajectories it is still difficult to make a correct visualisation of the whole slope because there are always certain gaps between the measurements.

C.2.2 Stereo photography with Python

With stereo photography a 3D visualisation can be made out of two pictures from different angles and/or positions. Every photo must be taken from the exact same positions and the cameras must be calibrated in order for a reliable result to be obtained. To determine the reliability and applicability of the stereo photo technique some tests have been executed in the wave flume of DMC. The procedure of creating a 3D visualisation out of the two photos consists of the following steps.

Capturing the structure

The structure used for the tests is a structure that was already present in the flume and is a structure with an oblique orientation. For the tests two cameras were placed on tripods to ensure that they remained at the same location. The set-up of the cameras and the design of the used structure are depicted in figure C.5.

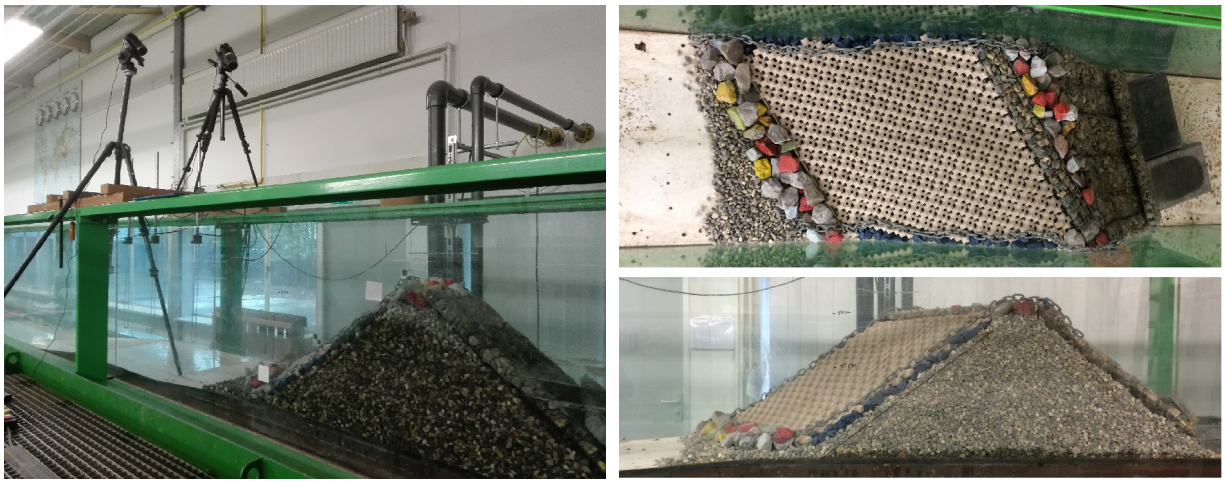

(a) Camera setup **(b)** Test structure, top and side view

Figure C.5: Capturing the structure

Twenty pictures were taken with both cameras of a checkerboard at differing locations and with differing angles. The pictures of the checkerboard are used to calibrate the cameras. After this both cameras captured the structure two times both with different lighting in order to assess the accuracy of the method.

Camera calibration

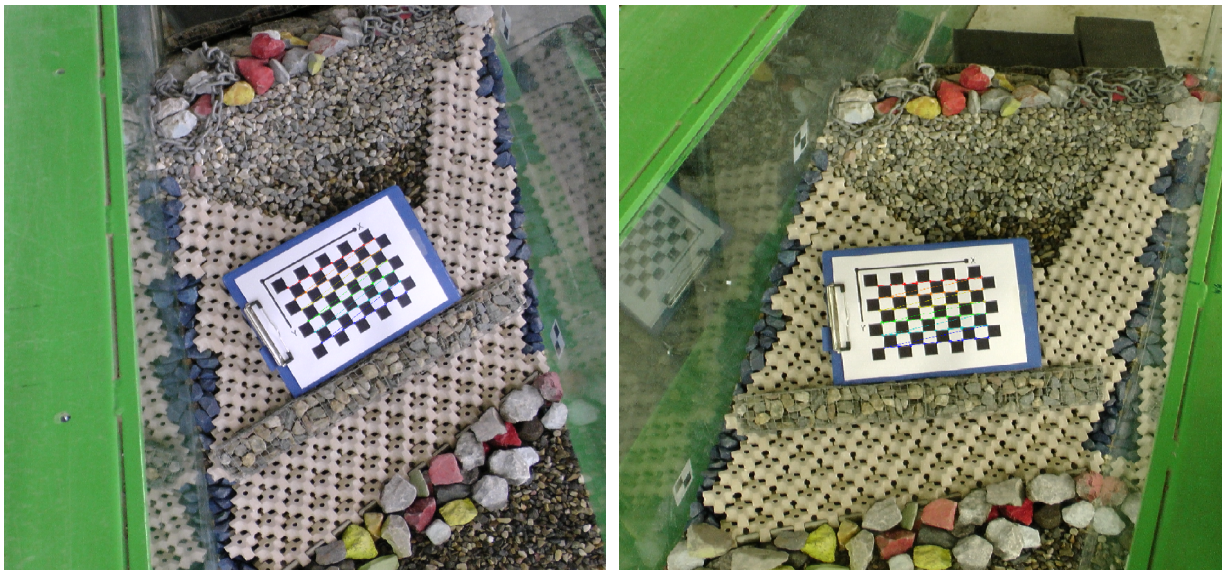

(a) Left camera **(b)** Right camera

Figure C.6: Checkerboard for camera calibration

The calibration of the cameras exists out of multiple steps, for this test the steps were performed with Python and the Python package of OpenCV. First the pictures of both

cameras are loaded into python, the camera parameters of both cameras and the error of the calibration are determined. OpenCV can calculates the parameters by detecting the checkerboard in the pictures and determines the exact location of all inner corner points. Because the real world size of the checkerboard squares is known the exact location and angle of the checkerboard and the distortion of the camera lens can be determined. The detection of the checkerboard is depicted in figure C.6.

The calibration of the cameras is checked by re-projecting the real world points into the image and measuring the difference between the projected and the detected points. The mean error of the points per photo is shown in figure C.7. The mean error of all photos is 0.075 mm, which is very small.

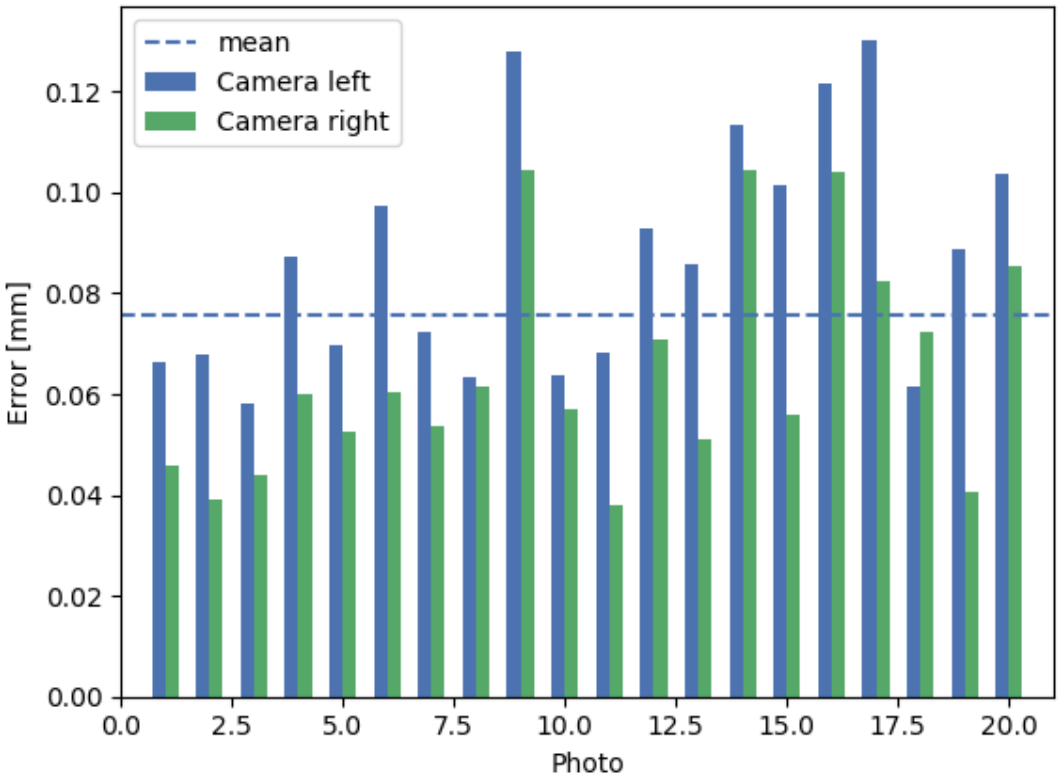

Figure C.7: Re-projection errors

After calibration of the separate cameras the cameras are calibrated together. OpenCV is able to determine the positions of the cameras relative to each other, again with the location of the checkerboards inner corner points.

Rectification of images

With all aspects of the two cameras known the images of the test-structure can be rectified such that all corresponding points are on the same horizontal location in the picture. This is checked by drawing horizontal lines across the pictures and determine if the horizontal position of all features are the same. The rectified images are depicted in figure C.8

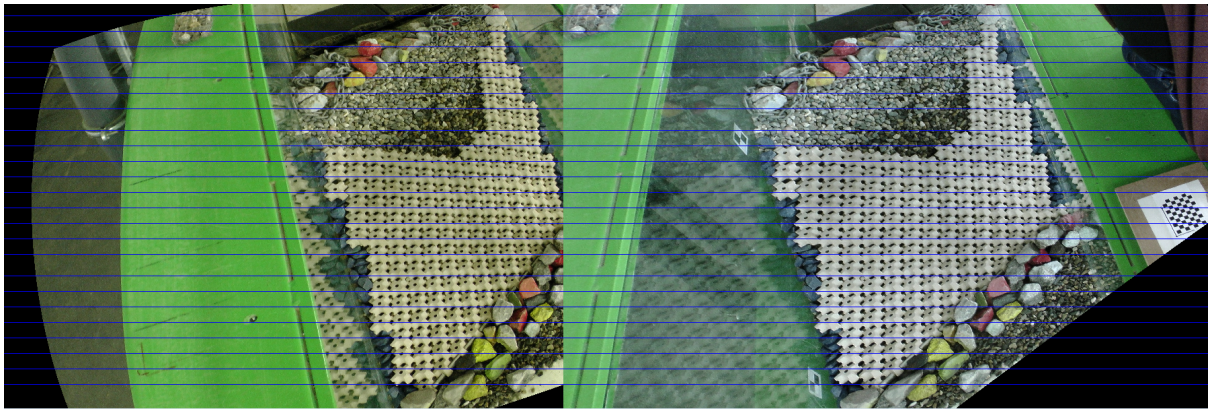

Figure C.8: Result of rectification

Disparity map

Because all pixels of the two pictures have been aligned horizontally each pixel in a row can be matched to a pixel in the same row of the other picture. In this case a Semi-Global Block-Matching (SGBM) was applied, which matches the pixels by matching the neighbouring pixels in five directions, applies smoothing and takes into account that the pixels have a certain sequence.

After matching the pixels the distance between the pixels on the separate photos is measured. From the distance between the pixels it is possible to calculate the distance between the camera and the real world coordinate of the pixel. Because the photos are taken from different locations the object has a different location in the respective pictures. The closer the object is to the camera, the smaller the shift on the pictures is. This distance is called the disparity and is visualised by projecting the disparity in grayscale on the first picture. In this case it resulted in the disparity map shown in figure C.9.

With difficulty it is possible to locate the position of the armour units by the repetitive pattern of disparity clouds. However there are a lot of black patches which indicates that no match has been found and no disparity has been calculated. It is possible to reduce the amount of blackness by adapting the parameters of the SGBM, but this results in an increase of noise. This noise is caused by matches which are not really matches and thus become erroneous points.

Compute 3D point cloud

The disparity map that has the optimal balance between the reduction of blackness without a large increase of noise is used to produce a 3D point cloud. With the combination of de calculated disparity and the location of the pixel in the image, the XYZ-coordinates of each pixel can be calculated with camera parameters from the calibration. Resulting in the point cloud depicted in figure C.10.

The 3D point cloud is of poor quality due to the gaps and noise in the disparity map. After many attempts of computing the disparity, this was the best result that could be obtained. Possibly it is possible with further tweaking of the SGBM parameters or by applying an other algorithm to improve the disparity map and thereby the 3D point cloud. However it is expected that the improvement will not be enough to obtain an accurate result. The geometry is too complex with its many corners and repetitive pattern to find the correct matches based on pixels and their neighbouring values without inducing a lot of noise.

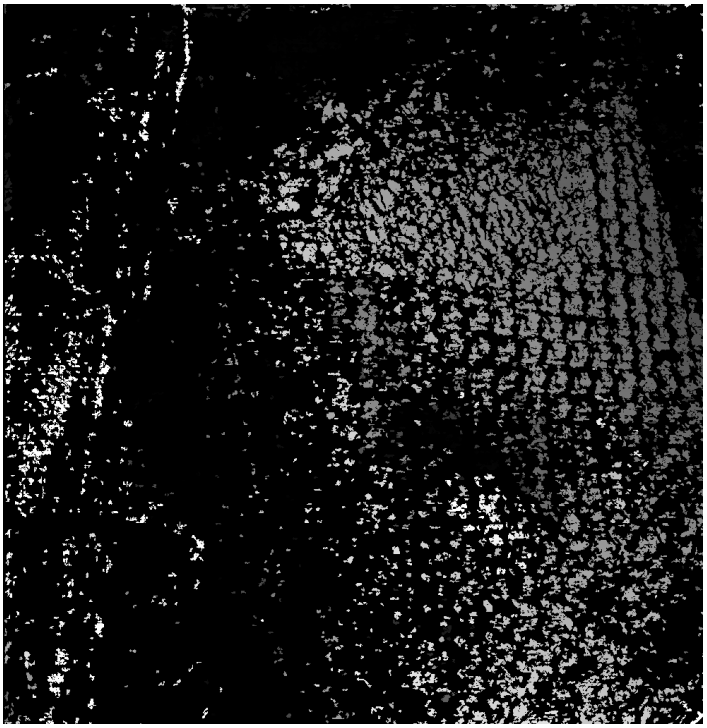

Figure C.9: Disparity map

Remarks
The use of Stereo photography is very time efficient. The calibration of the cameras takes around 20 photos and some computations and after this it only takes two photos to perform the measurements.

However, the two cameras need to be kept in the exact same place during all the test. There is a high risk that the cameras will be moved during adjustments of the set-up which will effect the results. Besides that, the mayor problem is that the accuracy of the method is insufficient. The accuracy could be improved by adding a pair of cameras to a total of four cameras, but this amount of cameras is not available and using the same camera at multiple locations decreases the time efficiency and accuracy.

C.2.3 Autodesk Recap

Autodesk Recap is a program of Autodesk which can operate and align point clouds. The program has an additional tool called Recap Photo which can generate a 3D mesh and point cloud out of a large amount of pictures. A minimum amount of 20 pictures is recommended by the program, but for good quality the amount should be around 40 to 60 pictures. To assess the accuracy of the method two models have been made with different lighting and the deviation of the models is determined. In this section the process of creating the models and the accuracy of the models is described.

Capturing the structure
To obtain a 3D result 40 to 60 pictures should be taken, all from different angles and preferably all with the whole structure on the image. To make sure that all angles of the structure are captured it was chosen to start at the left side diagonally above the structure. From this position photos were taken from left to right, every time it was no longer possible to capture the whole structure because the side of the flume, a lower

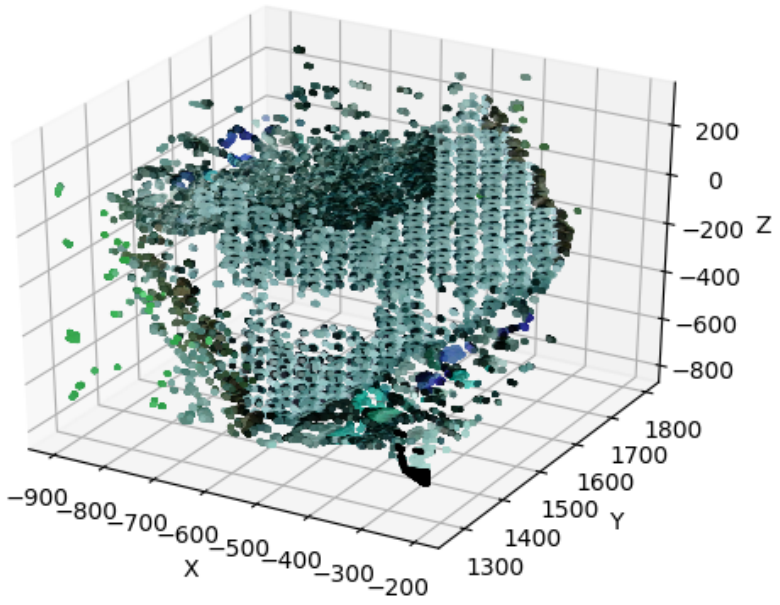

Figure C.10: Resulting 3D point cloud

position was chosen and the process was repeated. It is important to have enough space between the structure and the wave gauges, in order to be able to capture the full structure at the lower levels within the flume.

Model set up

When the pictures have been taken, they are uploaded at the site of Autdesk Recap Photo. To make sure that all models have the same axial system, four targets were placed close to the structure. After the photos have been uploaded the targets can be selected manually and given an XYZ-coordinate. By repeating this process for all models the models are be placed in the same location with the same coordinates. Because the targets are selected manually there will be a slight error during the selection. However all targets must be selected in four different pictures for every model as is depicted in figure C.11. This procedure will make the relative average mistake small and within a few millimeters. The XYZ-coordinates of the targets are measured manually and therefore prone to inaccuracies. Still the error will be within half a centimeter. Because the error is exactly the same for all models, it is not expected to influence the results. Since it is a systematic error it will cause distortion in the model, but the effects of the measurements of the roughness will be small.

After the coordinates are set it can be chosen which output format is required. The format of Recap Photo is a rcm file, the format that can be opened in all Autodesk programs is the rcs file. In order to open the file in Autodesk Recap an rcs file has to be made. Autodesk Recap saves the file in an rcp file, which is a point cloud file and is able to export the file as an pts file. The pts file can be imported into python for further analysis.

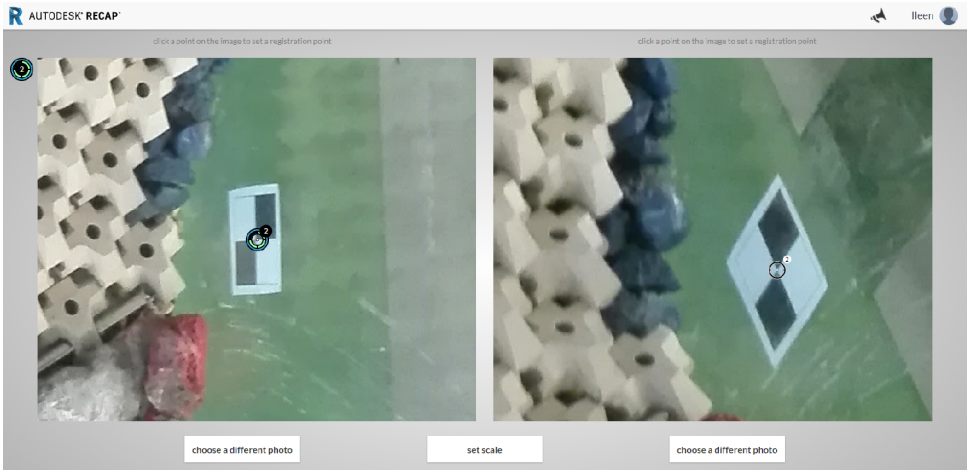

(a) Manually select target in four pictures

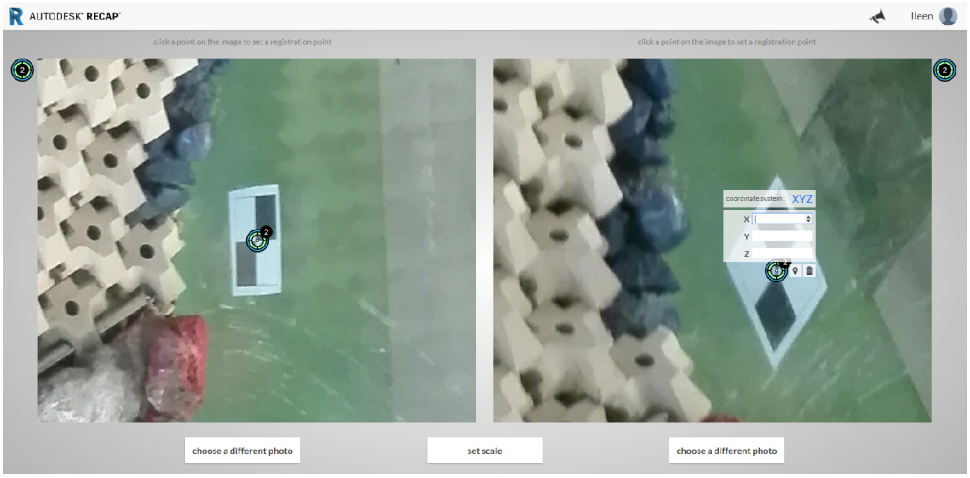

(b) Add measured coordinates to selected target

Figure C.11: Set axial system of Recap model

Model results

When all settings have been set the pictures are submitted and after about 20 minutes the model is created and the selected output formats can be downloaded. Recap Photo has its own tool for comparing models and this is how the models with different lighting have been compared. The result is showed in figure C.12.

In the Recap Photo tool it is an option to align the models. However it is not know what procedures Recap undertakes during this aligning. Besides, because of the targets the models are already be aligned. After the comparison it is indeed shown that the models are very well aligned and that the difference between the models, that is in fact the error, is around two millimeters.

For the region of interest which is the middle section of the structure the error is two millimeters or less for both the area with and without the Xbloc^{Plus}. The area that is green has an error of less than one millimeter. Only the top right area of the structure has a relative large error. This could also be caused by the diagonal shape of the structure which made it harder to capture this area in all the images. Therefore it is expected that the results for the real structure will be better than the test structure.

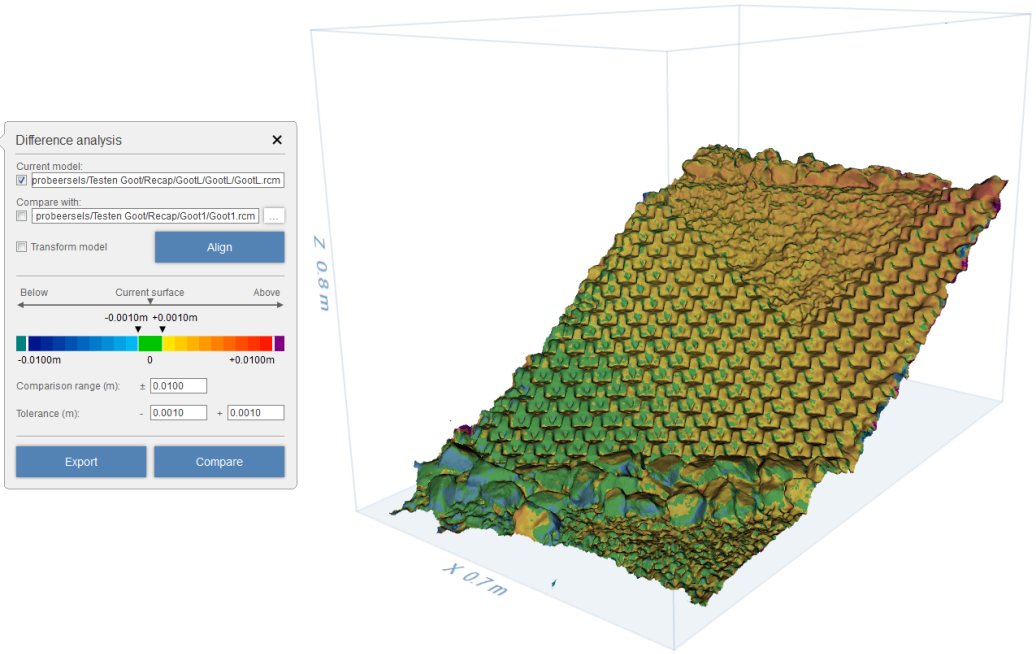

Figure C.12: Result of comparing two models

ReCap update

Between the testing of the measurement techniques and the performing of the real model tests the ReCap program had been updated. The main difference was that the program no longer worked online, but was a real desktop program. The overall process of the model creation remain the same as above. Beneficial is that the zoom function for the target registration was more powerful and thus more accurate. Additionally it was chosen to register the targets on eight different pictures instead of four to further decrease the error.

Appendix D: Test documentation

Each test consisted out of multiple runs which had a stepwise increase of wave height. The overview of all runs and their wave heights per series is given in this appendix. Subsequently, the under layer profile configurations of each test in the series is given. Followed by the before and after pictures of each test, when possible complimented with the before and after measurements of the 3D-models. Finally all calculated angles and relative angles over every test is given.

D.1 Overviews tests and runs

Test	Run	H_s	$H_{0.1\%}$	T_p	Observations
1	60%	0.06391	0.1243	0.9884	
	80%	0.08338	0.1613	1.138	
	100%	0.1023	0.1895	1.286	
	120%	0.1218	0.2151	1.399	
	130%	0.1316	0.2128	1.414	
	140%	0.1381	0.2383	1.552	
	150%	0.1456	0.2274	1.58	
	160%	0.1536	0.2341	1.571	

Table D.1: Overview tests and runs series 1

Test	Run	H_s	$H_{0.1\%}$	T_p	Observations
1	60%	0.06375	0.1223	0.9884	More plunging waves due to irregularity
	80%	0.08324	0.1569	1.138	
	100%	0.1024	0.1894	1.286	
	120%	0.1226	0.2213	1.399	
	130%	0.1323	0.2194	1.446	
2	60%	0.06091	0.1183	0.9884	More plunging waves due to irregularity
	80%	0.0815	0.1546	1.138	
	100%	0.101	0.1874	1.286	
	120%	0.1191	0.2117	1.399	
	130%	0.1295	0.2142	1.414	
	140%	0.139	0.2357	1.552	
	150%	0.1477	0.2278	1.58	
	160%	0.1544	0.2375	1.62	
3	60%	0.06115	0.1179	0.9884	Movement of 3rd whit and red row at high waves
	80%	0.08097	0.1528	1.153	
4	60%	0.06213	0.1225	0.9884	More plunging waves due to irregularity

	80%	0.08202	0.1588	1.138	
	100%	0.1021	0.1873	1.286	
	120%	0.1222	0.2123	1.399	
	130%	0.1316	0.2205	1.414	
	140%	0.1417	0.2471	1.552	
	150%	0.1498	0.2273	1.58	
5	60%	0.065	0.1253	0.9884	
	80%	0.08434	0.1626	1.138	
	100%	0.1038	0.1937	1.261	
	120%	0.1234	0.2224	1.399	
	130%	0.134	0.218	1.414	
	140%	0.1438	0.2427	1.552	
	150%	0.1536	0.2388	1.58	
	160%	0.1626	0.2488	1.571	

Table D.2: Overview tests and runs series 2

Test	Run	H_s	$H_{0.1\%}$	T_p	Observations
1	60%	0.06716	0.1322	0.9884	
	80%	0.08681	0.1706	1.138	
	100%	0.1056	0.1904	1.286	
	120%	0.1255	0.2212	1.34	
	130%	0.1358	0.2289	1.414	
	140%	0.1473	0.2591	1.552	
	150%	0.1558	0.2467	1.497	
	160%	0.1651	0.2625	1.62	
2	60%	0.06889	0.1305	0.9884	Calibration incorrect
	80%	0.08985	0.1775	1.138	Calibration incorrect
	100%	0.1099	0.1942	1.286	Calibration incorrect
	120%	0.1305	0.2316	1.34	Calibration incorrect
	130%	0.1411	0.2315	1.414	Calibration incorrect
	140%	0.1521	0.2632	1.552	Calibration incorrect
	150%	0.1461	0.2262	1.497	Recalibration conducted
	160%	0.1542	0.2361	1.62	
3	60%	0.06217	0.1185	0.9884	Irregularity outside influence of waves
	80%	0.08227	0.162	1.138	
	100%	0.1014	0.1823	1.286	
	120%	0.1207	0.2157	1.399	Rotation unit at 2nd white row
	130%	0.1303	0.2071	1.414	Rotated unit stable
	140%	0.1404	0.2448	1.552	Rotation neighbouring unit
	150%	0.1474	0.2326	1.58	Extraction of unit
4	60%	0.06217	0.1182	0.9884	
	80%	0.08223	0.1603	1.138	
	100%	0.1016	0.1858	1.286	
	120%	0.1215	0.2132	1.399	
	130%	0.1311	0.2145	1.414	
	140%	0.1394	0.2475	1.552	

150%	0.147	0.2301	1.58	Measurements of two gauges only
160%	0.1545	0.2368	1.6	Measurements of two gauges only

Table D.3: Overview tests and runs series 3

Test	Run	H_s	$H_{0.1\%}$	T_p	Observations
1	60%	0.06324	0.1218	0.9884	
	80%	0.08292	0.1586	1.138	
	100%	0.1025	0.1891	1.286	Settlements causes gaps in upper slope
	120%	0.1221	0.2196	1.399	
	130%	0.1316	0.2213	1.414	
	140%	0.1423	0.2398	1.552	
	150%	0.1465	0.2255	1.58	
	160%	0.153	0.2237	1.571	
2	60%	0.0625	0.1211	0.9884	
	80%	0.08283	0.1572	1.138	
	100%	0.1016	0.1844	1.286	
	120%	0.1212	0.2154	1.399	
	130%	0.1317	0.2158	1.414	
	140%	0.1418	0.2421	1.552	
	150%	0.1499	0.2348	1.58	
	160%	0.157	0.2344	1.571	

Table D.4: Overview tests and runs series 4

Test	Run	H_s	$H_{0.1\%}$	T_p	Observations
1	60%	0.06291	0.1219	0.9884	
	80%	0.08223	0.1603	1.138	
	100%	0.1023	0.1875	1.286	
	120%	0.1233	0.2191	1.399	
	130%	0.1322	0.2149	1.414	
	140%	0.142	0.2466	1.552	
	150%	0.1513	0.2392	1.58	
	160%	0.159	0.2462	1.62	
2	60%	0.06039	0.1154	0.9884	
	80%	0.0812	0.1589	1.138	
	100%	0.1006	0.1878	1.286	
	120%	0.1192	0.2117	1.399	
	130%	0.129	0.208	1.414	
	140%	0.138	0.2386	1.552	
	150%	0.145	0.2298	1.58	
	160%	0.1532	0.2379	1.62	
3	60%	0.06354	0.1246	0.9884	
	80%	0.08334	0.1661	1.138	
	100%	0.1033	0.1855	1.286	
	120%	0.1204	0.2147	1.399	
	130%	0.1297	0.2104	1.414	

	140%	0.1399	0.2443	1.552	
	150%	0.1547	0.2475	1.61	Measurements of two gauges only
	160%	0.1651	0.2799	1.62	Measurements of two gauges only

Table D.5: Overview tests and runs series 5

Test	Run	H_s	$H_{0.1\%}$	T_p	Observations
1	60%	0.06247	0.1174	0.9884	
	80%	0.08233	0.1581	1.138	
	100%	0.1015	0.1898	1.286	
	120%	0.1221	0.2146	1.399	
	130%	0.1314	0.2138	1.414	
	140%	0.1408	0.2419	1.552	
	150%	0.1495	0.2326	1.58	
	160%	0.1571	0.2456	1.571	
2	60%	0.06034	0.1177	0.9884	
	80%	0.08223	0.1603	1.138	
	100%	0.1005	0.1844	1.286	
	120%	0.1197	0.213	1.399	
	130%	0.1283	0.2129	1.414	
	140%	0.1377	0.2363	1.552	
	150%	0.1456	0.2276	1.58	
	160%	0.1525	0.2307	1.62	
3	60%	0.06083	0.116	0.9884	
	80%	0.08128	0.1562	1.138	
	100%	0.1005	0.1837	1.286	
	120%	0.12	0.2125	1.399	
	130%	0.1293	0.2098	1.414	
	140%	0.1384	0.2414	1.552	
	150%	0.1466	0.2268	1.58	Extraction of armour unit 3rd white row
	160%	0.1519	0.232	1.62	Progression of failure due to unit at edge
4	60%	0.06135	0.1166	0.9884	
	80%	0.08199	0.1609	1.138	
	100%	0.1012	0.1843	1.286	Rotation of unit 3rd white row
	120%	0.1212	0.2101	1.399	Rotated unit stable
	130%	0.1299	0.2126	1.414	Rotated unit stable
	140%	0.1393	0.2372	1.422	Rotated unit extracted
5	60%	0.06085	0.1148	0.9884	
	80%	0.08165	0.1574	1.138	
	100%	0.1012	0.1863	1.286	
	120%	0.121	0.2115	1.399	
	130%	0.1301	0.213	1.414	
	140%	0.1391	0.2393	1.552	
	150%	0.1467	0.2247	1.58	
	160%	0.1542	0.2355	1.571	

Table D.6: Overview tests and runs series 6

Test	Run	H_s	$H_{0.1\%}$	T_p	Observations
1	60%	0.06292	0.1233	0.9884	More plunging waves due to irregularity
	80%	0.0822	0.158	1.108	
	100%	0.1022	0.1878	1.261	Brittle failure due to lifting of armour layer at convex section
2	60%	0.06072	0.1195	0.9884	More plunging waves due to irregularity
	80%	0.08114	0.1574	1.138	
	100%	0.1005	0.18	1.286	
	120%	0.1199	0.213	1.399	
	130%	0.1296	0.2095	1.446	
	140%	0.1392	0.2369	1.552	
	150%	0.1475	0.2392	1.61	
	160%	0.1545	0.2368	1.6	
3	60%	0.06143	0.1205	0.9884	More plunging waves due to irregularity
	80%	0.0813	0.1538	1.108	
	100%	0.1004	0.1839	1.286	
4	60%	0.06074	0.1194	0.9884	More plunging waves due to irregularity
	80%	0.0813	0.1537	1.138	
	100%	0.1011	0.1805	1.286	
	120%	0.121	0.2125	1.399	
	130%	0.1296	0.2126	1.446	
	140%	0.139	0.2383	1.552	Rotation of two units at 3rd neutral row, stable unit further rotations and ultimately extractions
5	60%	0.06099	0.1185	0.9884	More plunging waves due to irregularity
	80%	0.08139	0.1559	1.138	
	100%	0.1001	0.1794	1.286	
	120%	0.1205	0.2174	1.399	
	130%	0.1298	0.2085	1.446	
	140%	0.1389	0.2376	1.552	Multiple lifts of armour layer visible, failure due to extraction of unit 3rd neutral row
6	60%	0.06092	0.1194	0.9884	More plunging waves due to irregularity
	80%	0.08135	0.1548	1.138	
	100%	0.1007	0.1851	1.286	
	120%	0.1203	0.2242	1.34	

Table D.7: Overview tests and runs series 7

D.2 Profile configurations

The profiles of the under layer of each test is depicted per series. For series 2, 3 and 7 the profiles are averaged over the x axis. For series 4 and 5 the profiles are averaged over the y axis. Series 6 does not have an overall shape, therefore the deviation from the design profile is given.

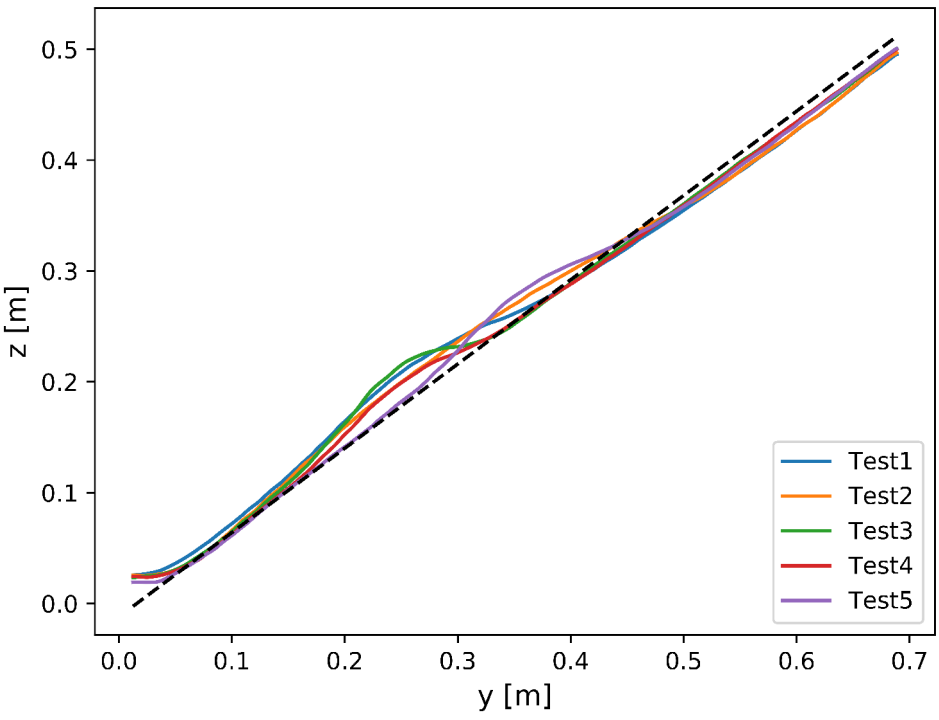

Figure D.1: Profiles series 2

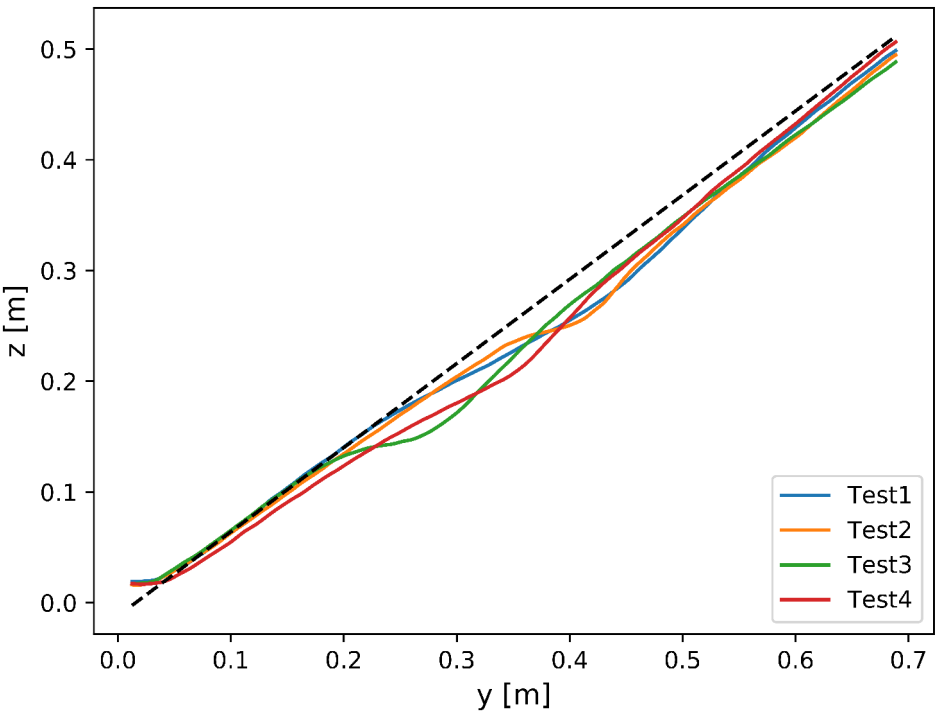

Figure D.2: Profiles series 3

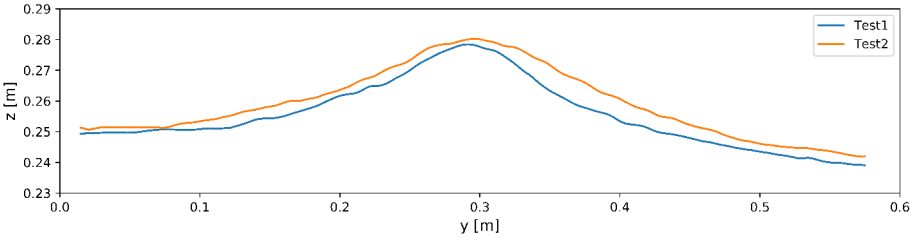

Figure D.3: Profiles series 4

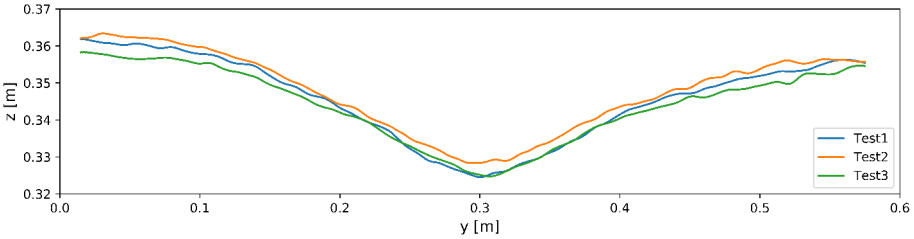

Figure D.4: Profiles series 5

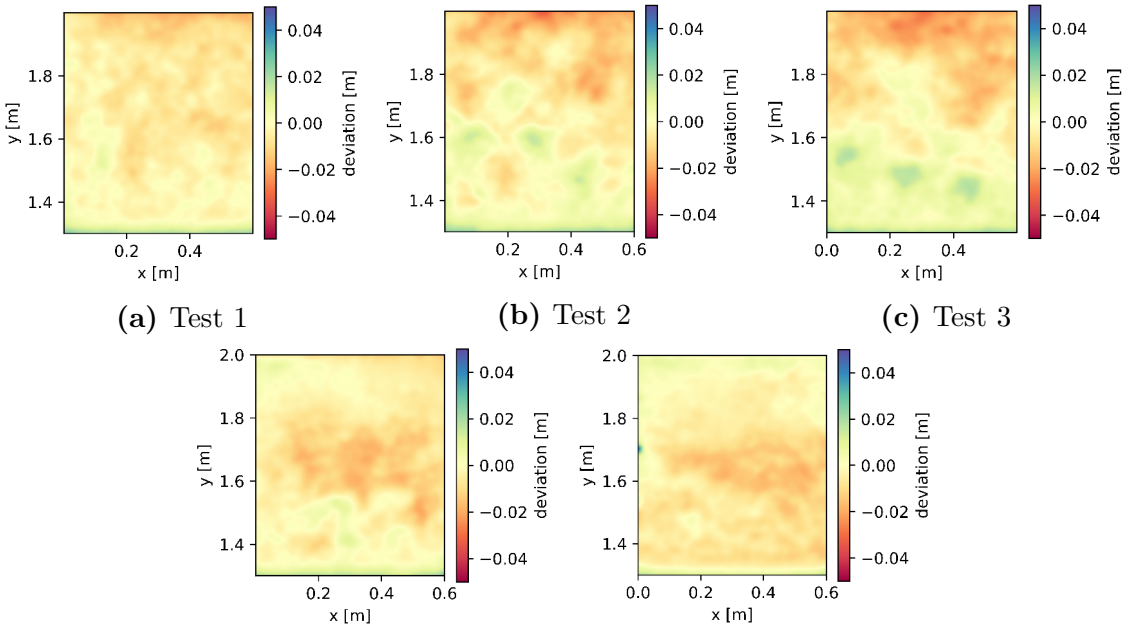

(a) Test 1 **(b)** Test 2 **(c)** Test 3

(d) Test 4 **(e)** Test 5

Figure D.5: Configurations series 6

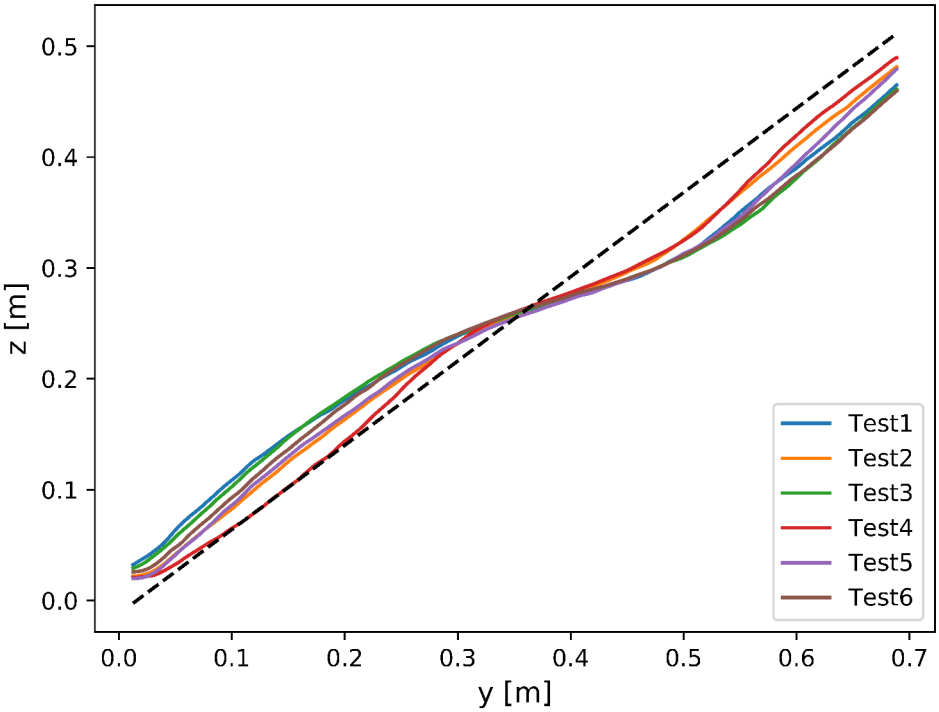

Figure D.6: Profiles series 7

Videos of the full 3D ReCap Models can be found at `https://www.youtube.com/channel/UC5qs_X7Ve3Cfa4XGQT2v8jw`. In these videos the models rotate over 360° and for each layer and test has its own video.

D.3 Comparison start and end of tests

Pictures have been made during the tests before and after each run. The picture before the first run and the picture after the last run of each test is displayed in this section. Additionally before and after each test a ReCap model has been made, the difference between the models can also be seen. In some cases the damage was to severe for a model to be useful, so for some tests the difference could not be depicted.

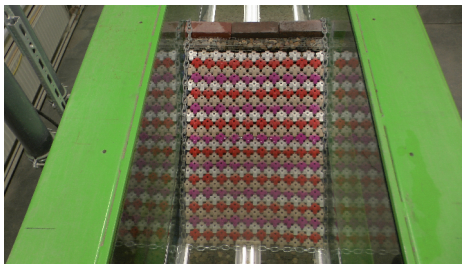

(a) Start

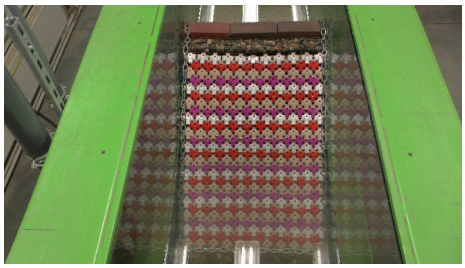

(b) End

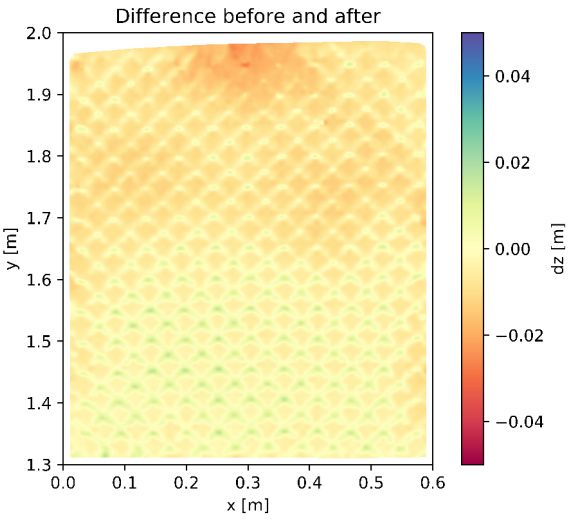

(c) Measured difference

Figure D.7: Series 1

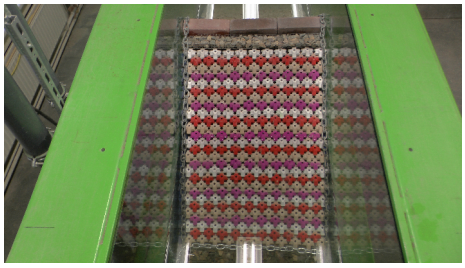

(a) Start

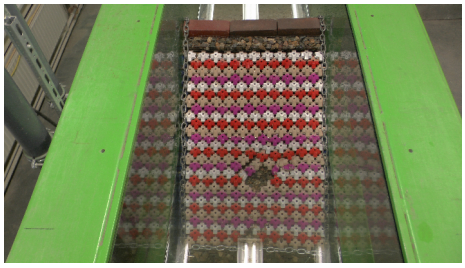

(b) End

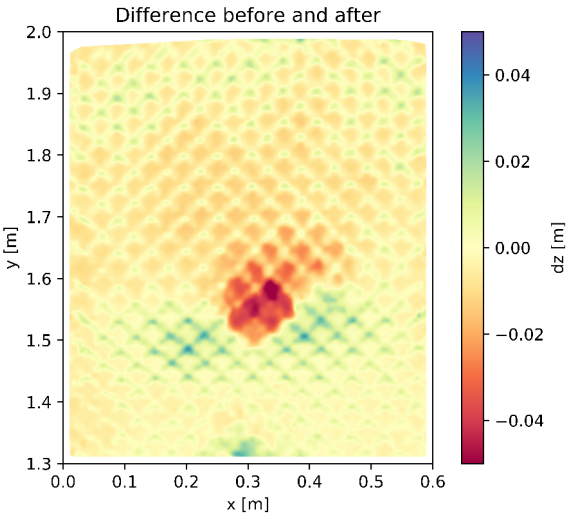

(c) Measured difference

Figure D.8: Series 2, Test 1

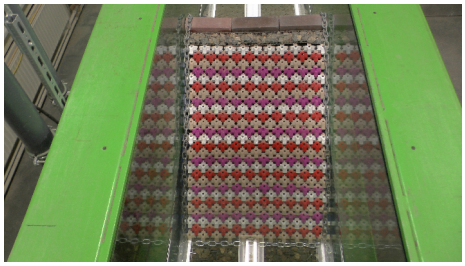

(a) Start

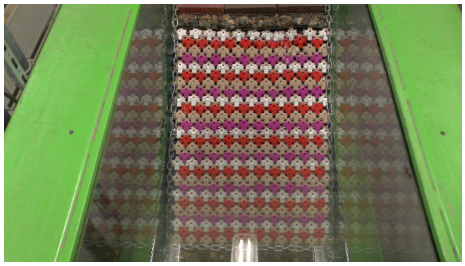

(b) End

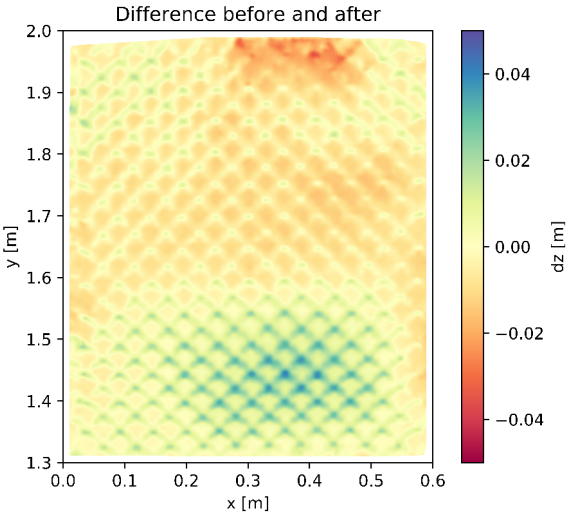

(c) Measured difference

Figure D.9: Series 2, Test 2

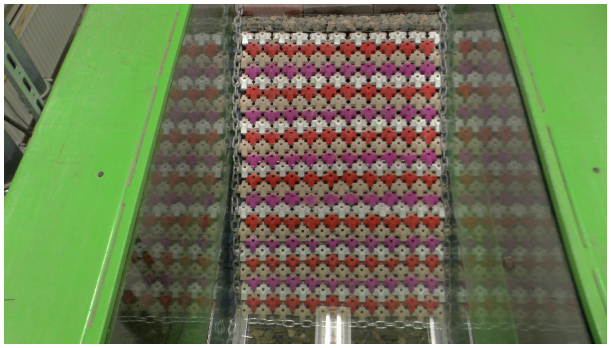

(a) Start

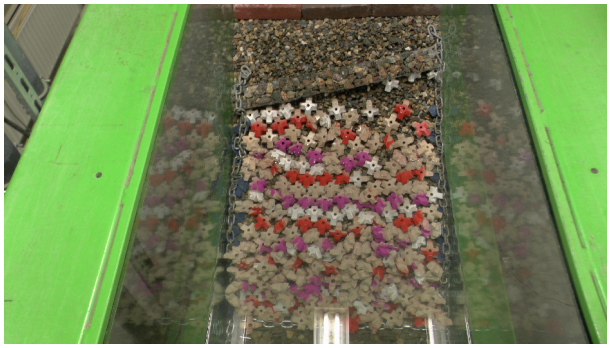

(b) End

Figure D.10: Series 2, Test 3

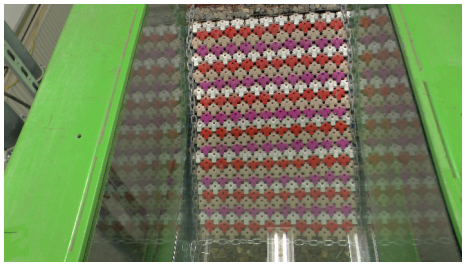

(a) Start

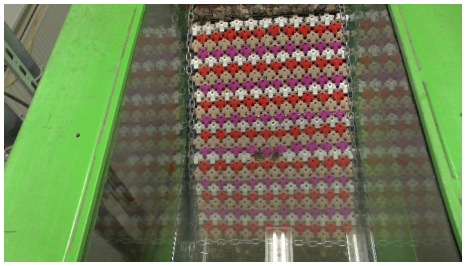

(b) End

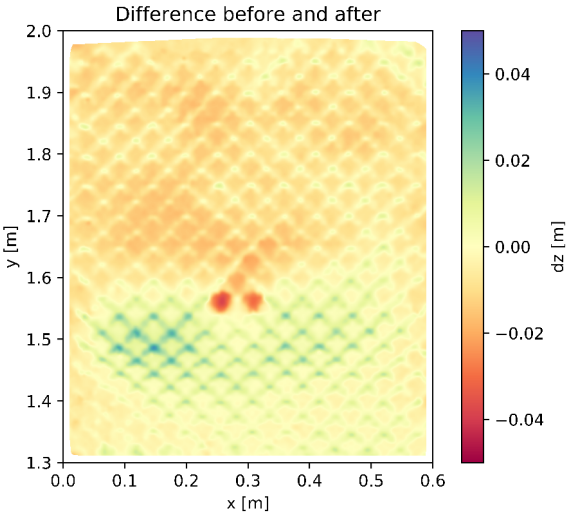

(c) Measured difference

Figure D.11: Series 2, Test 4

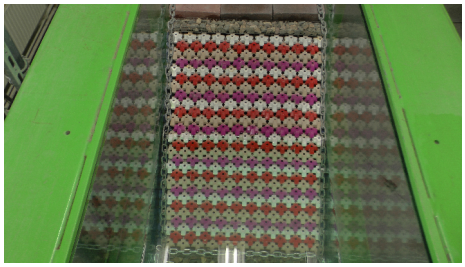

(a) Start

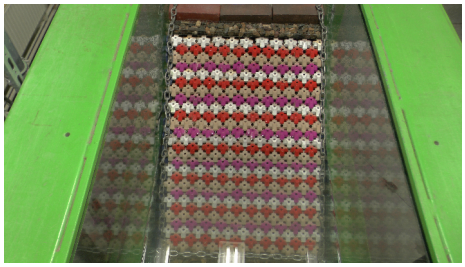

(b) End

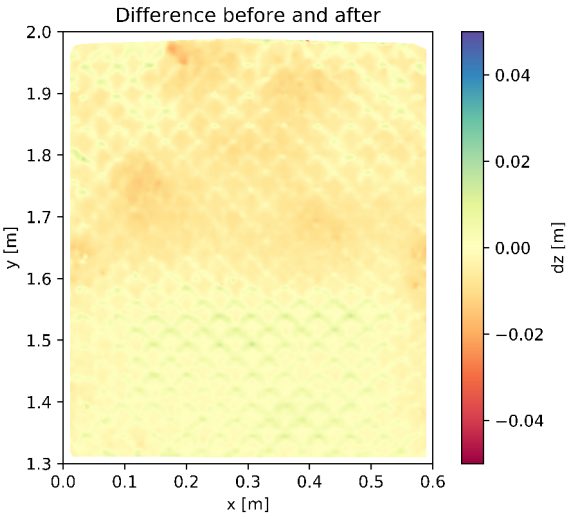

(c) Measured difference

Figure D.12: Series 2, Test 5

(a) Start

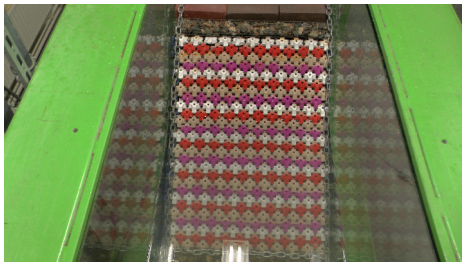

(b) End

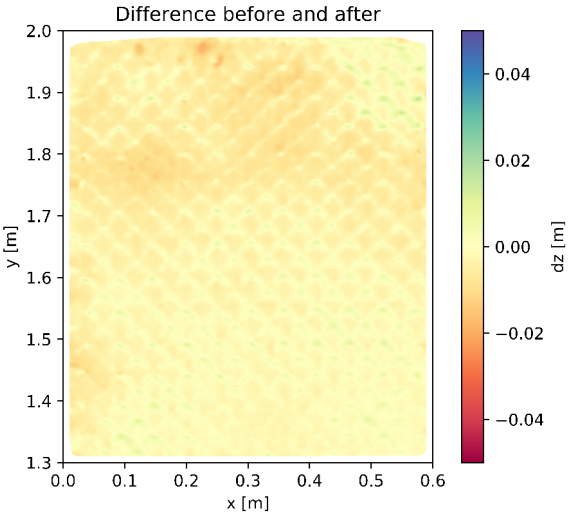

(c) Measured difference

Figure D.13: Series 3, Test 1

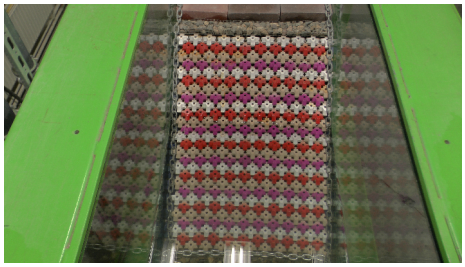

(a) Start

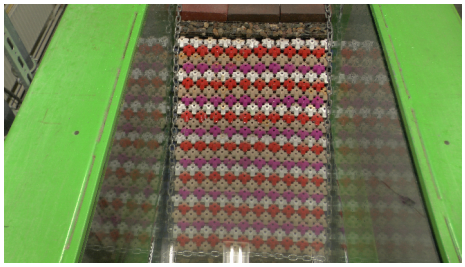

(b) End

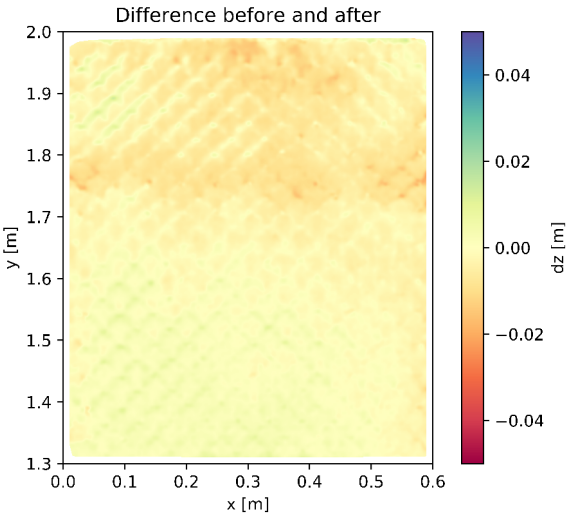

(c) Measured difference

Figure D.14: Series 3, Test 2

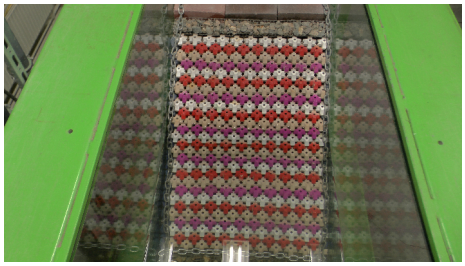

(a) Start

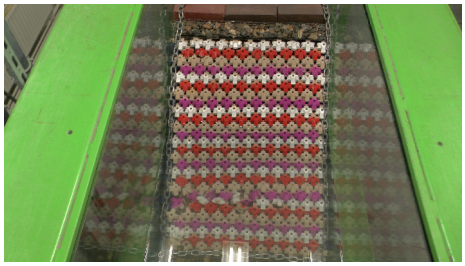

(b) End

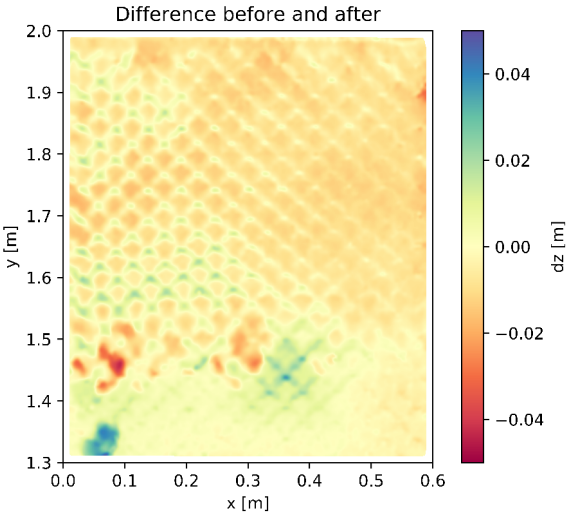

(c) Measured difference

Figure D.15: Series 3, Test 3

(a) Start

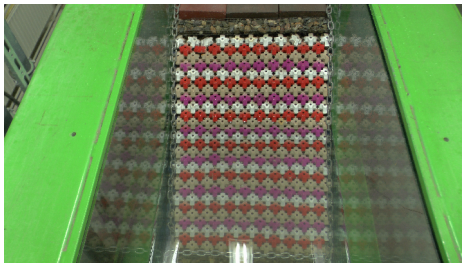

(b) End

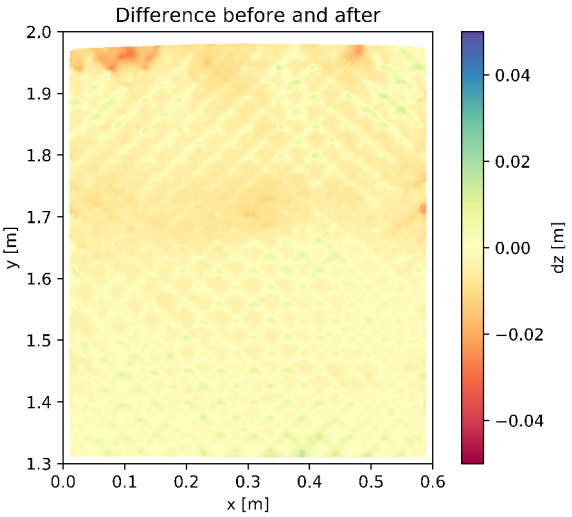

(c) Measured difference

Figure D.16: Series 3, Test 4

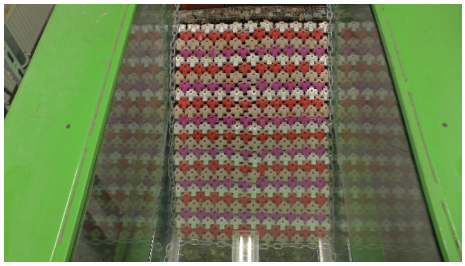

(a) Start

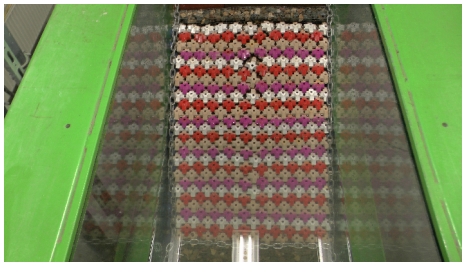

(b) End

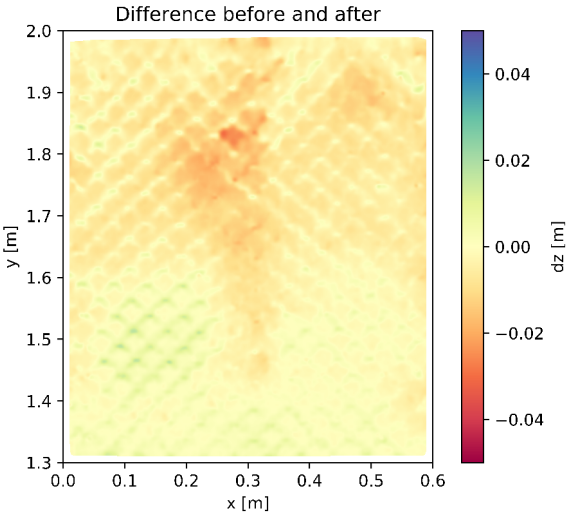

(c) Measured difference

Figure D.17: Series 4, Test 1

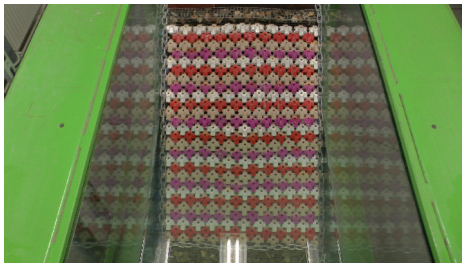

(a) Start

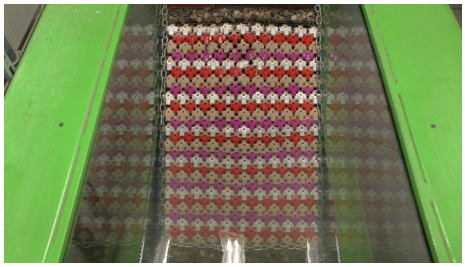

(b) End

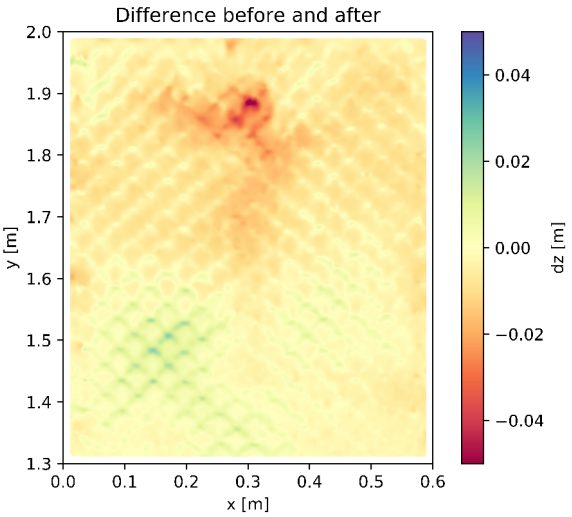

(c) Measured difference

Figure D.18: Series 4, Test 2

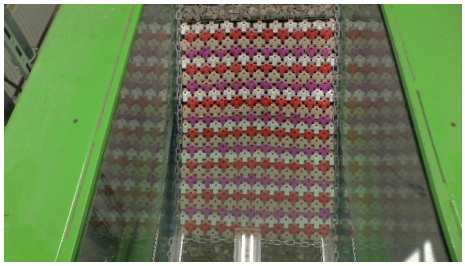

(a) Start

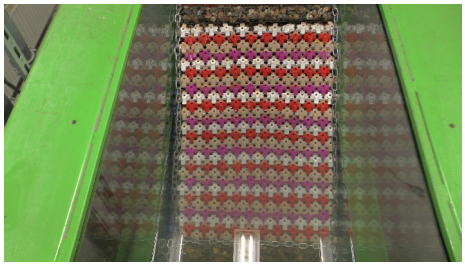

(b) End

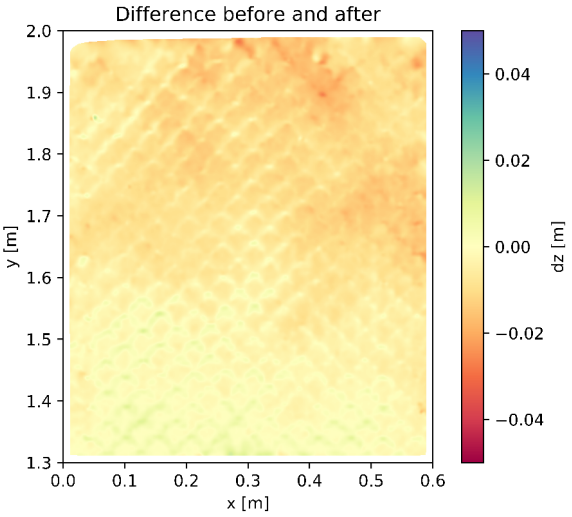

(c) Measured difference

Figure D.19: Series 5, Test 1

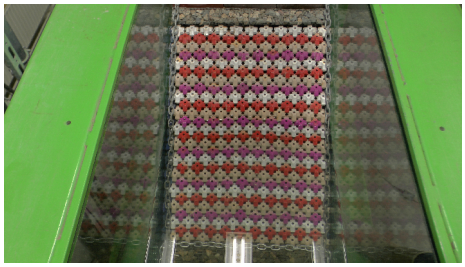

(a) Start

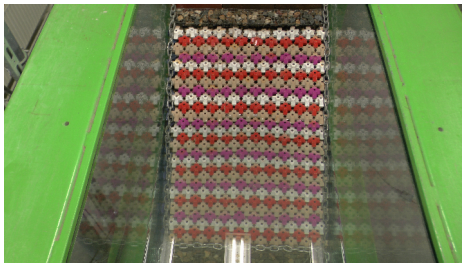

(b) End

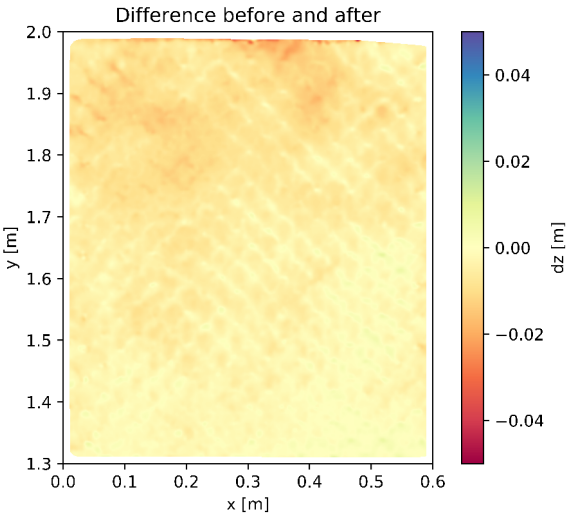

(c) Measured difference

Figure D.20: Series 5, Test 2

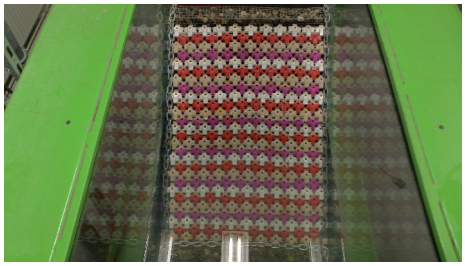

(a) Start

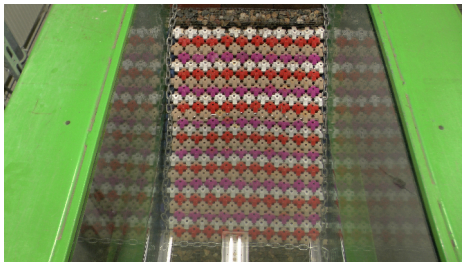

(b) End

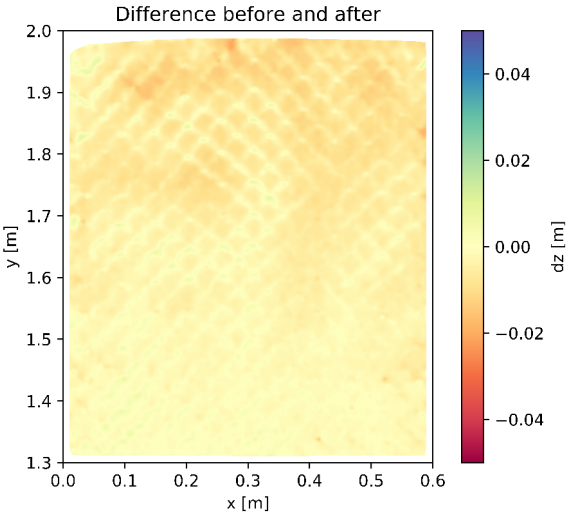

(c) Measured difference

Figure D.21: Series 5, Test 3

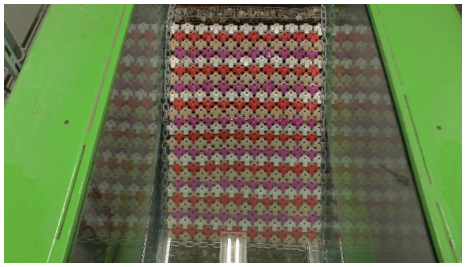

(a) Start

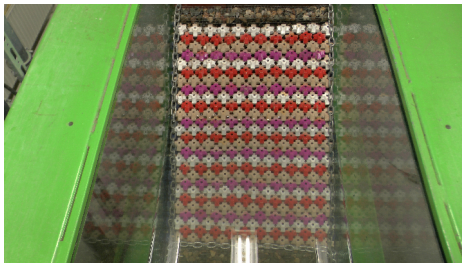

(b) End

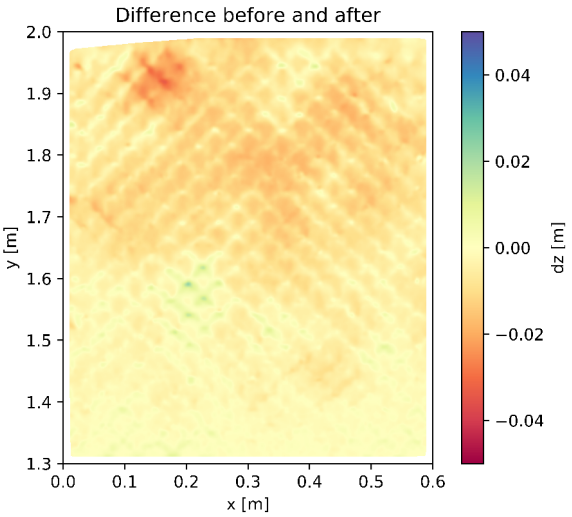

(c) Measured difference

Figure D.22: Series 6, Test 1

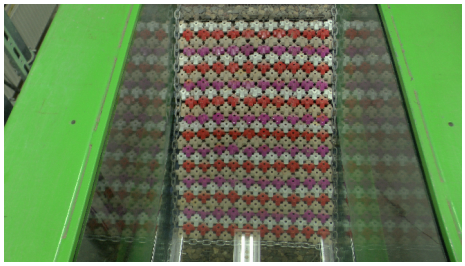

(a) Start

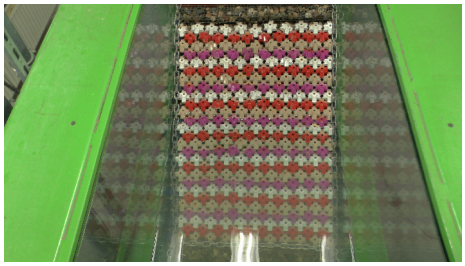

(b) End

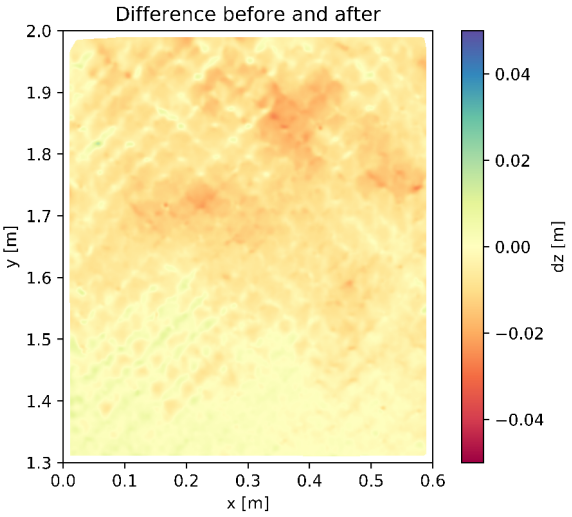

(c) Measured difference

Figure D.23: Series 6, Test 2

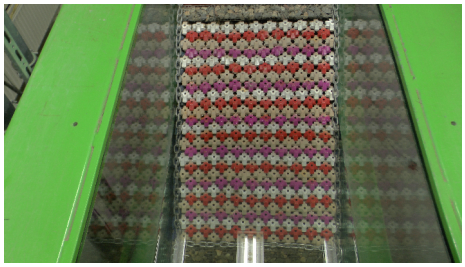

(a) Start

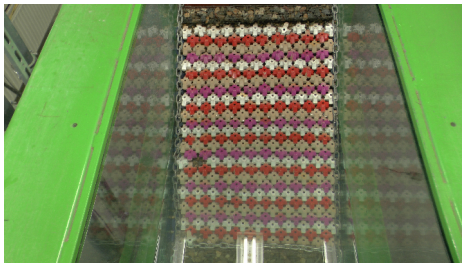

(b) End

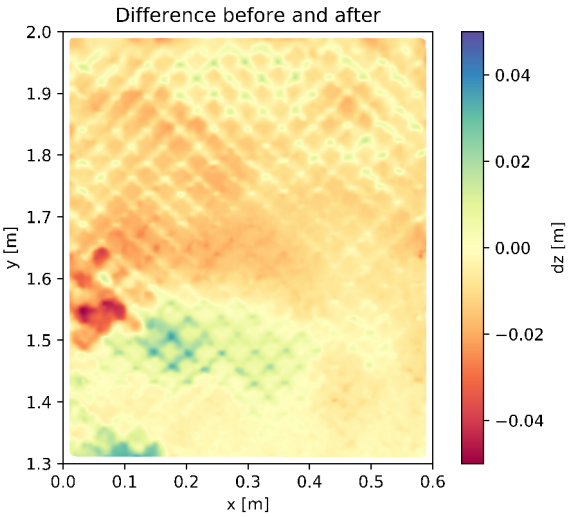

(c) Measured difference

Figure D.24: Series 6, Test 3

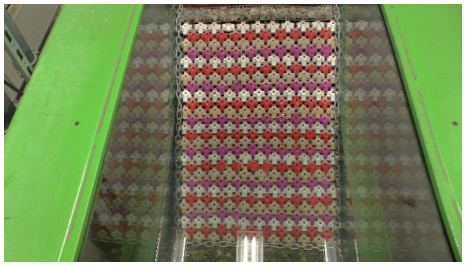

(a) Start

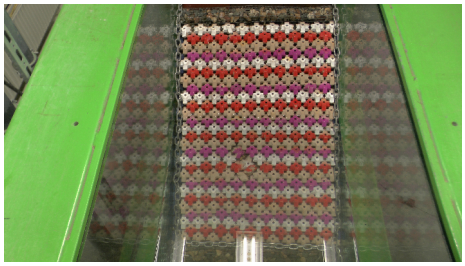

(b) End

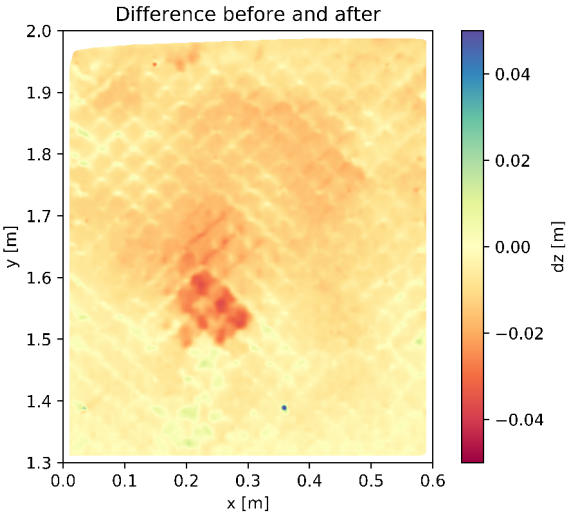

(c) Measured difference

Figure D.25: Series 6, Test 4

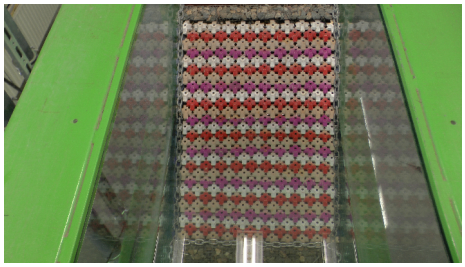

(a) Start

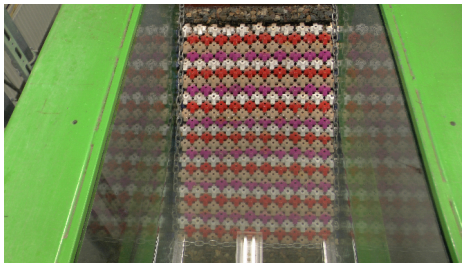

(b) End

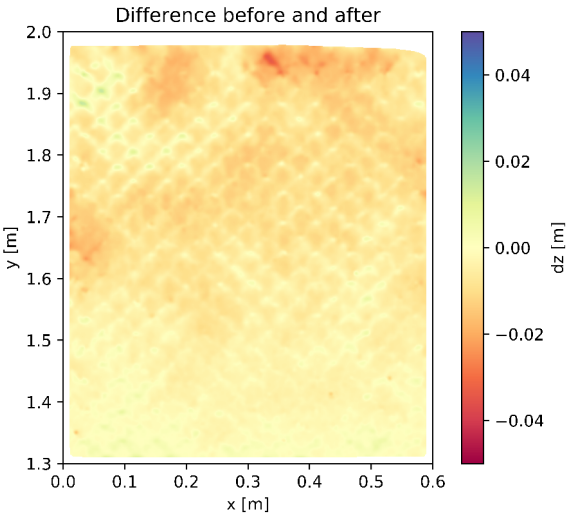

(c) Measured difference

Figure D.26: Series 6, Test 5

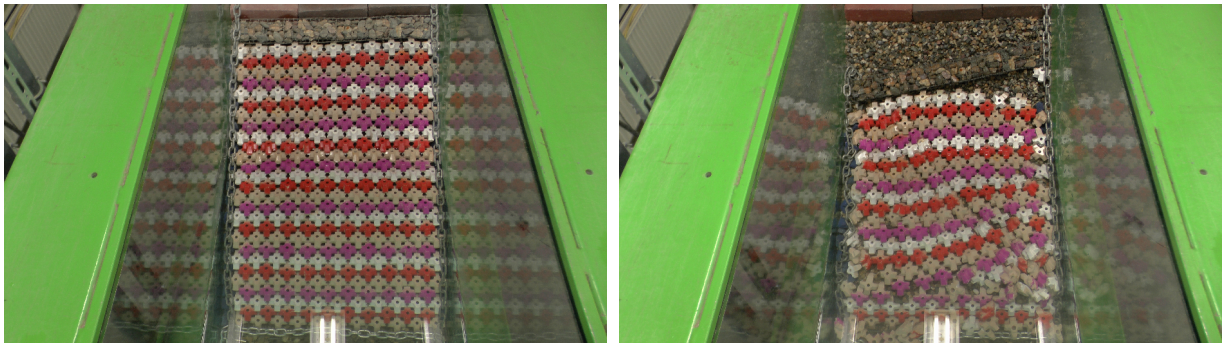

(a) Start **(b)** End

Figure D.27: Series 7, Test 1

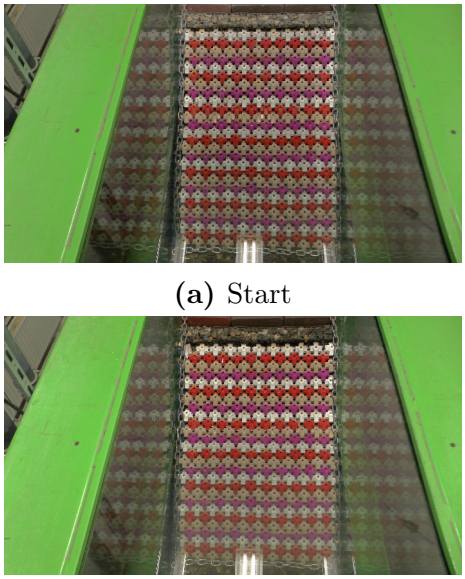

(a) Start

(b) End

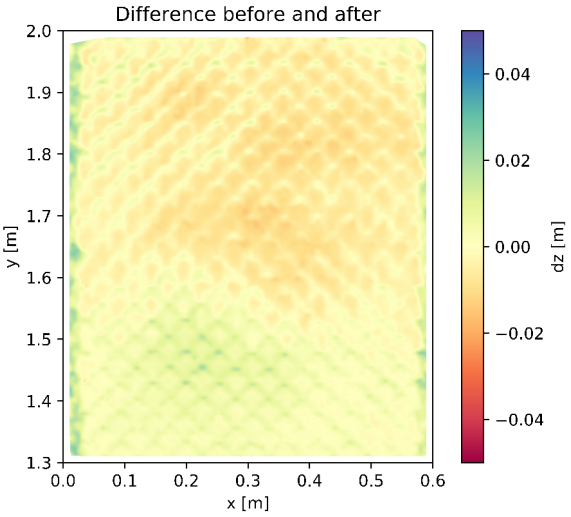

(c) Measured difference

Figure D.28: Series 7, Test 2

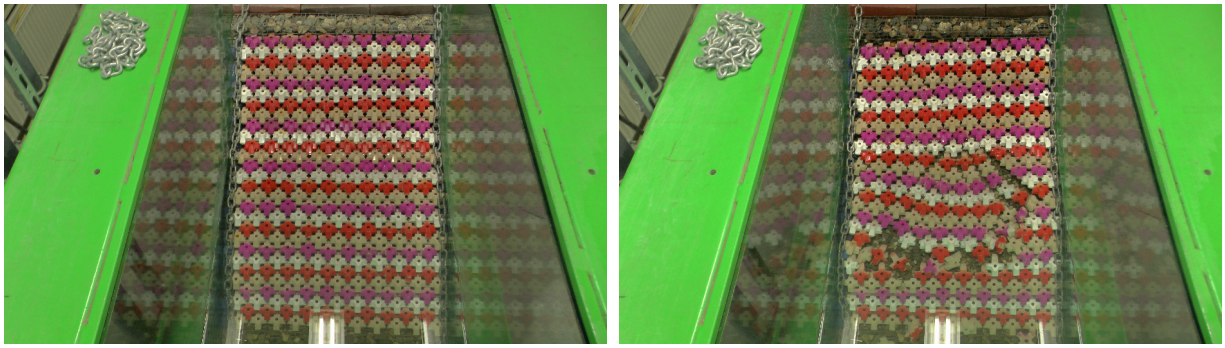

(a) Start **(b)** End

Figure D.29: Series 7, Test 3

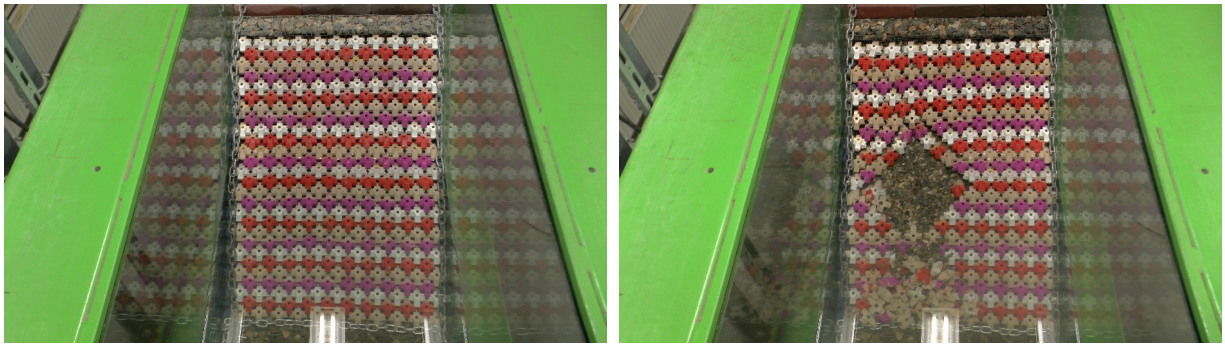

(a) Start **(b)** End

Figure D.30: Series 7, Test 4

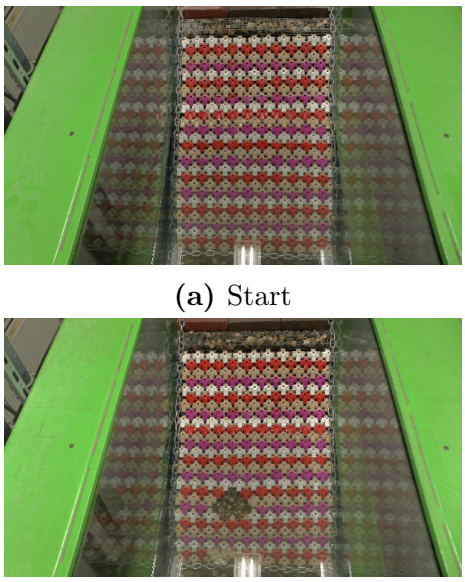

(a) Start

(b) End

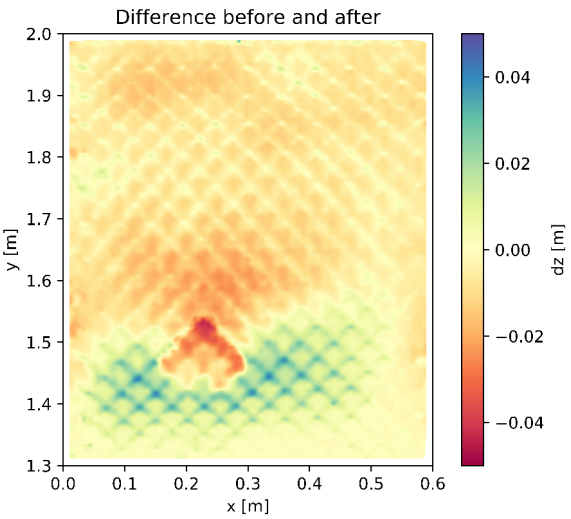

(c) Measured difference

Figure D.31: Series 7, Test 5

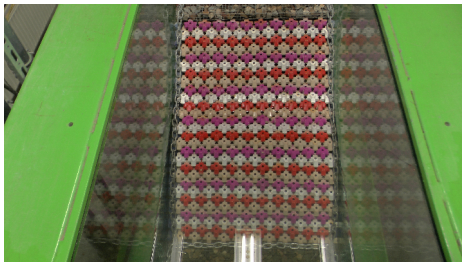

(a) Start

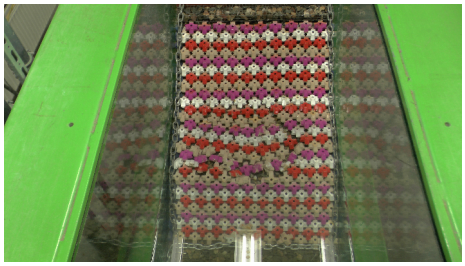

(b) End

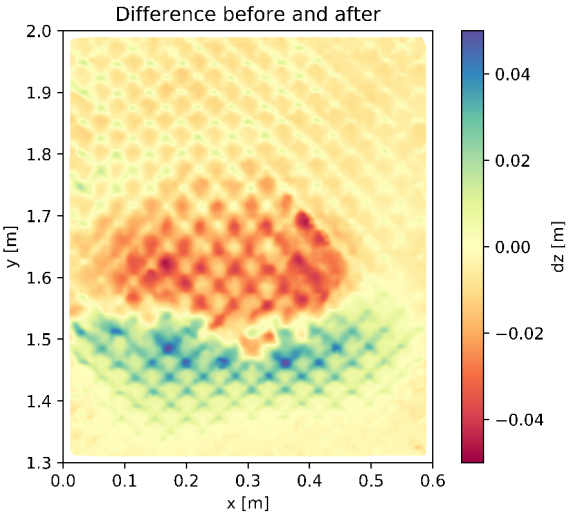

(c) Measured difference

Figure D.32: Series 7, Test 6

D.4 Calculated angles

Out of the 3D-models from ReCap the angles of the units and the angles of the under layer at the unit locations were extracted. With the angles the relative angles between the neighbouring units have been calculated. The results of both processes for all tests have been depicted in this section.

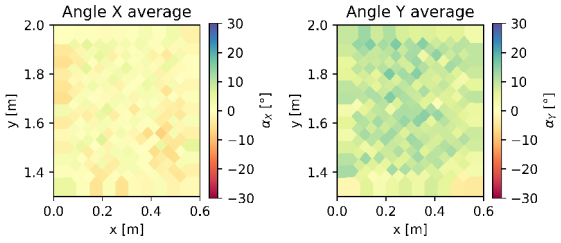

(a) Armour layer angles

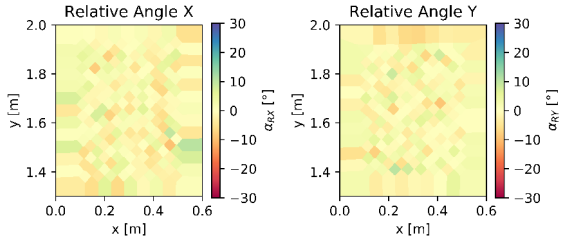

(b) Armour layer relative angles

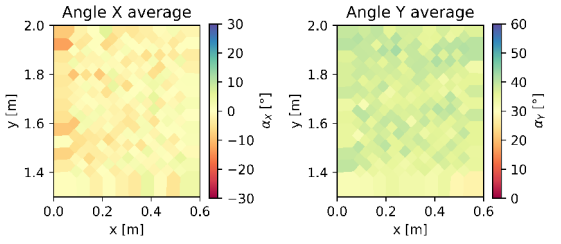

(c) Under layer angles

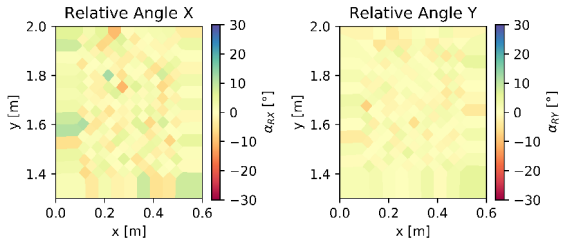

(d) Under layer relative angles

Figure D.33: Series 1

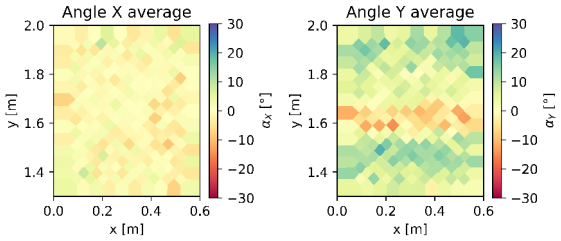

(a) Armour layer angles

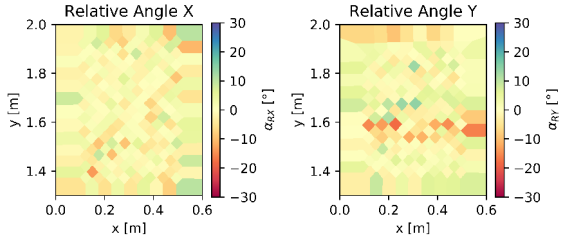

(b) Armour layer relative angles

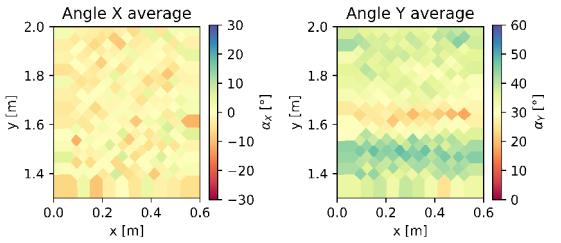

(c) Under layer angles

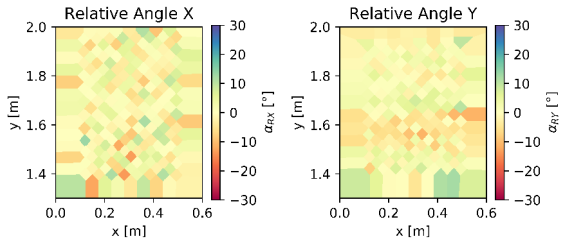

(d) Under layer relative angles

Figure D.34: Series 2, test 1

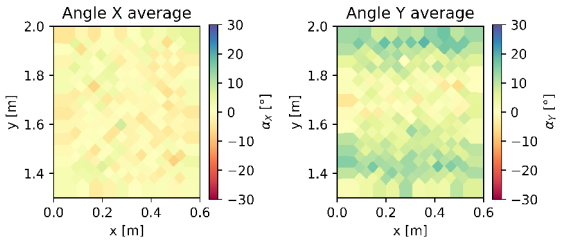

(a) Armour layer angles

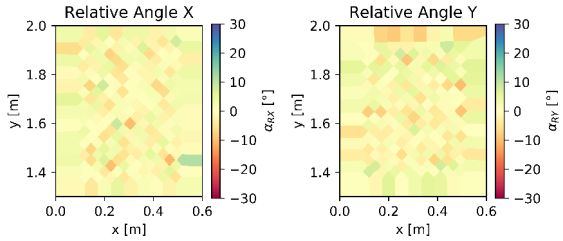

(b) Armour layer relative angles

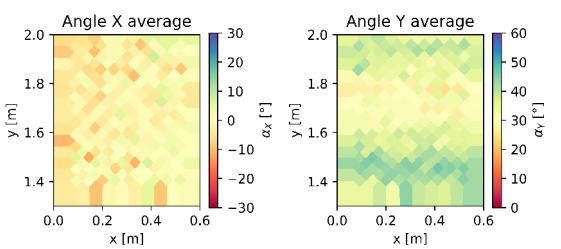

(c) Under layer angles

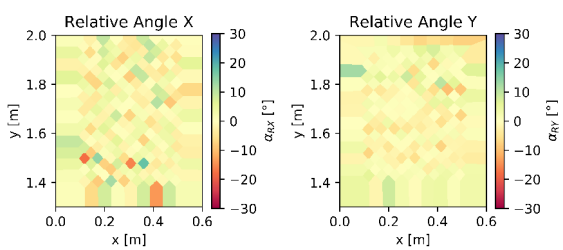

(d) Under layer relative angles

Figure D.35: Series 2, test 2

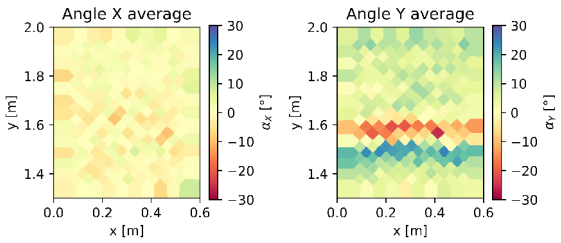

(a) Armour layer angles

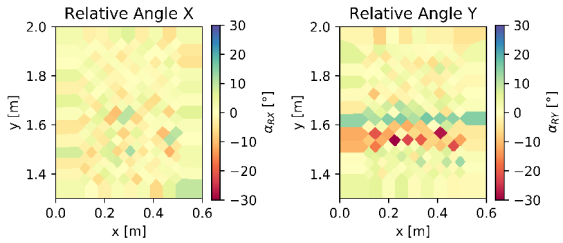

(b) Armour layer relative angles

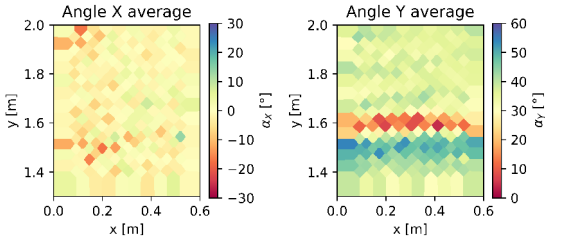

(c) Under layer angles

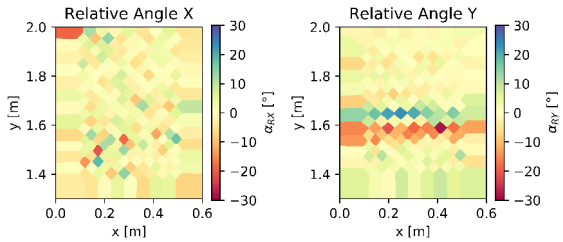

(d) Under layer relative angles

Figure D.36: Series 2, test 3

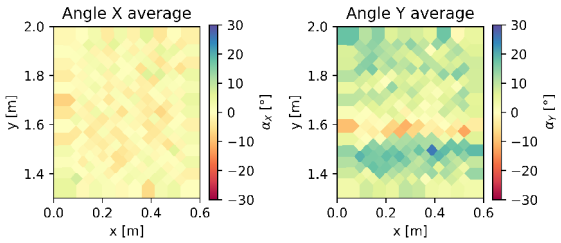

(a) Armour layer angles

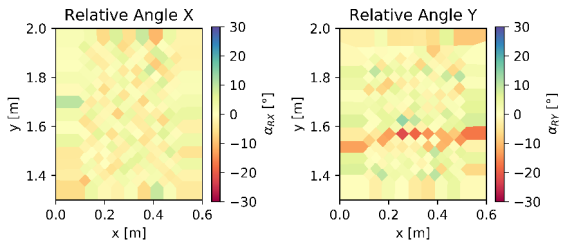

(b) Armour layer relative angles

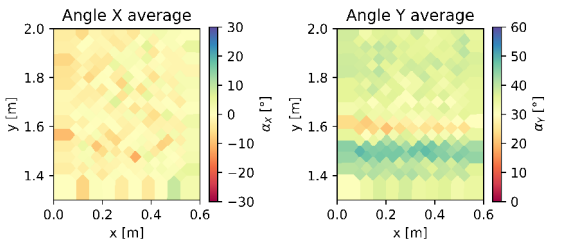

(c) Under layer angles

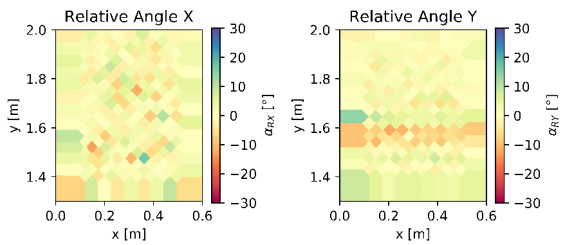

(d) Under layer relative angles

Figure D.37: Series 2, test 4

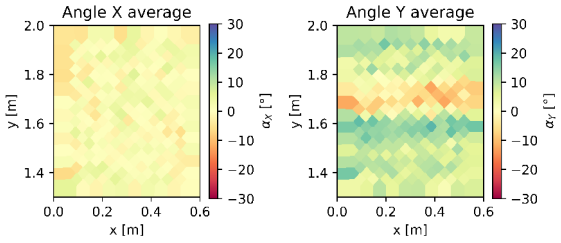

(a) Armour layer angles

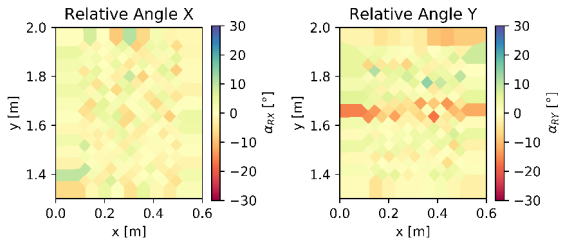

(b) Armour layer relative angles

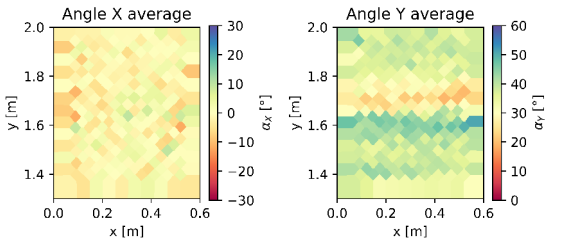

(c) Under layer angles

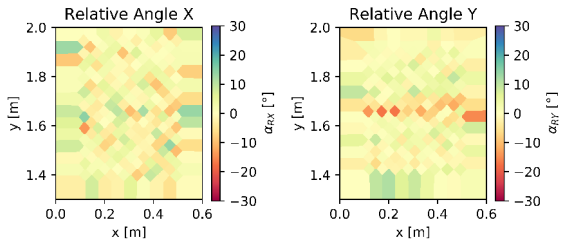

(d) Under layer relative angles

Figure D.38: Series 2, test 5

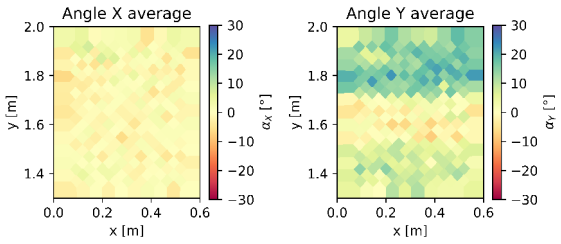

(a) Armour layer angles

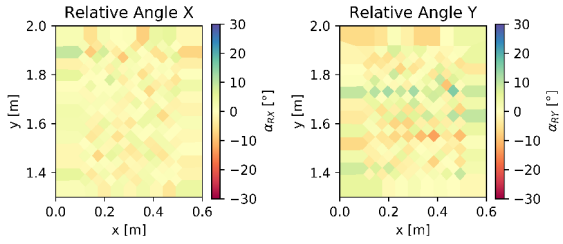

(b) Armour layer relative angles

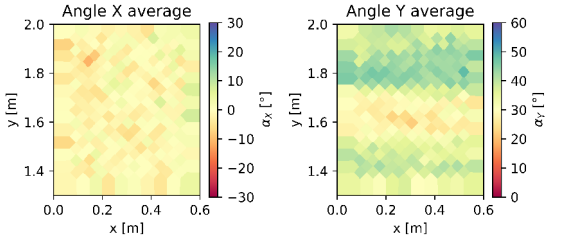

(c) Under layer angles

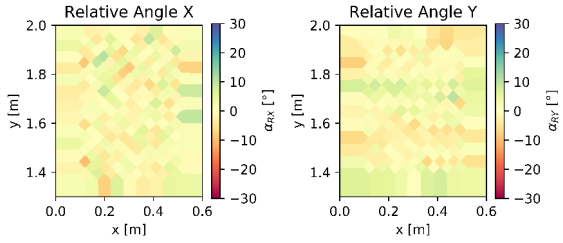

(d) Under layer relative angles

Figure D.39: Series 3, test 1

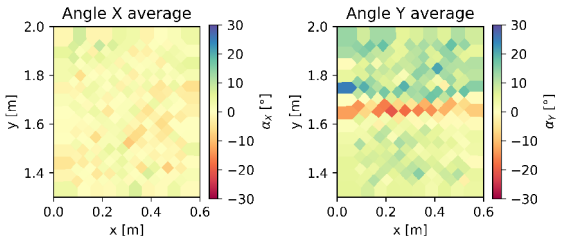

(a) Armour layer angles

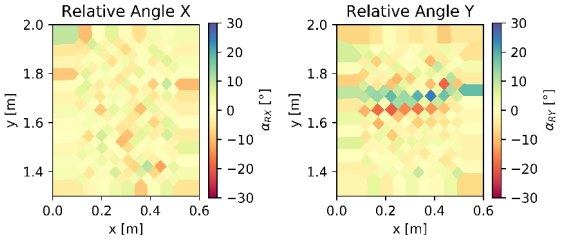

(b) Armour layer relative angles

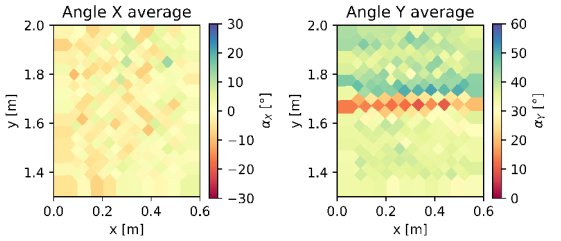

(c) Under layer angles

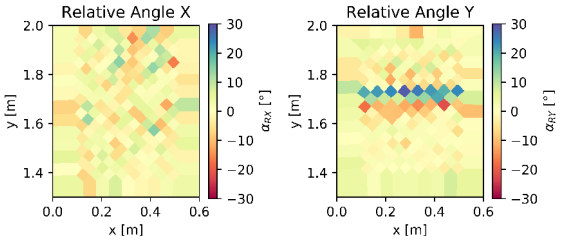

(d) Under layer relative angles

Figure D.40: Series 3, test 2

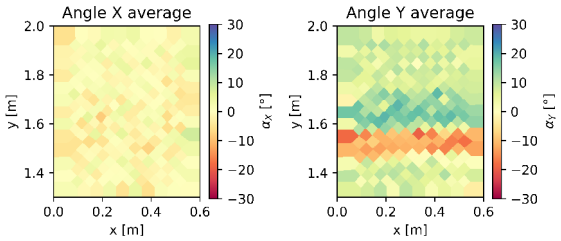

(a) Armour layer angles

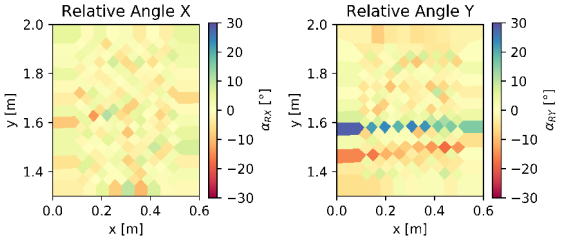

(b) Armour layer relative angles

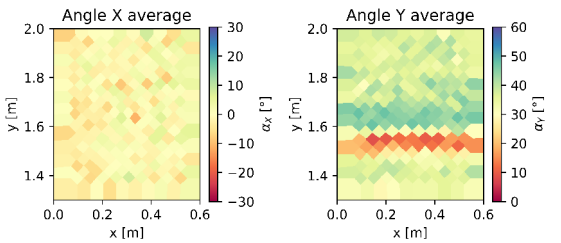

(c) Under layer angles

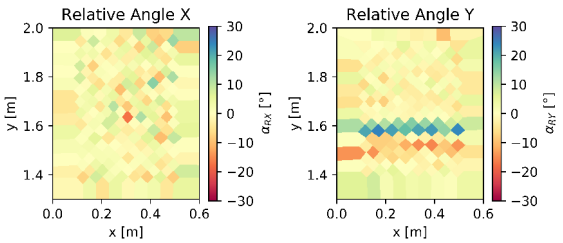

(d) Under layer relative angles

Figure D.41: Series 3, test 3

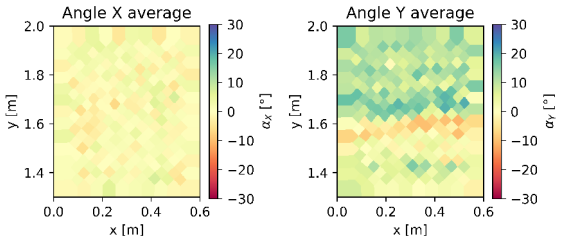

(a) Armour layer angles

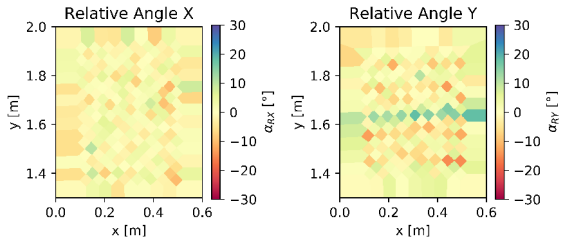

(b) Armour layer relative angles

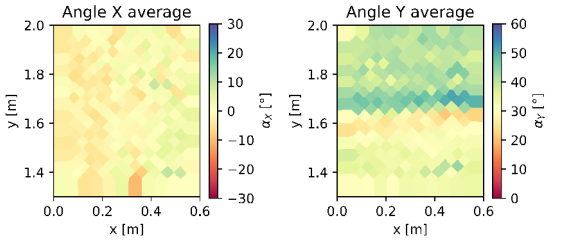

(c) Under layer angles

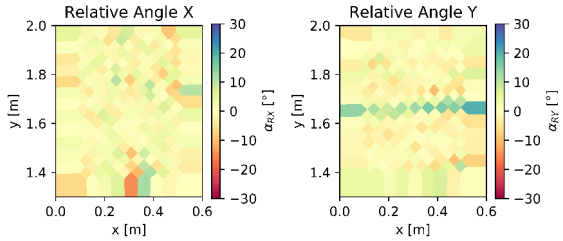

(d) Under layer relative angles

Figure D.42: Series 3, test 4

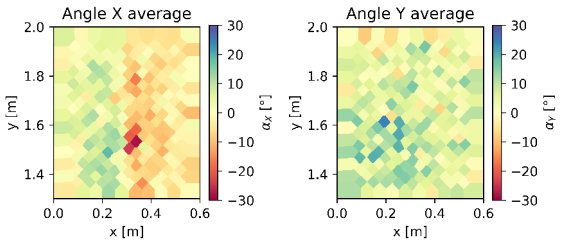

(a) Armour layer angles

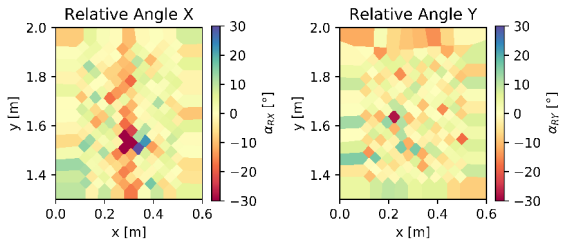

(b) Armour layer relative angles

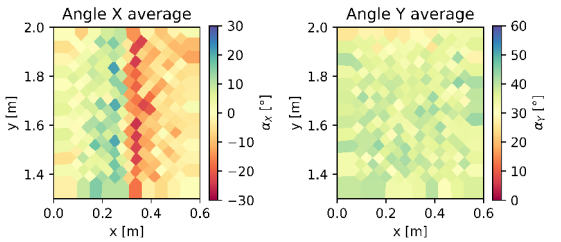

(c) Under layer angles

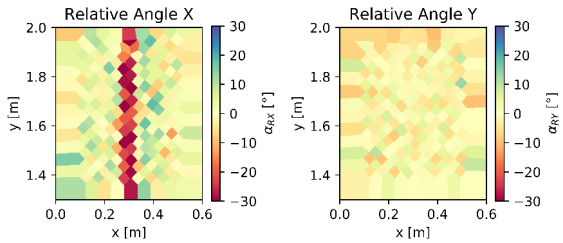

(d) Under layer relative angles

Figure D.43: Series 4, test 1

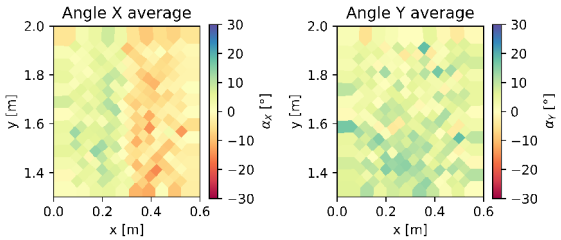

(a) Armour layer angles

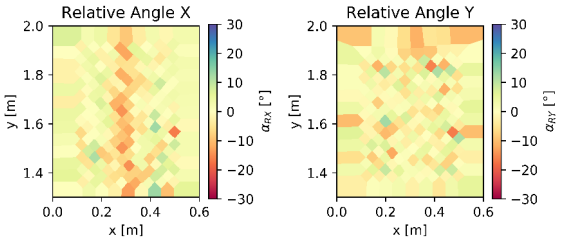

(b) Armour layer relative angles

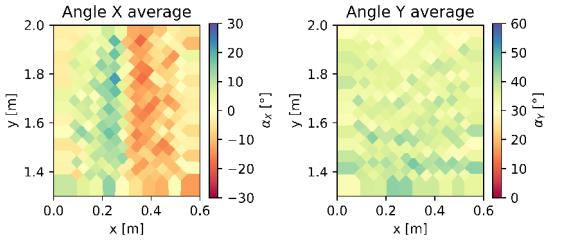

(c) Under layer angles

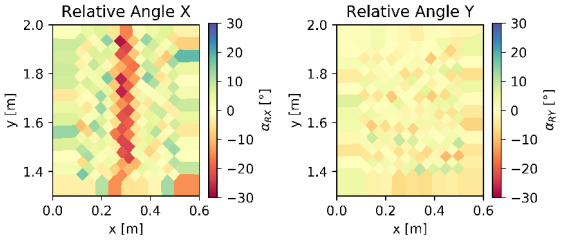

(d) Under layer relative angles

Figure D.44: Series 4, test 2

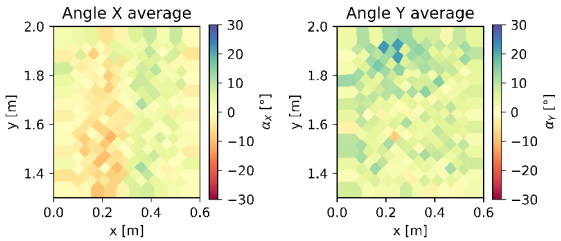

(a) Armour layer angles

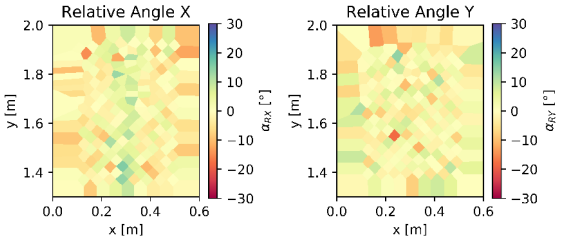

(b) Armour layer relative angles

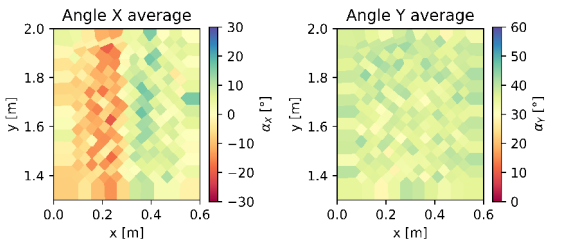

(c) Under layer angles

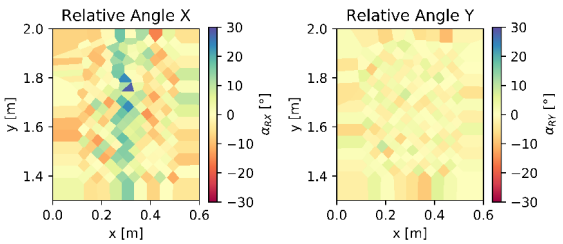

(d) Under layer relative angles

Figure D.45: Series 5, test 1

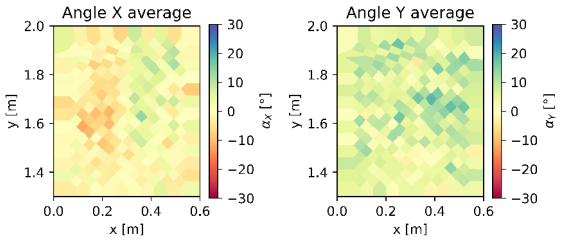

(a) Armour layer angles

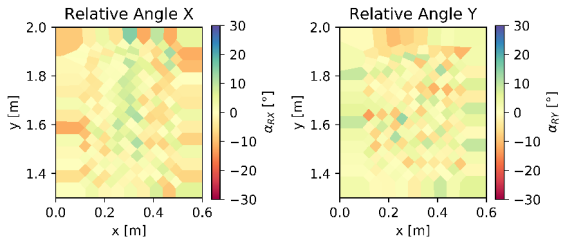

(b) Armour layer relative angles

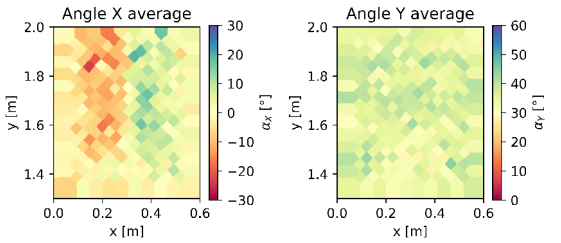

(c) Under layer angles

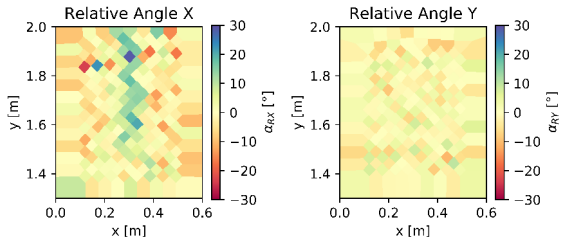

(d) Under layer relative angles

Figure D.46: Series 5, test 2

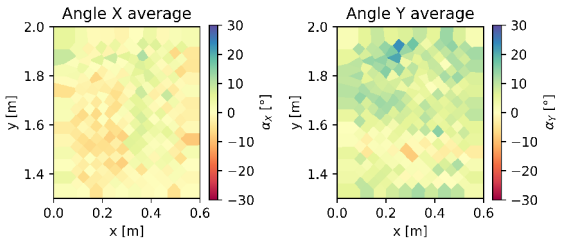

(a) Armour layer angles

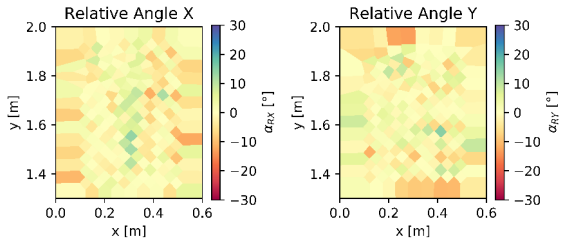

(b) Armour layer relative angles

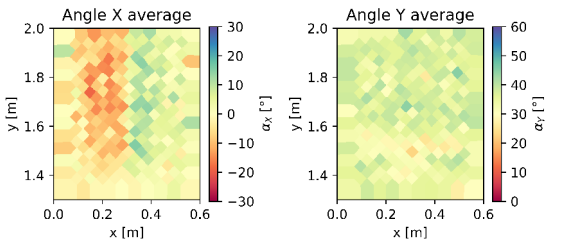

(c) Under layer angles

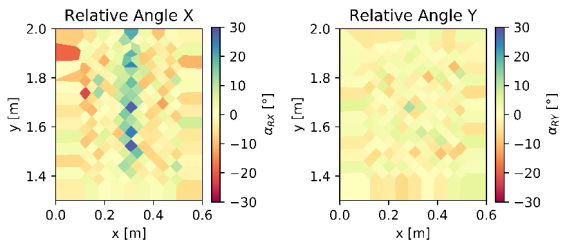

(d) Under layer relative angles

Figure D.47: Series 5, test 3

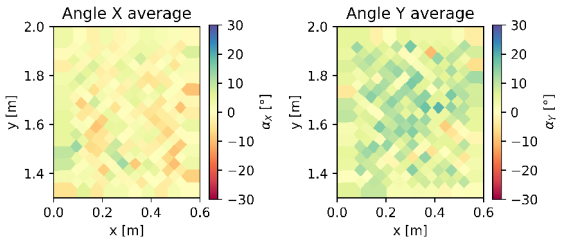

(a) Armour layer angles

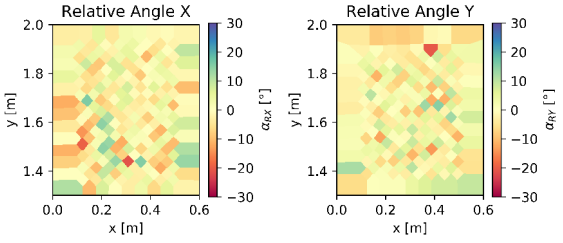

(b) Armour layer relative angles

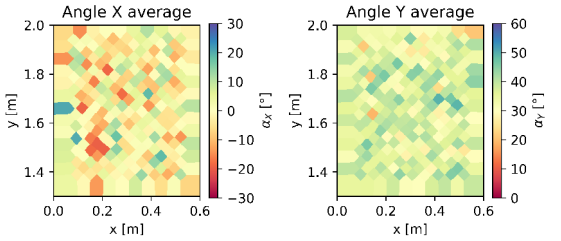

(c) Under layer angles

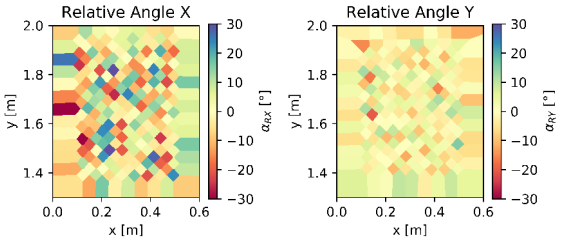

(d) Under layer relative angles

Figure D.48: Series 6, test 1

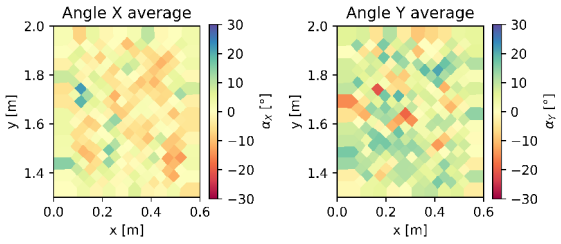

(a) Armour layer angles

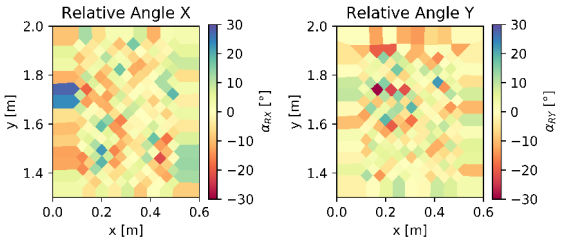

(b) Armour layer relative angles

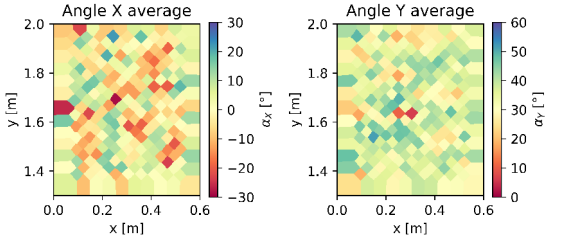

(c) Under layer angles

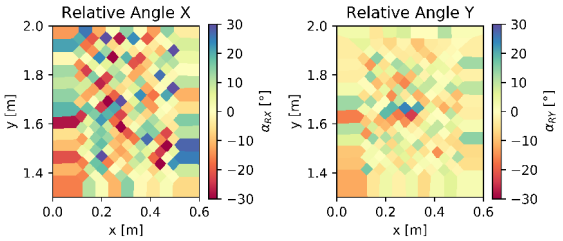

(d) Under layer relative angles

Figure D.49: Series 6, test 2

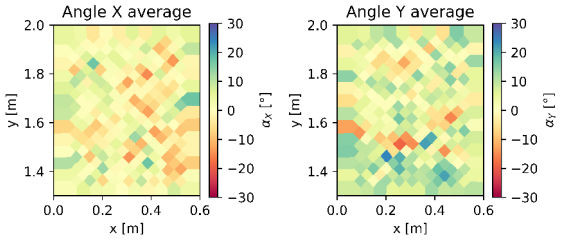

(a) Armour layer angles

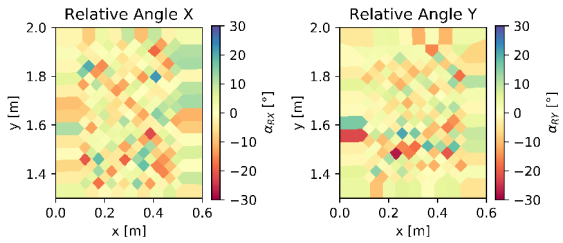

(b) Armour layer relative angles

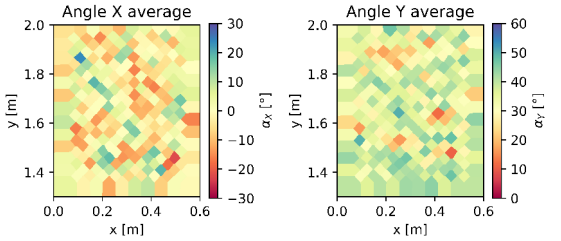

(c) Under layer angles

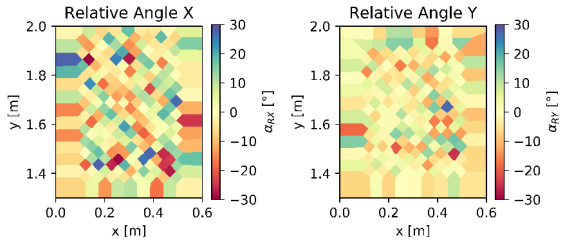

(d) Under layer relative angles

Figure D.50: Series 6, test 3

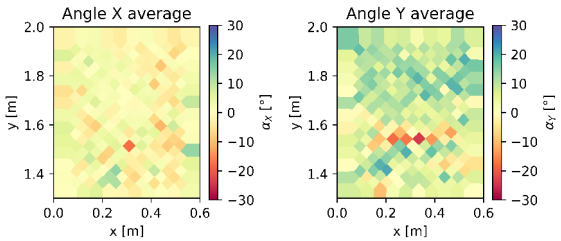

(a) Armour layer angles

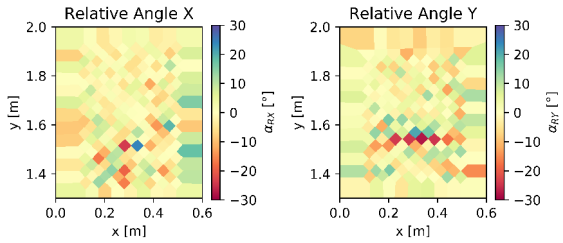

(b) Armour layer relative angles

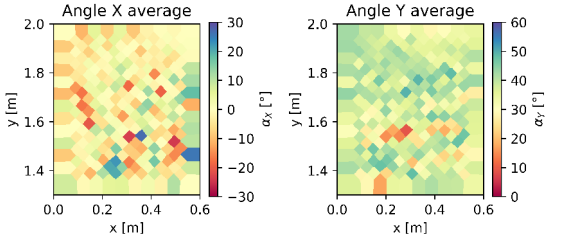

(c) Under layer angles

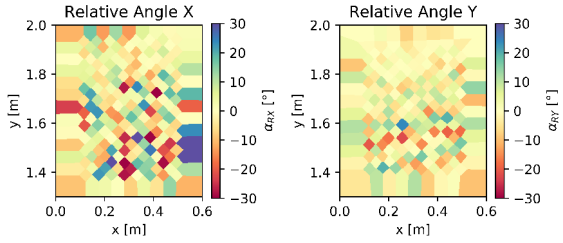

(d) Under layer relative angles

Figure D.51: Series 6, test 4

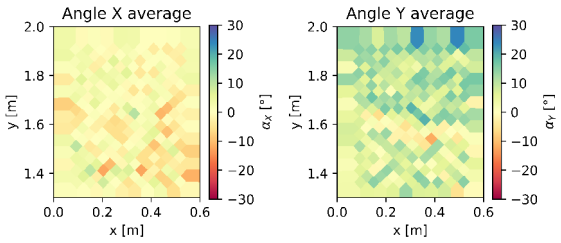

(a) Armour layer angles

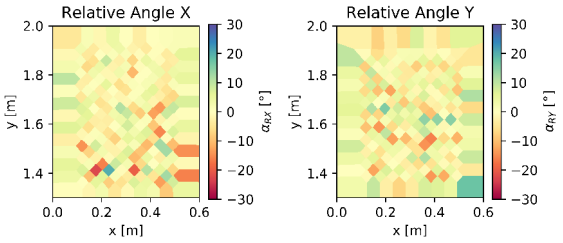

(b) Armour layer relative angles

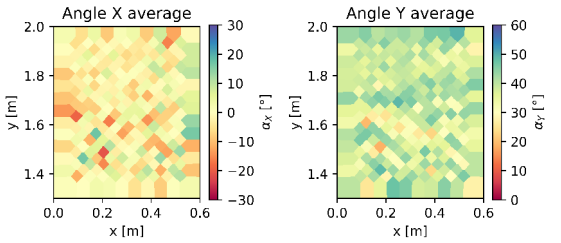

(c) Under layer angles

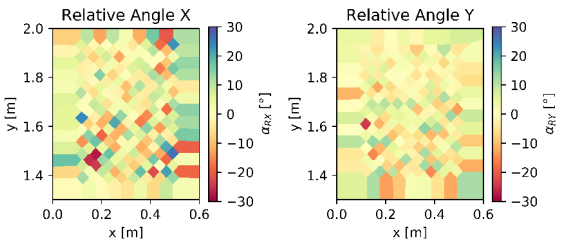

(d) Under layer relative angles

Figure D.52: Series 6, test 5

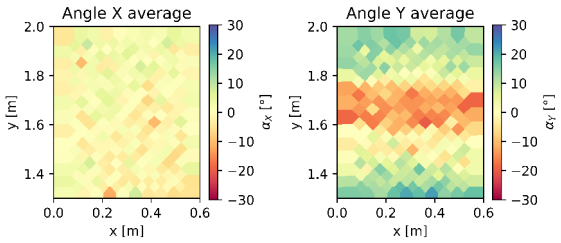

(a) Armour layer angles

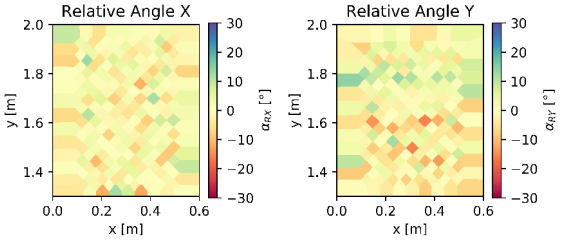

(b) Armour layer relative angles

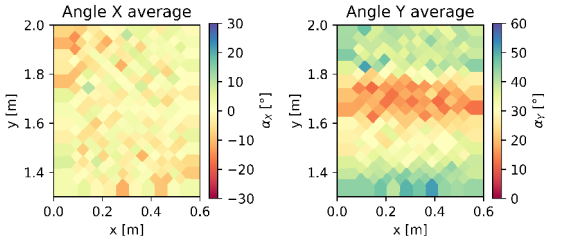

(c) Under layer angles

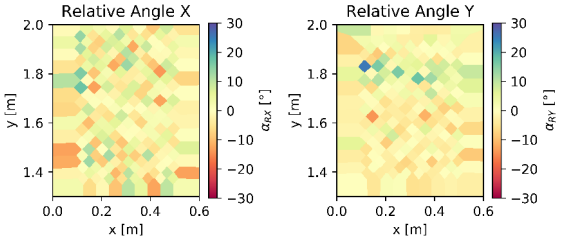

(d) Under layer relative angles

Figure D.53: Series 7, test 1

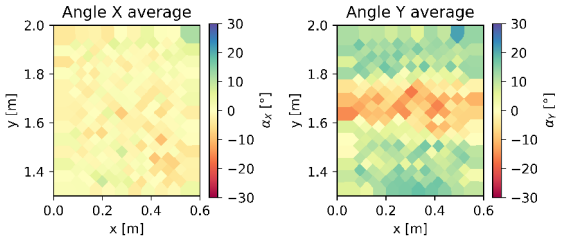

(a) Armour layer angles

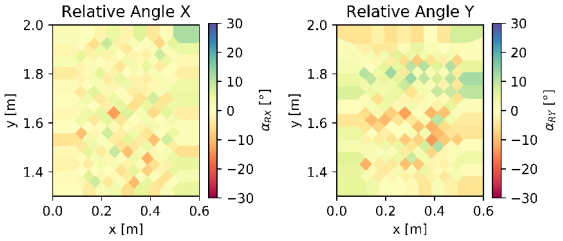

(b) Armour layer relative angles

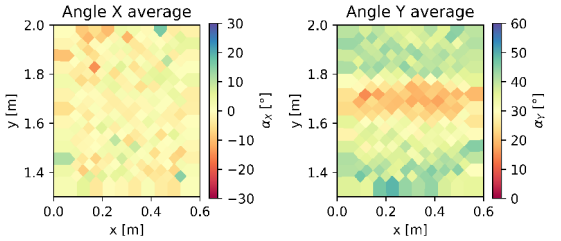

(c) Under layer angles

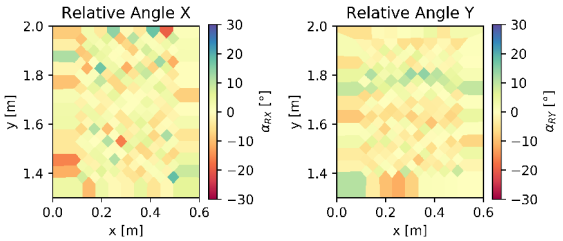

(d) Under layer relative angles

Figure D.54: Series 7, test 2

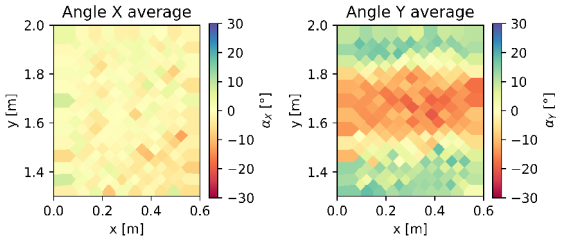

(a) Armour layer angles

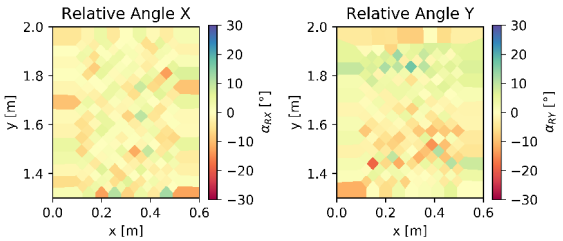

(b) Armour layer relative angles

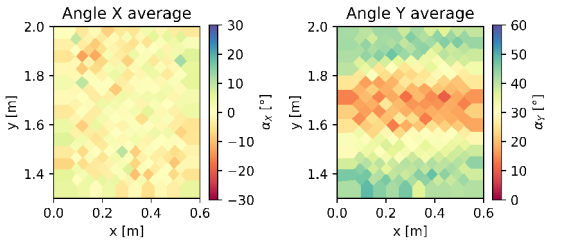

(c) Under layer angles

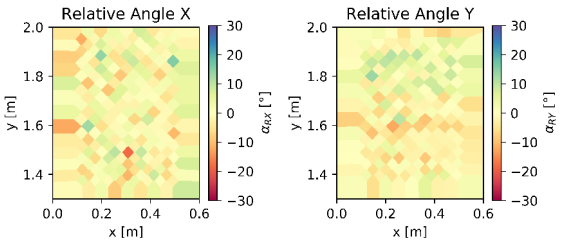

(d) Under layer relative angles

Figure D.55: Series 7, test 3

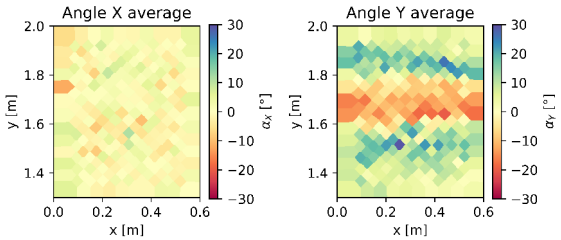

(a) Armour layer angles

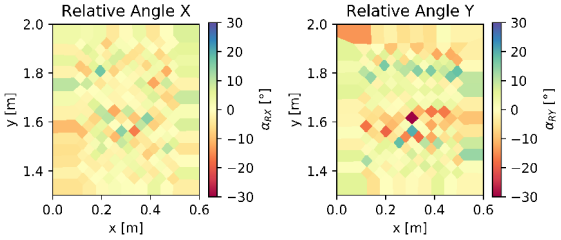

(b) Armour layer relative angles

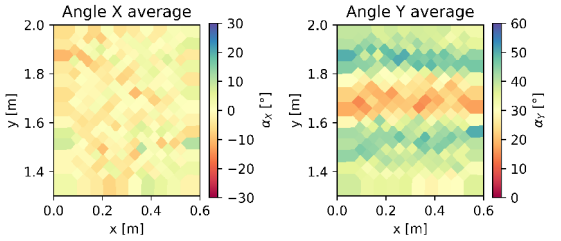

(c) Under layer angles

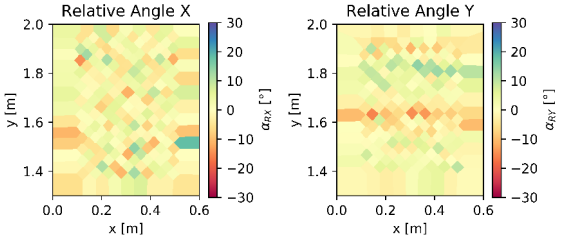

(d) Under layer relative angles

Figure D.56: Series 7, test 4

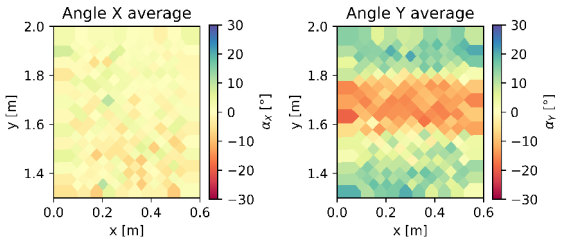

(a) Armour layer angles

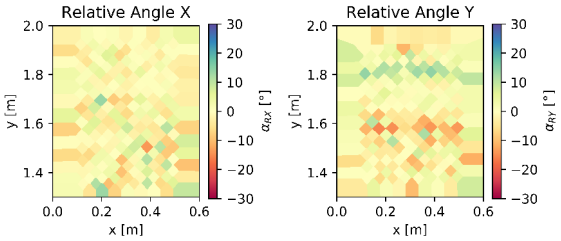

(b) Armour layer relative angles

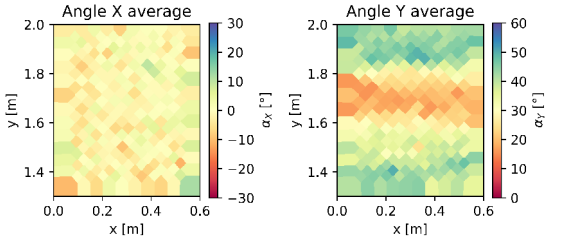

(c) Under layer angles

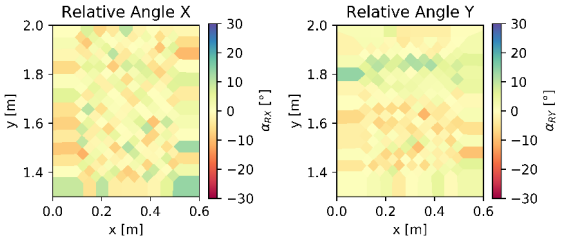

(d) Under layer relative angles

Figure D.57: Series 7, test 5

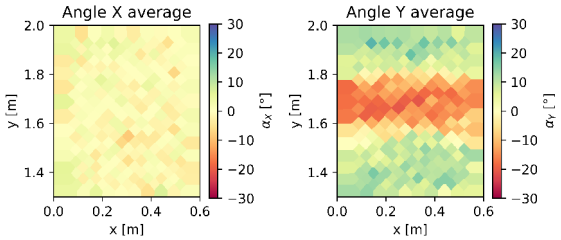

(a) Armour layer angles

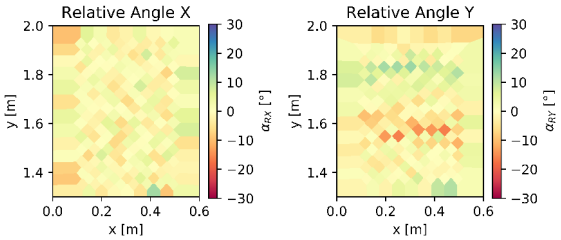

(b) Armour layer relative angles

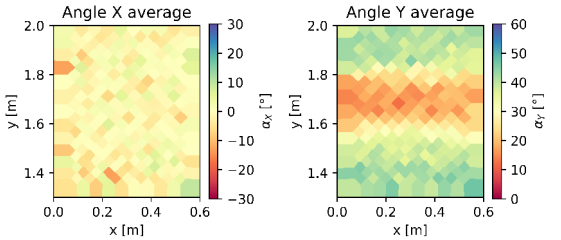

(c) Under layer angles

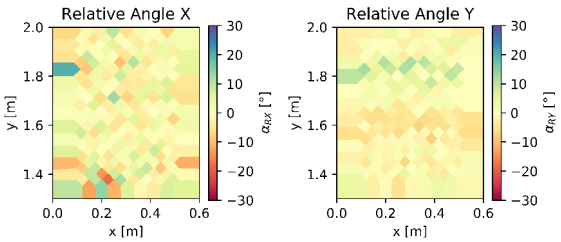

(d) Under layer relative angles

Figure D.58: Series 7, test 6

Appendix E: First simplified model of arching mechanism

In the two tests with large S-profiles the armour layer failed in a brittle fashion. The convex section of the profile was lifted up and consequentially the armour layer broke and failed, without any previous loss of interlocking. Further analysis was done of the forces over the cross section to understand the cause of the sudden failure. The analysis is a first estimation of the forces that have an influence. Multiple factors have been assumed to be negligible and have not been taken into account.

The following mechanisms are thought to play a role. The size of the forces in the S-profile are expected to be the same as for a straight profile, but the distribution has changed. The resistance is reduced due a reduction of weight resting on the steep lower part of the slope (1) and a reduction of the weight resting on the convex section (3). The force due to the overpressure and the drag of the down-rush are still present and are not expected to be decreased. The weight of the upper part of the slope (4) induces a buckling effect, thereby increasing the initial distortion by an axially applied force. Resulting in the units on top of the convex section (2), to be pushed away from the slope and fail.

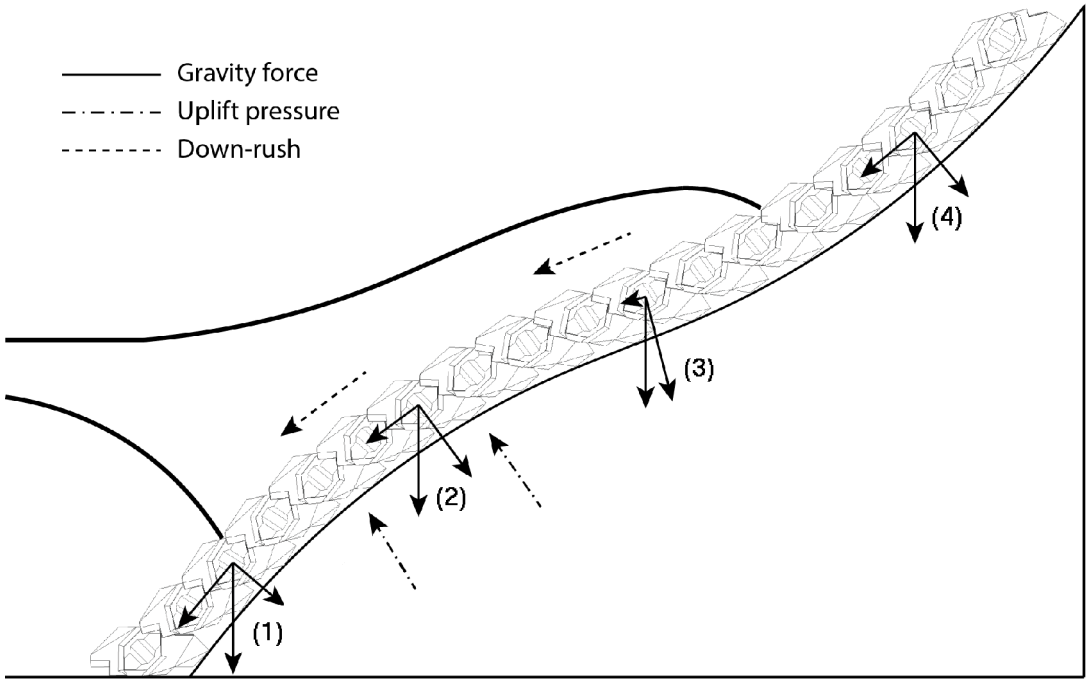

Figure E.1: Overview of directions main acting forces on a S-profile

Factors of the whole profile are influencing the total behaviour. The cross section is simplified and only the main factors are taken into account and made into a simplified model. This model is used to increase the understanding of the mechanism and is verified by checking the correlation with the test results.

First the simplified forces on a single unit are analysed at a straight slope and in the concave and convex section of the S-profile. The main forces on the units are the normal

forces (Fn) in line with the units, the gravity force (Fz) with a parallel and a perpendicular component and the pressure force (Fp). The drag force (Fp) is also present, but has been left out of this simplified model. The normal forces do not act at one location due to multiple contact points between the units and a contact point with the under layer. A simplification is made by assuming that the normal force acts in line with the center of gravity.

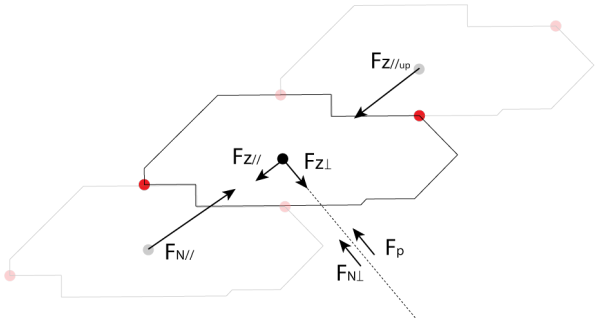

Figure E.2: Straight slope

For a straight slope the forces are depicted in figure E.2. The normal forces from the units below and weight from the units above are exactly in line with the center of gravity of the unit. It is assumed that also the pressure force and the perpendicular normal force have their point of application in the center of gravity, so there is no resulting moment. No failure occurred for a straight slope, which indicates that the pressure force is smaller than the perpendicular component of the gravity force for all performed test runs.

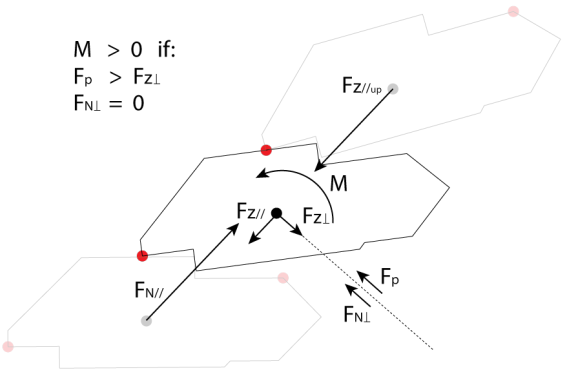

Figure E.3: Concave section

At the concave sections the slope is steeper, resulting the gravity and normal forces parallel to the slope to be increased. In figure E.3 it can be seen that the rotation between the units have caused the parallel forces to be slightly out of line. The difference in arm between the rotation point at the nose of the unit is however small and therefore the influence is expected to be small. Due to the increase of the parallel component of the gravity force, the perpendicular component has been reduced. Since the pressure force has remained the same it is possible for the pressure force to be larger and push the unit

away from the slope. Because of the rotation point at the nose of the unit and the high amount of interlocking between the units this is only possible when multiple units are moved. Still it can be concluded that units in the concave section have the preference to rotate in counter-clockwise direction and move away from the slope.

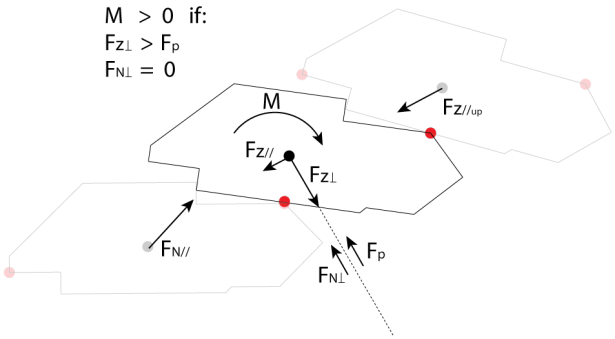

Figure E.4: Convex section

The forces of a unit in a convex section is seen in figure E.4. Here it can be seen that also for the convex section the gravity and normal forces are no longer in line. The rotation point is now located underneath the wings of the units, causing the center of gravity to be slightly behind the rotation point. The difference in arm between the gravity and normal forces and the location of the center of gravity in relation to the point of rotation, both cause a moment in clockwise direction. This moment is counteracted by the pressure force and the presence of the under layer. If the contact with the under layer however would be temporarily absent due to shifts in the lower part over the cross section, the combination of the resulting moment and the increased perpendicular component of the gravity force will cause the unit to move toward the slope.

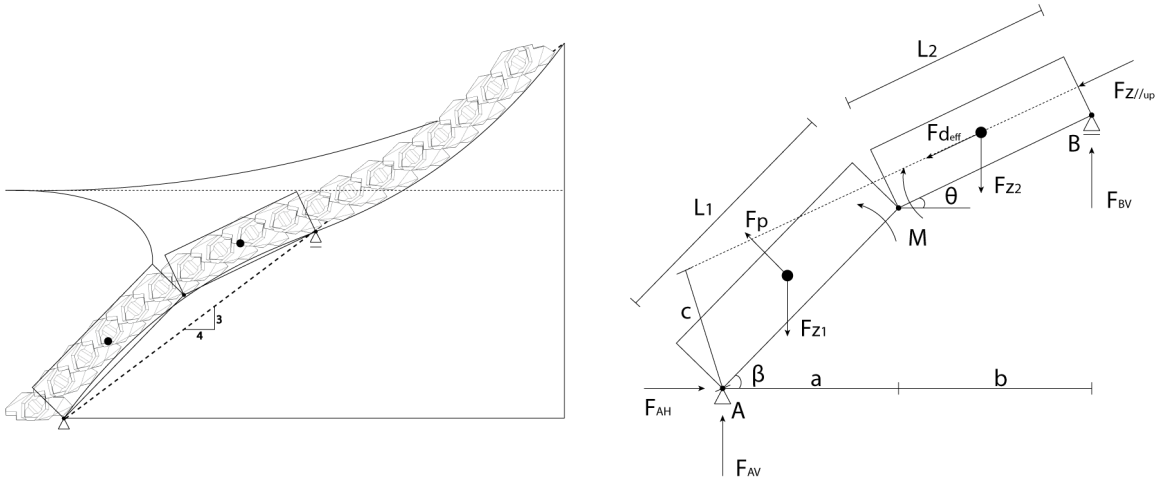

(a) Schematized S-profile **(b)** Simplified model

Figure E.5: Schematization of S-profile into simplified model

The knowledge on the force on a single unit in the different sections is used to model the full slope. The downward part of the S-profile is a straight slope, but it is a steeper

slope than the units are designed for. Therefore the forces on the units are the same as depicted for the concave section. At the concave section the normal forces between the units are very large and the interlocking is strong. To simplify the model the steep downward section of the slope is modelled as a rigid body. At the convex section the normal forces between the units are reduced, but since the units are still interlocked they are also modelled as a rigid body to simplify the model. The transition between the steep downward slope and the convex section is the point of breakage, modelled with a hinge. The point of breakage is at the transition between the units that want to rotate forward (figure E.3) and want to rotate backward (figure E.4). This is the location with the largest positive deviation from the design profile, where also failure was observed during the model tests. With these simplifications the S-profile can be schematised in to a model as depicted in figure E.5. The top part of the profile is modelled by a force on the rigid bodies, depicted as $Fz_{//up}$. The size of this force will vary as function of the steepness of the upper slope.

A further simplification is made by applying the pressure force (Fp) only on the lower rigid body and the effective drag force (Fd_{eff}) only on the upper rigid body. This simplification is valid because the pressure force increases with the distance from the still waterline and thus has the main effect of the lower part of the slope. The effective drag force is assumed to act in the direction parallel to the slope and thus has its main effect on the upper rigid body. The effective drag force is the drag force of the down rush minus the friction of the under layer.

When the moment around point A is taken this results in the following equation:

$$M_A = -1/2a\ Fz_1 + 1/2L_1\ Fp + c\ Fd_{eff} + c\ Fz_{//up} - (a + 1/2b)\ Fz_2 + F_{BV}(a + b)$$

with:

$$a = L_1 cos(\phi)$$
$$b = L_2 cos(\theta)$$
$$c = (a + 1/2b) tan(\beta - \theta)$$

As was expected the moments that induce the rotation are forced by Fp, Fd_{eff} and $Fz_{//up}$. The resistive force is the weights of the rigid bodies. In the equation also F_{BV} forces the rotation. This force however is the normal force of the rigid bodies on the under layer and does not force the rotation. At the moment of rotation the armour units are lifted from the under layer and the normal force is no longer present. Therefore the F_{BV} is taken to be zero in the model.

The Fz, Fd_{eff} and Fp, are assumed to be the same per unit length for all tests. An increase in L1 also increases a, but to a lesser extend. Resulting the increase in arm for Fp to be larger than for Fz_1. The increase in arm for Fd_{eff}, $Fz_{//up}$ and Fz_2, is approximately the same, thereby increasing the forcing of the rotation. An increase of L2 will increase the arm of Fz_2, but will also increase the Fd_{eff}. The total effect of L2 is expected to be of minor importance.

An increase of ϕ results in an decrease of the arm of Fz_1 and Fz_1 and an increase of the arm of Fd_{eff} and $Fz_{//up}$. Thereby only decreasing the resistive forces and increasing the forcing of the rotation. The opposite is true for an increase of θ. This would reduce the arms of Fd_{eff} and $Fz_{//up}$, and thereby reduces the forcing of the rotation. The major

influence of ϕ explains why the mechanism is so sensitive for the deviation from the design profile, since a large deviation causes a large ϕ. That the mechanism is more effective for S-profiles is caused by the sensitivity for θ. The long transitional area which is almost flat causes a small value for θ and thus a lower stability. Also an increase of $\mathrm{Fz}_{//\mathrm{up}}$ has a direct influence on an increase of the forcing of the rotation. In the S-profiles this increase is caused by the steep upper slope.